January 2019

Low Temperature Multi Effects Desalination-Mechanical Vapor Compression Powered by Supercritical Organic Rankine Cycle

Eydhah Almatrafi
University of South Florida, almatrafi@mail.usf.edu

Low Temperature Multi Effects Desalination-Mechanical Vapor Compression Powered by Supercritical Organic Rankine Cycle

by

Eydhah Almatrafi

A dissertation submitted in partial fulfillment
of the requirements for the degree of
Doctor of Philosophy
Department of Mechanical Engineering
College of Engineering
University of South Florida

Major Professor: Yogi Goswami, Ph.D.
Elias Stefanakos, Ph.D.
Rasim Guldiken, Ph.D.
Thomas Crisman, Ph.D.
Frank Pyrtle III, Ph.D.

Date of Approval:
December 13, 2018

Keywords: Thermal Desaliantion, MED-MVC, SORC, Solar-MED-MVC

DEDICATION

I dedicate this work to my parents.

ACKNOWLEDGMENTS

First and foremost, praises and thanks to the God, the Almighty, for His showers of blessings throughout my research work to complete the research successfully.

This work would not have complete without the great support I received from my advisor, committee members, and family.

I would like to express my sincere gratitude to my advisor, Dr. D. Yogi Goswami, for providing me this opportunity to pursue higher studies in the field of engineering. I am also indebted to my committee members: Dr. Elias Stefanakos, Dr. Rasim Guldiken, Dr. Thomas Crisman, and Dr. Frank Pyrtle III. Their kind insights was very precious to me. Each of my dissertation committee members has inspired my work in unique and highly significant ways. I would like to thank my friends in Clean Energy Research Center (CERC) for their support and motivation during my research at USF. I thank Dr. Jotsh, Mrs. Barabara, Francesca, Chatura, Arun, Kelly, and Deigo for their constant help.

I am extremely grateful to my parents (Ibrahim and Fatimah), and my brothers and sisters (Helal, Bandar, Mohammed, Asmaa, Ibtesam, Khalel and Bashaer) for their love, prayers, caring, and sacrifices for educating and preparing me for my future. I am very much thankful to my wife (Reem) and my son (Husam) and daughter (Fatimah) for their love, and understanding.

I thank King Abdul-Aziz University (KAU) for their support throughout the study and the research. Finally, my thanks go to all the people who have supported me to complete the research work directly or indirect.

TABLE OF CONTENTS

LIST OF TABLES

LIST OF FIGURES

ABSTRACT

Utilizing low grade heat sources such as geothermal, solar or waste heat has received a high attention in recent years. A lot of research has discussed using Organic Rankine Cycle (ORC) as subcritical or supercritical in power generation. However, very few studies extend their research in utilizing ORC in other applications such as desalination. For reverse osmosis (RO) desalination, which is considered a membrane technology, the use of supercritical-ORC in low grade heat sources is more favorable than subcritical-ORC. Thus, studies of utilizing either subcritical-ORC or supercritical-ORC for thermal desalination that use power and heat from Rankine cycle are rare or have not been done yet. Thermal desalination technologies are dominant for desalination in the Gulf Corporation Countries (GCC) and are getting more focus to treat high concentration feed and provide drinking water due to shortage of clean water in the world.

This study proposes a novel system that combines a supercritical-ORC with multi-effect desalination and mechanical vapor compressor (MED-MVC) for desalination using low grade heat sources at temperatures less than 150 °C. A numerical model was developed, which was used to conduct performance, exergy and economic analyses under various parameters such as: salinity of the feed, temperature of motive steam and pressure of ORC. The proposed system was compared with different MED combinations with respect to specific energy consumption and unit cost of water produced.

CHAPTER 1: INTRODUCTION

1.1 General Background

Clean drinking water availability is one of the most important issues today. According to the United Nations World Water Development Report published in 2014 : Water and Energy, 47% of world population will be living in areas of high water stress by 2030 and by 2025, 1.8 billion people are expected to be living in countries or regions with absolute water scarcity, and two-thirds of the world's population could be living under water stressed conditions [1]. There are many reasons for that, such as limited fresh water sources, increased annual demand of fresh water, and the intensive energy needed for desalination making it less favorable for countries with limited sources of fossil fuels.

Only 3 % of earth's water is fresh water while the rest is saline and found in the oceans and seas. About one third of the fresh water is stored underground that is not easily accessible, and a large part in the form of ice covering mountainous regions, Antarctic and Arctic far away from the population. Only 0.03% of earth's water is usable by humans in the form of rivers and lakes that is distributed unevenly on the earth as shown in Figure 1. The demand of fresh water has been increasing annually by 5% and is currently 9,087 billion m^3, 75% of which is dependent on rainwater for agriculture [2].

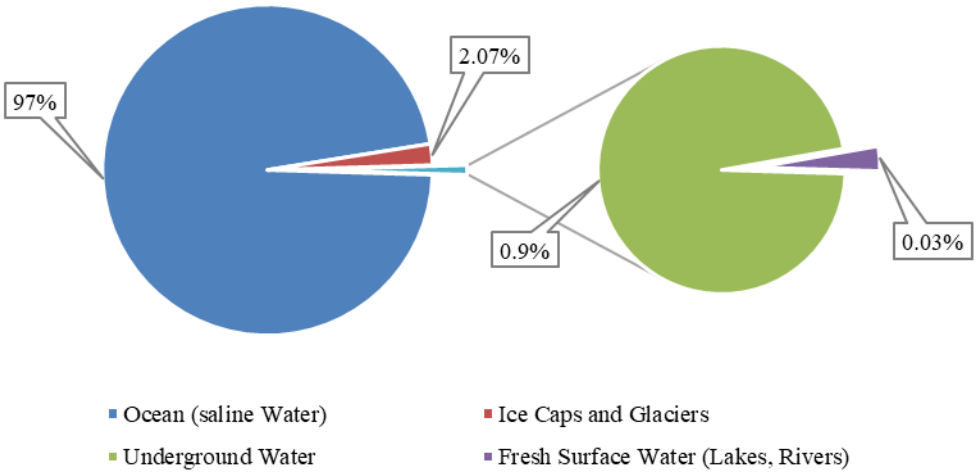

Figure 1 Earth's water distribution by source.

The main reasons for the increasing demand of fresh water are the exponential population and economic growth in industrial and agricultural businesses. According to the United Nations World Water Development Report published in 2015: Water for a Sustainable World, water use has been growing at more than twice the rate of population increase in the last century [3]. Stress on fresh water resources is faced by developed and developing countries for domestic, agricultural, and industrial uses. Figure 2 shows how fresh water has been used in developing and developed countries. The Energy Information Agency (EIA) estimated that water consumption will be increased up to 60% by 2040 [4]. The natural water cycle including surface and ground water, estimated at a total volume of about 4,500 billion m^3, will not meet the demand in 2030 which is predicted to be 6,900 billion m^3 [5,6]. Desalination technologies can bridge the gap between demand and availability of fresh water since the saline water is abundant and easily accessible.

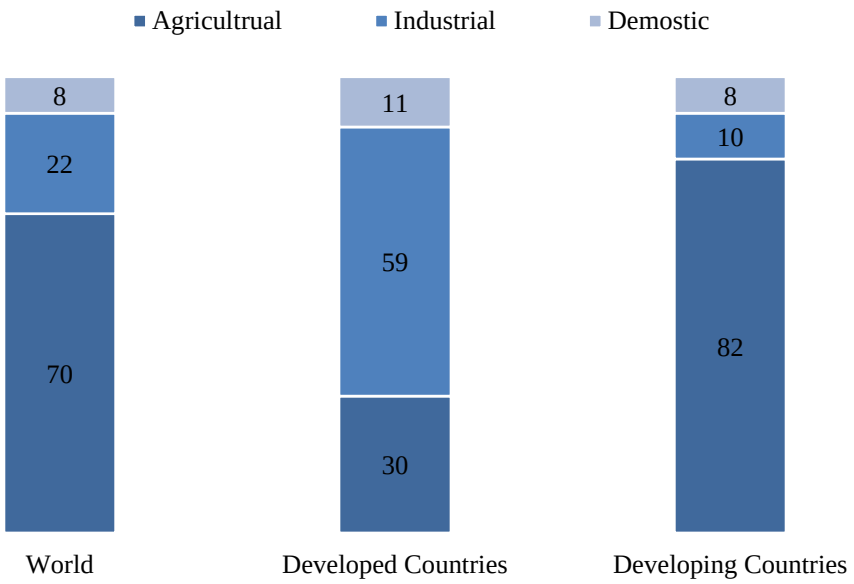

Figure 2 Fresh water uses in developing, developed countries and the world.

Desalination, which is the process of removing dissolved salts from water, thus producing water from seawater or brackish water, has the promise to face the challenge of limited of fresh water. There are more than 18,400 desalination plants worldwide producing about 31.68 billion m^3/year that represent 4.3% of the fresh water demand for domestic and industrial uses (not including agriculture) [7]. The installed capacity of desalination has increased by about 10% annually from 2010 to 2016 through the world based on Global Water Intelligence Report [8]. This increase in the capacity includes desalination plants that treat brine water, with salinity greater than 50,000 (ppm); saline water, which has salinity 20,000-50,000 (ppm) and brackish water that has salinity 500-2,000 (ppm). The desalination technology is desalting the seawater and provide water within the limit of 500 ppm that defined by WHO (world Health Organization).

Desalination can be classified based on the process as either phase change or membrane desalination, as depicted in Figure 3. In phase change desalination processes, the feed water is heated and evaporated at saturation pressure to obtain salt free water vapor while the remaining

concentrated brine is discharged. The product is of good quality and the process is suitable for high salinity concentration. Multi-stages flash (MSF) and multi-effects desalination (MED) are examples of phase change processes. Phase change processes account for about 40% of the desalination market worldwide and more than 70% of desalination market treat feed with salinity greater than 35,000 ppm. In membrane processes, seawater passes through a membrane by applying high pressure in a reverse osmosis (RO) and or membrane distillation (MD) process to collect desalinated water or by applying electrical potential in an electro–dialysis (ED) process to extract the salt ions from seawater. Membrane desalination processes account more than 60% of the desalination market worldwide as shown in Figure 4.

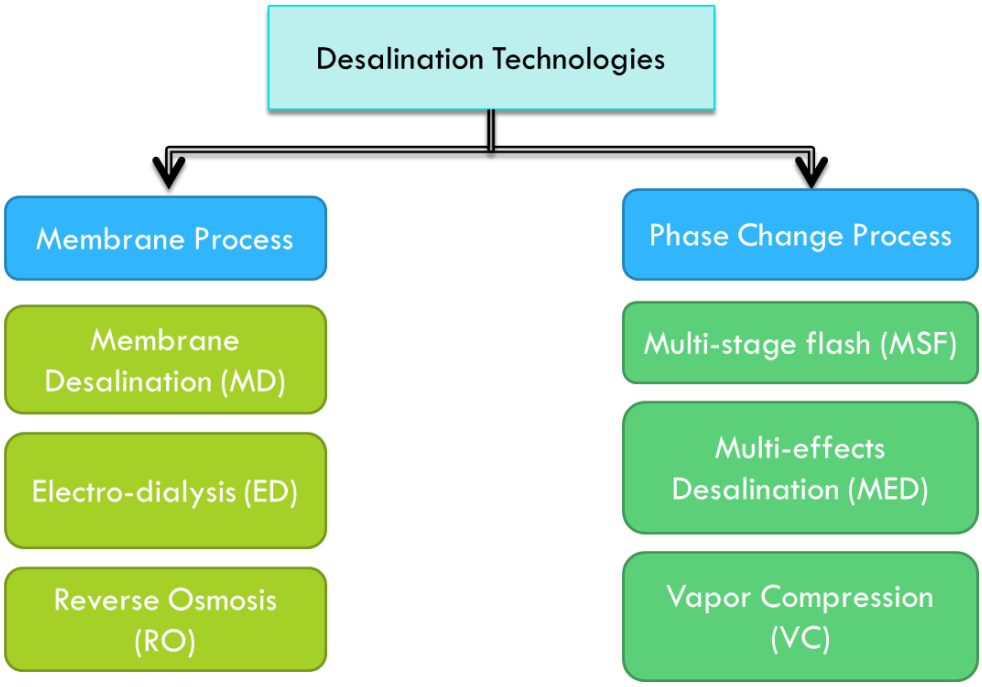

Figure 3 Classification of desalination technologies by process.

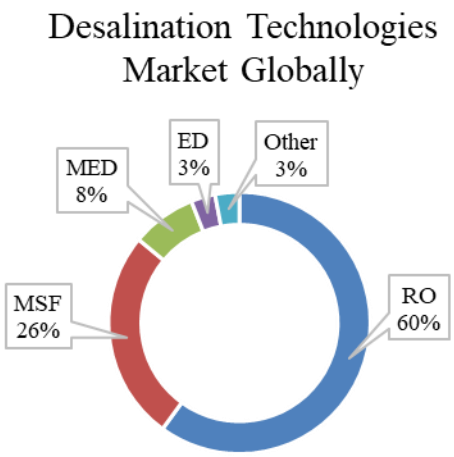

Figure 4 Desalination technologies market in global.

Desalination processes require a huge amount of energy to separate the dissolved salts from seawater as illustrated in Table 1. The total equivalent energy used in water sector that includes pumping water and desalination was estimated by EIA at 120 million tons of oil equivalent (Mtoe). About 60% of that required energy comes directly from electricity which was about 4% of electricity net generation globally in 2015 where desalination accounted for 20% of the total energy consumption that mainly came from fossil fuels [4,9]. The EIA estimated 60% of energy consumption in the water sector in 2040 will be from desalination plants [4]. Due to the environmental impact of using fossil fuels in desalination and limited access for many developing and underdeveloped countries to fossil fuels, using solar energy and renewable energy is a valuable option instead of fossil fuels since it is accessible worldwide and is a clean energy source.

Table 1 Energy requirement and unit product cost for conventional desalination systems [10–18].

	Specific thermal energy Consumption (kWh/m^3)	Specific Electricity Power Consumption (kWh/m^3)	Total Equivalent Energy Consumption (kWh/m^3)	Specific Cost of Water Production ($\$/m^3$)
Reverse Osmosis (RO)	0	4-7	4-7	0.64-1.98
Electro-Dialysis (ED)	0	2.6-5.5	2.6-5.5	0.6-1.05
Multi-Stage Flash (MSF)	52 - 78	3-5	19 - 27	0.56-1.75
Multi-Effects Desalination (MED)	40 - 65	1.5-2.5	14.5-21	0.52-1.5
Mechanical Vapor Compressor (MVC)	0	7-12	7-12	0.89-2.48
Thermal Vapor Compressor (TVC)	63	1.6-1.8	16.26	0.87-2

Solar energy is the most appropriate of all renewable energy options to compete with fossil fuels for desalination since both heat and power can be utilized in desalination. According to a detailed market analysis report of desalination by renewable energy, two-thirds of renewable desalination installation in the world is powered by solar energy [19]. Solar energy can be used for desalination by producing either the thermal energy or electricity via solar pond, flat plate collector, evacuated tube collector, parabolic trough, solar dish, central receiver tower or photovoltaic (PV) cells to drive the phase change or membrane processes. Solar desalination systems are classified into two categories: direct and indirect collection systems. Direct collection systems use solar energy to produce distillate directly in the solar collector, whereas indirect collection systems have two subsystems: one for solar energy collection and the other for desalination as shown in Figure 5. Papapetrou et al. [19] studied the roadmap of implementing renewable energy in desalination market with respect to the development status and capacity of production as shown in Figure 6 that shows solar organic Rankine driven desalination system has the potential for low capacity water production though it is in an early stage of research. The renewable energy powered desalination accounts for less than 1% of total installed capacity in the desalination

market, 62% based on RO and 43% powered by PV [19–21]. The costs of production for different renewable energy powered desalination systems are shown in Figure 7. Solar driven MED is estimated to be the lowest cost among all technologies although it is in an advanced stage of research with small applications. For high capacity production, CSP-MED is recommended while for small capacity, solar-MED is more favorable.

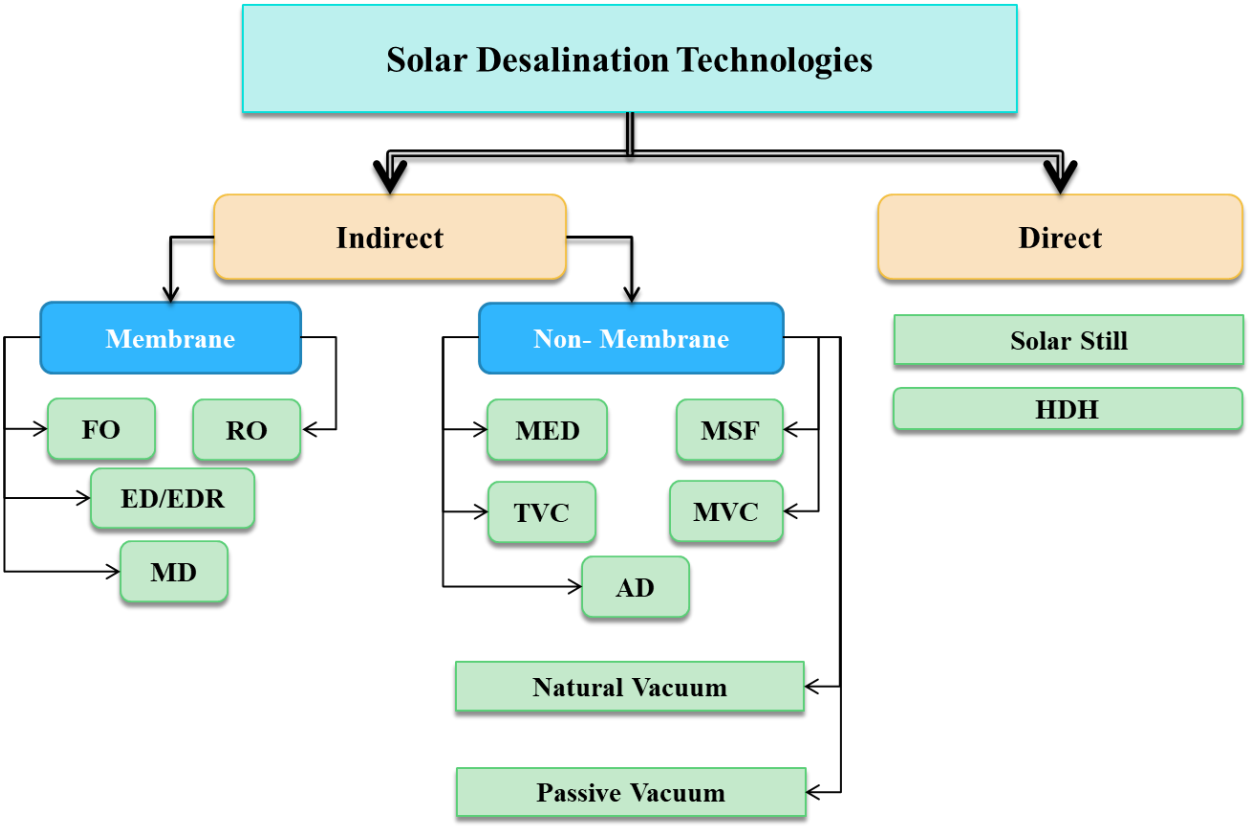

Figure 5 Solar desalination technologies.

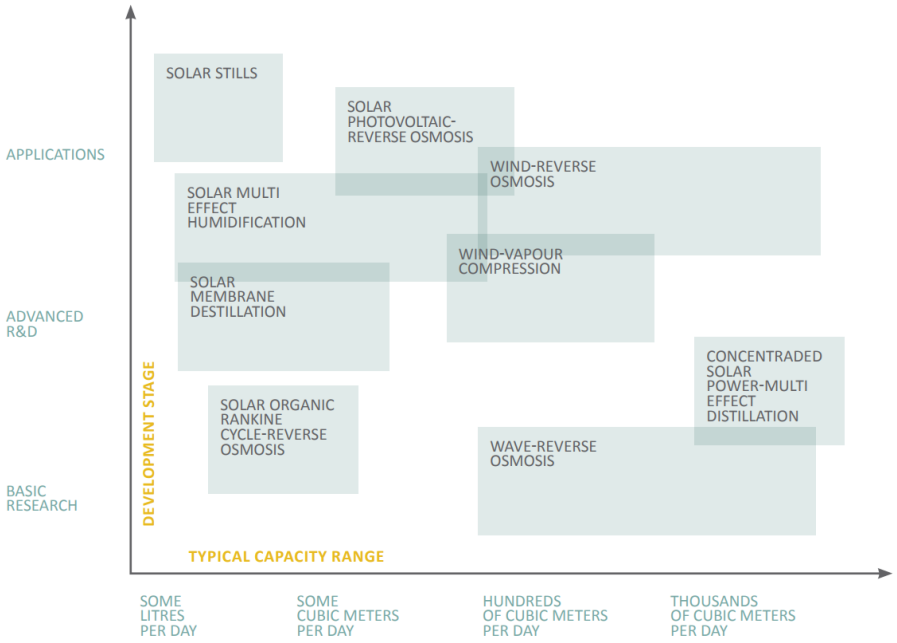

Figure 6 Development status and capacity range of renewable energy driven desalination [19].

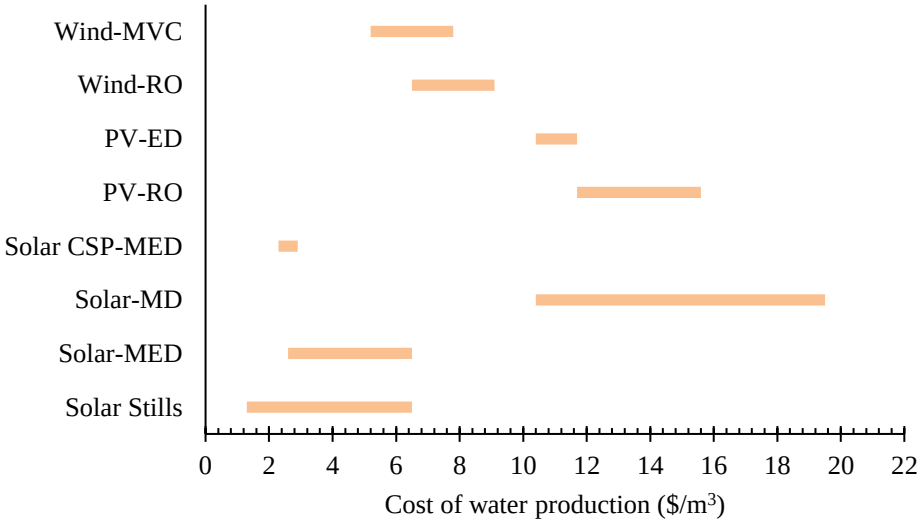

Figure 7 Cost of production for different renewable energy powered desalination systems.

There are many references in the literature that describe the current status and future development of solar desalination. Delyannis reviewed the historic development of solar desalination technologies [22,23]. Li et al. [24] presented a comprehensive review of the current

solar desalination research powered by direct or indirect solar energy. Although not commercialized yet, hybrid desalination systems that use solar, fossil fuels and low grade waste heat sources have a potential to be cost effective. Sharon et al. [25] performed a comprehensive performance analysis of solar desalination technologies that includes direct and indirect methods (membrane and phase change process) based on specific energy consumption, performance ratio, efficiency, and recovery ratio. Key findings about solar assisted MED that are mentioned in the most recent literature are summarized in Table 2 and further detailed in Chapter 2.

Table 2 Summary of key findings about MED in solar desalination in published literature.

Reference	Key Finding about Solar-MED
Delyannis, E. (1987,2003) [9,10]	Reviewed solar parabolic dish concentrator powered MED-TVC and evacuated tube collector powered MED that has a capacity 120 m^3/day in UAE.
Li, C. et al. (2013) [24]	Solar-MED is a proven technology where solar-MED-RO (hybrid) and co-generation solar system have an enormous potential.
Sharon, H. (2015) [25]	Solar-MED different configurations are mature technologies, and more favorably for large production. The cost of solar pond coupled MED is in range 0.71-0.89 \$/m^3 and CSP powered MED 2.4-2.8 \$/m^3.
Al-Karaghouli, A and Kazmerski, L (2013) [16]	MED and RO are the best candidate for CSP coupling. Where the cost of energy in MED for low temperature heat sources is up to 60% and for co-generation is less. The cost of energy for RO is about 44%.
Hetal, K. et al. (2014) [26]	They conducted that solar-MED shares 13% of the installed capacity among distribution of renewable energy powered desalination and most suitable desalination technology is MSF and MED for solar power.
Qiblawey, H and Banat, F. (2008) [27]	The cost of solar powered MED has dropped from 3.2 \$/m^3 to 2 \$/m^3 when the capacity is increased from 500 m^3/day to 5000 m^3/day.
Palenzuela, P. et al. (2015) [28,29]	Compared the cost of large scale CSP powered MED and RO in different configuration in the Mediterranean basin and the Arabian Gulf, found. They recommend combination of CSP with MED for the Arabian Gulf.

1.2 Motivation for the Present Research

Middle East and North Africa is a region with high dependence on non-renewable water resources which face the challenge of depletion. In Saudi Arabia a study performed on the main and secondary aquifers for about 10 years has shown that the amount of available water has been decreased by about 40% [30,31]. GCC are the highest desalination producers and account for more

than 30% of the total global desalination capacity. Thermal desalination represented by MSF and MED accounts about 71% as shown in Figure 8 [32,33]. In Saudi Arabia, the total water produced by desalination has increased by 40% between 2010-2016 based on the Electricity & Cogeneration Regulatory Authority (ECRA) annual reports represented in Figure 9 [34]. GCC countries consume about 38 million tons of oil equivalent per year to meet their needs in water. The World Bank and EIA have projected that the amount of desalinated water will almost double by 2050. That brings three main challenges; making desalination technologies friendlily to the environment by reducing CO_2 emissions, increasing the performance of desalination technologies to reduce the energy consumption, and developing and implementing renewable energy desalination technologies where they are cost effective.

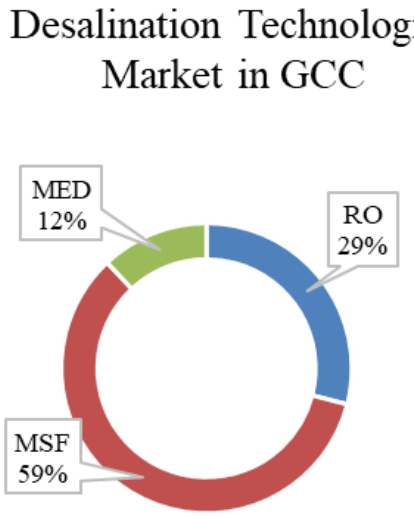

Figure 8 Desalination technologies market in GCC.

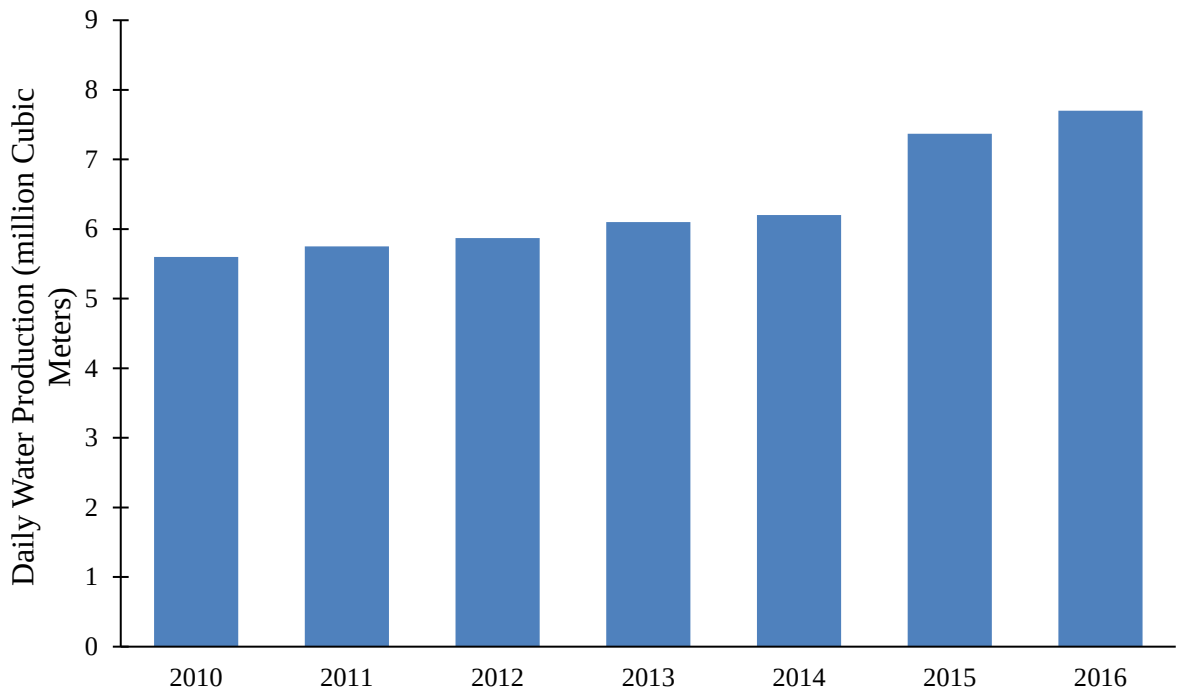

Figure 9 Actual production of desalinated water in Saudi Arabia in period 2010 – 2016.

Shifting to RO desalination plants that use less energy, reforming the policies in the agricultural sector by using treated waste water and implementing solar in the current thermal desalination systems in GCC may lift the burden of intensive fossil fuels use in desalination and minimize the side effects of GHG emissions[35].

US Department of Energy (DOE) has called for research proposals to reduce the specific thermal energy consumption of solar-MED, to less than 30 kWh_{th}/m^3 and the unit costs to be less than 0.5 $\$/m^3$ for seawater and 1.5 $\$/m^3$ for small capacity and high concentration brine more than 100,000 ppm. This will be fantastic opportunity for GCC since thermal desalination is dominant there and the conventional MED costs in the range of 0.8-1.2 $\$/m^3$. The variation of total costs of produced water ($\$/m^3$) from conventional desalination technologies is listed in Table 1 based on many factors, such as, the specific energy required, the degree of salinity (ppm) and the scale of production (m^3/day).

While the membrane desalination by reverse osmosis have the highest share in the market for desalination, it has a limitation that it is not able to treat water with a salinity of more than 100,000 ppm and cannot achieve 50% recovery at water above 50,000 ppm. The pressure limit for the current commercial RO is 8.3 MPa. Beyond this limit the membrane spacers collapse and are not appropriate to flow water[36]. Al-Karaghouli et al. analyzed the impact of increasing the salinity on the performance of RO desalination plant (2000 m^3/day) located in Umm Qasr in Arabian Gulf where salinity is in the range of 38,000-42,500 ppm[37]. Their results are shown in Figure 10. The cost of water production was increased by almost 5% and the specific energy consumption was increased about 23% because of the increase in the osmotic pressure by 10%. Moreover, the recovery ratio, defined as the mass of fresh water produced over mass of the feed, was decreased by 40% and the quality of water produced was decreased by 11%. That shows the need for using thermal desalination for high concentration feed.

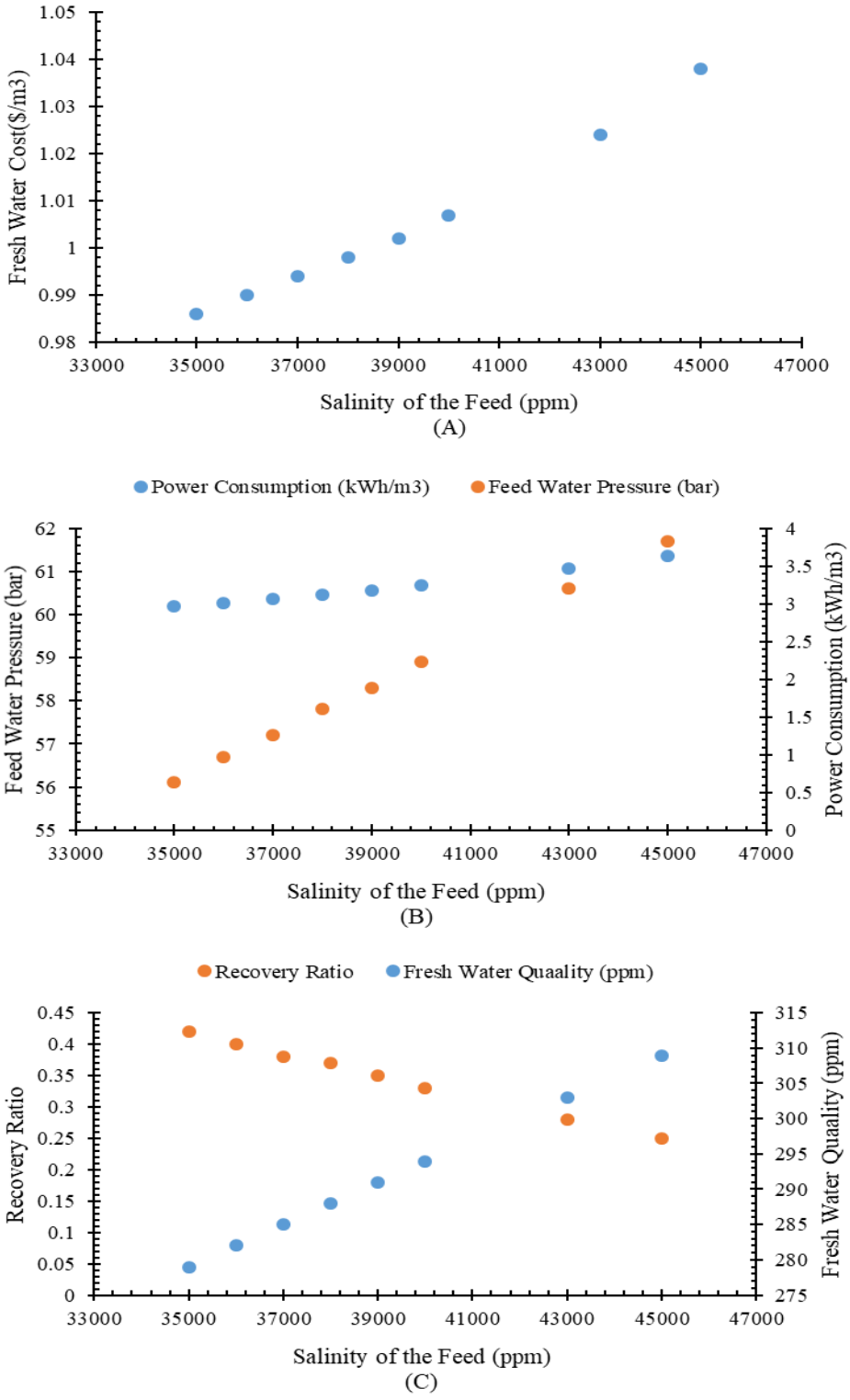

Figure 10 Effect of seawater salinity on (A) Water production cost, (B) RO power consumption and pressure feed, (C) Recovery ratio and quality of fresh water produced.

Although multi-stage flash desalination (MSF) has higher share of market among the thermal desalination technologies in the world, it has higher energy consumption, higher temperature operation, and higher capital costs compared with multi-effect desalination (MED). Therefore, MED has attracted more attention in the MENA region from energy prospective. In addition, MED can be operated at a low temperature below 90°C avoiding scaling and fouling issues. This range of low-temperature operation gives MED an advantage to be compatible with low grade heat sources such as geothermal, solar or waste heat.

One of the major improvements in MED would be eliminating the down condenser totally or partially. Most of the studies in the literature are focused on solar MED-TVC coupled with a power cycle or a stand-alone system driven by a solar technology while a few have discussed MED-MVC. Mechanical vapor compressor assisted MED is more attractive since it makes it possible to operate a MED system by electricity, eliminating the external steam [38]. For solar energy powered MED-MVC either PV or a solar thermal power could be used. Most recent studies on MED-MVC are summarized on Table 3.

Based on our review, a system that has not been investigated in the literature is using supercritical ORC powered MED-MVC for low and medium temperature heat sources. The advantage of using a supercritical ORC as opposed to a subcritical ORC is that the heating process does not go through the two phase region, creating a better thermal match in the heat exchanger with less exergy destruction and ultimately a higher cycle efficiency. Due to the availability of low and medium temperature heat sources such as waste heat, solar or geothermal, a detailed study of a MED-MVC operated by a supercritical-ORC will add value to the knowledge base of desalination to meet the energy challenge.

Table 3 Most recent literature studies on MED-MVC.

	El-Dessouky et al., 2000[39]	Aybar et al., 2002[40]	Helal et al., 2006[41]	Nafey et al., 2008[42]	Sharaf et al., 2011[43]	He et al., 2018[44]
Solar System	-	-	PV	-	PTC	-
Power cycle	-	-	-	-	ORC, 350°C	Transcritical CO_2, 85 °C
Number of effects	3	1	1	2	16	1
Mass of water production daily, m^3/d	3000	250	120	1500	4545	111.456
Top steam Temperature, °C	70	87.00	59	65	60	85
Temperature of brine in last effect, °C	62.9	81.35	18	60	46.8	-
Salt concentration of intake seawater, ppm	36000	-	45000	42000	46000	-
Recovery Rate	0.49	-	0.44	0.35	0.333	-
Specific energy consumption, kWh/m^3	6.3	11.47	15.6	9.4	4.18	13.99

1.3 Research Objective

The main goal of this research is to study a novel system coupling a solar supercritical organic Rankine cycle with low-temperature multi-effects desalination assisted by mechanical vapor compressor (solar-Supercritical-ORC-LT-MED-MVC) treating high concentration feed and to analyze this system thermodynamically and economically. The proposed system has the potential to meet the two goals set by USDOE for solar-MED, which are specific thermal energy consumption less than 30 kWh_{th}/m^3 and the specific cost less than 1.5 $\$/m^3$. A brief description of the contents of the chapters in this dissertation is given below:

Chapter one highlights the general background of the desalination, current water demand and future trend, solar desalination current status, motivation of the research and the research objective of the present work.

Chapter two presents a literature review associated with solar assisted multi-effects desalination systems with different combinations such as solar-MED, solar-MED-TVC and solar-MED-MVC, focusing on ORC driven thermal desalination and mapping it with the DOE goals.

Chapter three discusses the components of the proposed innovative system that include four sub-systems; solar sub-system, supercritical-ORC sub-system, LT-MED sub-system and MVC sub-system.

Chapter four presents the performance analysis and discusses using organic fluid to drive the proposed system for low grade heat sources optimizing the pressure of the power cycle and comparing ORC and supercritical-ORC with the motive steam temperature, pressure of the power cycle, salinity of the feed, and the number of effects as variables.

Chapter five presents an exergy analysis of the proposed system with the motive steam temperature, pressure of the power cycle, salinity of the feed, and the number of effects as the variables.

Chapter six provides a comparison of the proposed system with solar-MED and solar-MED-TVC in terms of specific energy consumption and solar field size, which shows the advantage of using supercritical-ORC to run thermal desalination.

Finally, chapter seven summarizes the conclusions and future recommendations.

CHAPTER 2: SOLAR ASSISTED MED, A REVIEW

2.1 Introduction

The improvements of membrane and energy recovery devices are driving the specific energy and costs of RO desalination lower, resulting in a high market share for desalination technologies. However, high salinity feed, high temperature feed, and the presence of organic and inorganic pollutants increases the cost of RO in replacements and pretreatment processes and can potentially cause the plant to shut down [45]. During harmful algae blooms (HAB) in the Arabian Gulf, RO plants were shut down for two months in Oman and UAE [46]. Therefore, thermal desalination is dominant in GCC although it consumes more energy than RO.

Thermal desalination, which is a phase change process, consists of a series of evaporation and condensation process. Multi stage flash (MSF) and multi-effects desalination (MED) are major desalination technologies for saline feed. The MED process has the ability to operate at low temperatures (less than 70°C), minimizing the risk of scale formation in the tube surface. MED has two clear advantages over the MSF process: lower power consumption and higher performance efficiency [47]. Reduction of oil consumption and air pollution resulting from desalination processes is the driving force for researchers to implement solar energy in desalination process.

Solar assisted multi-effect desalination (MED) is considered an indirect solar desalination system that is composed of two subsystems: a solar subsystem that converts solar energy into either heat or electricity, and an MED subsystem where the motive steam needed to the process is heated totally, partially or compressed by vapor compressors. Therefore, solar can assist MED by providing heat or power. There are many different arrangements to achieve this such as

photovoltaic (PV) collectors powering MED-MVC, solar thermal collector, such as solar pond (SP), flat plate collector (FPC), evacuated tube collector (ETC), parabolic trough collector (PTC) or central receiver tower, providing heat to MED or MED-TVC directly or driving a heat engine that drives MED, MED-TVC or MED-MVC.

In this chapter, a comprehensive review of solar assisted MED is presented. Non-conventional systems such as hybrid, co-generation and zero liquid discharge (ZLD) are also discussed. The systems studied in the literature are mapped against the DOE goals regarding solar-MED that aim to have a specific thermal energy consumption less than 30 kWh_{th}/m^3, and a cost less than 0.5 $\$/m^3$ for seawater and 1.5 $\$/m^3$ for salinity greater than 100,000 ppm.

2.2 Solar Assisted MED

Direct use of solar thermal energy to run MED is the simplest combination as shown in Figure 11. The motive steam which enters the first effect to give the latent heat to start the series of evaporation and condensation processes in other effects is heated directly in the solar field via direct steam generator (DSG) or indirectly through a heat exchanger boiler connected to the solar field.

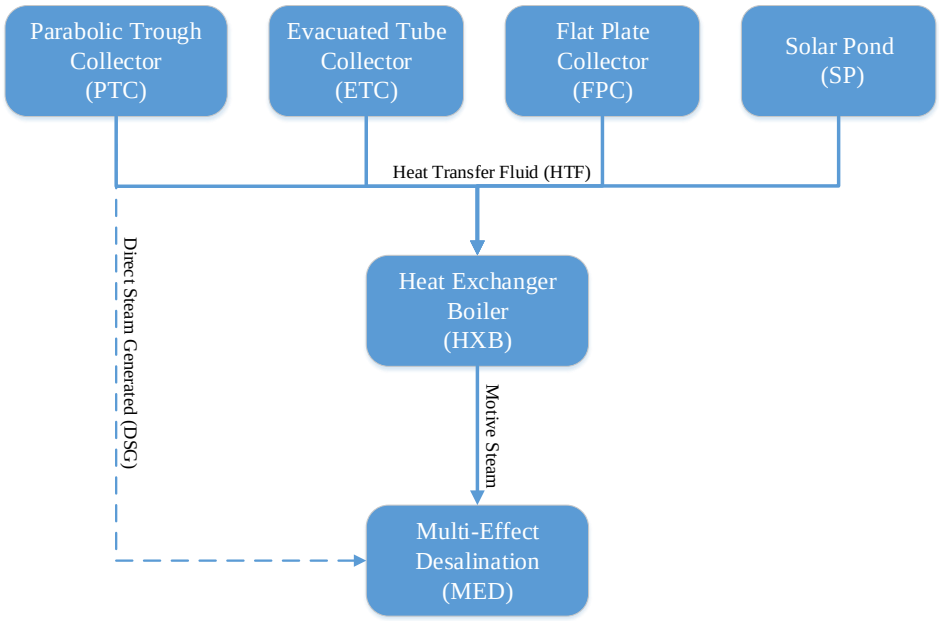

Figure 11 MED powered by different types of solar collectors.

Garcia-Rodriguez et al. [48] proposed MED driven by parabolic troughs based Direct Steam Generation (DSG). Garcia-Rodriguez et al. [49] compared the performance and the preliminary costs of three configurations of MED in Spain: a solar-fossil fuels powered MED plant with DSG using parabolic troughs, solar-fossil fuels powered MED plant using a HTF, and a conventional MED plant. However, this combination was not tested experimentally and estimating the cost of DSG parabolic trough is difficult since it is not commercial [50].

A solar pond, which is a combined solar collector and thermal energy storage, is composed of three layers: the upper convective zone (UCZ) that has lower salinity and low temperature, the non-convective zone (NCZ) that has salinity and temperature gradient, and lower convective zone (LCZ) that stores the heat at high salinity at temperatures up to 110 °C. Solar pond (SP) has the lowest cost among solar collectors, however, it requires a large area and its stability is affected by evaporation [51]. The El-Paso Solar Pond project in Texas studied the combination of a solar pond with different thermal desalination systems in 1987 including small multi-effect desalination,

multi-stage flash desalination, and membrane desalination focusing on the technical feasibility and thermal performance [52]. Al-Hawaj et al. [53] analyzed the performance of SP-MED for three years. The number of effects was 5, the capacity of production was 100 m^3/day, and the motive steam temperature was set at 90°C. They concluded that the optimum temperature of SP is in range of 80-90 °C. Tsilingiris [54] modeled a SP-MED system of 500 m^3/d capacity and a motive steam temperature of 75°C. The cost of production was 2 \$/m^3 and the specific thermal energy consumption was 75 kWh_{th}/m^3 with 14 effects of MED. Caruso et al. [55] tested a SP-MED for one year at the University of Ancona in Italy that had a capacity of 30 m^3/d and 4 effects of MED. The specific thermal energy consumption was 192 kWh_{th}/m^3.

A flat plate collector (FPC) driven MED was studied by Gerofi et al. [56] in 1983 in Sydney, Australia. Fresh water was pumped through the collectors and flashed in a tank producing motive steam to drive the MED. The specific cost using FPC was 4 \$/m^3 as compared to 5.10 \$/m^3 for evacuated tube collector (ETC) [57].

Evacuated tube collector (ETC) powered MED was tested experimentally in 1984 at United Arab Emirates (UAE). El-Nasher and Samad [58] reported 13 years of operation and performance of ETC-MED which had 18 effects producing 85 m^3/d for feed salinity of 55,000 ppm where the specific thermal energy consumption was 50 kWh_{th}/m^3 and the cost of water produced was 7-10 \$/m^3.

Parabolic troughs collector (PTC) powered MED was tested experimentally at the Platforma Solar de Almeria (PSA) in 1988 [59–62]. A system with 14 effects of MED, where the motive steam temperature was 70 °C, with a capacity of 72m^3/d and thermocline thermal energy storage (TES) required 2,672 m^2 of PTC for 24-hour operation. The specific thermal energy consumption was 63.33 kWh_{th}/m^3. Sharaf et al. [43] studied different arrangements of MED

coupled with PTC regarding the direction of the feed and motive steam such as; parallel feed (PF), forward feed (FF), preheated forward feed (FFH) and backward feed (BF). The system was designed to produce 100 m^3/day. The specific thermal energy consumption and the costs of unit water produced by MED-FFH and MED-PF were lower than MED-BF and MED-FF.

Table 4 shows the specific energy consumption and costs of water produced for solar-MED.

Table 4 Summary of solar-MED.

Author	Model or Exp.	Solar System	Number of Effects	Desalination Capacity (m^3/day)	Salinity of the Feed (ppm)	Motive Steam Temp. (°C)	Cost of Unit Produced ($/$m^3$)	Specific thermal energy Consumption (kWh_{th}/m^3)
Garcia-Rodriguez et al. [63]	Model	PTC-DSG	14	2400	35,000	<100	1.6-4[1]	62.67[2]
Tsilingiris [54]	Model	SP	14	500	40,000	75	~2	75
Caruso et al.[55]	Exp.	SP	4	30	42,000	65	3.04[1]	192
Gerofi et al.[56]	Model	FPC	-	100	35,000	76	4	64.8[3]
El-Nasher and Samad [58]	Exp.	ETC	18	85	55,000	76.5	7-10	50
Platforma Solar de Almeria (PSA) phase I [59–62]	Exp.	PTC	14	72	32,000	70	-	63.33
Sharaf et al.[43]	Model	PTC	16 effects, MED-PF	100	42,000		5.47	42.4
			16 effects, MED-FFH				5.75	46.25
			16 effects, MED-FF				12.87	143.8
			16 effects, MED-BF				7.139	65.2

[1] Reported Data was in Euro. The conversion based on 1 euro = $1.14.
[2] Based on PR of MED = 10 and 24-hour operation with TES, and latent heat at 100 °C = 2256 kJ/kg.
[3] Based on PR of MED = 10 and 24-hour operation with TES, and latent heat at 70 °C = 2333 kJ/kg.

2.3 Solar Assisted MED-TVC

A major development in MED has been promoted by the French company SIDEM that developed a combination of thermal vapor compressor (TVC) with MED. It built several plants in GCC each with a capacity of 6.5 million gallons per day (MIGD) [64]. The major benefit is recovering the lost heat of MED by entraining a small fraction of the vapor formed in the last effect which is at a low temperature and low pressure (<0.1 bar) through TVC and compressing it with motive steam that has a pressure of 3-20 bar. The combination of solar powered MED-TVC is shown in Figure 12.

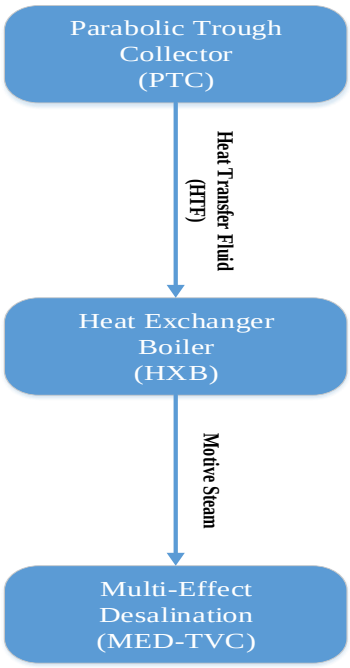

Figure 12 Schematic of solar-MED-TVC.

Parabolic trough collectors powered MED-TVC was tested at the solar thermal desalination project (STDP) in 1987-1994. The system had a capacity of 72 m^3/day and was composed of 14 forward feed multi-effects coupled to one-axis tracking PTC. The entrained vapor temperature was 35°C and the high pressure steam was at 16-26 bar. The thermal performance of MED was

increased from 9.4 to 12 [65]. The calculated specific thermal energy consumption is about 50 kWh_{th}/m^3. Sharaf et al. [66] analyzed parabolic troughs collector coupled with parallel feed MED –TVC composed of 5 effects that had a capacity of 4545 m^3/day. The cost of unit water produced was 1.323 $/$m^3$ and the calculated specific thermal energy consumption was 87.9 kWh_{th}/m^3.

Table 5 shows the specific thermal energy consumption and cost of unit water produced using solar-MED-TVC.

Table 5 Summary of solar assisted MED-TVC.

Author	Model or Exp.	Solar System	Number of Effects	Desalination Capacity (m^3/day)	Salinity of the Feed (ppm)	Motive Steam Temp. (°C)	Cost of Unit Produced ($/$m^3$)	Specific thermal energy Consumption (kWh_{th}/m^3)
Solar thermal desalination project (STDP) in 1987-1994 [65]	Exp.	PTC	14	72	32,000	70	-	50
Sharaf et al. [66]	Model	PTC	5	4545	46,000	60	1.323	87.9

2.4 Solar Assisted MED-MVC

Coupling mechanical vapor compressor with MED is considered more attractive and reliable compared to other heat pumps since it eliminates the down condenser. However MED-TVC plants have been installed with a capacity of more than 22,000 m^3/day while the maximum capacity of MED-MVC is reported at 5,000 m^3/day [67]. The combination of solar-MED-MVC could be driven by PV or solar-heat engine driven compressor as shown in Figure 13.

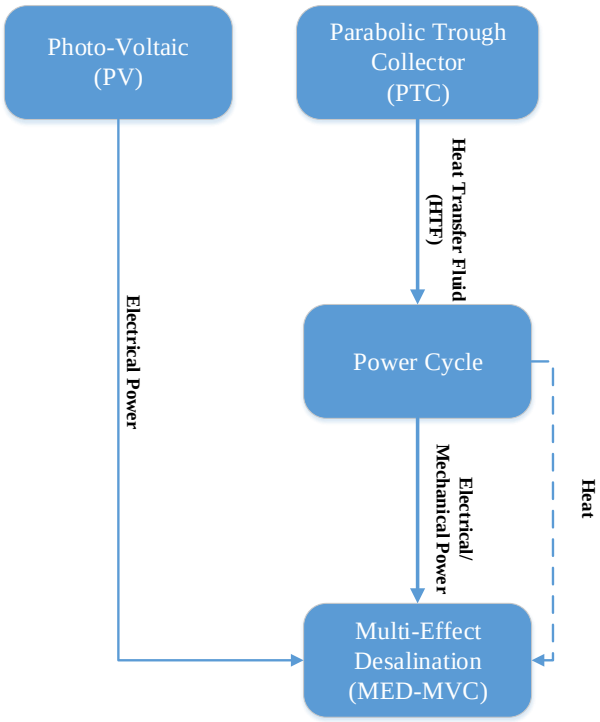

Figure 13 Solar assisted MED-MVC.

Helal and Al-Malik [41] suggested a hybrid PV/diesel powered MED-MVC system with a capacity of 120 m^3/day and a motive steam temperature of 59 °C. The feed was heated by distilled water and the difference between the saturation temperature and motive steam temperature was 4 °C. The specific energy consumption of the system was about 15.3 kWh_e/m^3.

Solar powered regenerative organic Rankine cycle (ORC) driven MED-MVC was studied by Sharaf et al.[66]. The design of PTC was based on LS-3 type and Thermiol-VP1 was used as the HTF providing to the ORC. The ORC was operated at 300 °C and 3.275 MPa, and toluene was used as the working fluid (T_c = 320 °C, P_c= 4.1 MPa). MED-MVC was composed of 16 effects with a motive steam temperature of 60 °C producing 4545 m^3/day. The specific energy consumption was 4.18 kWh_e/m^3 and the cost of unit produced was 0.94 $/$m^3$.

Table 6 shows the specific thermal energy consumption and cost of unit produced for solar-MED-MVC.

2.5 Solar Assisted Non-conventional MED

Decreasing the specific energy consumption and the cost of unit produced is considered the main goal in the desalination market. In co-generation plants, MED or MED-TVC is connected with power plants, as shown in Figure 14, to utilize the rejected heat and reduce the cost. Researchers have tested different power cycles based on the temperature of the heat source.

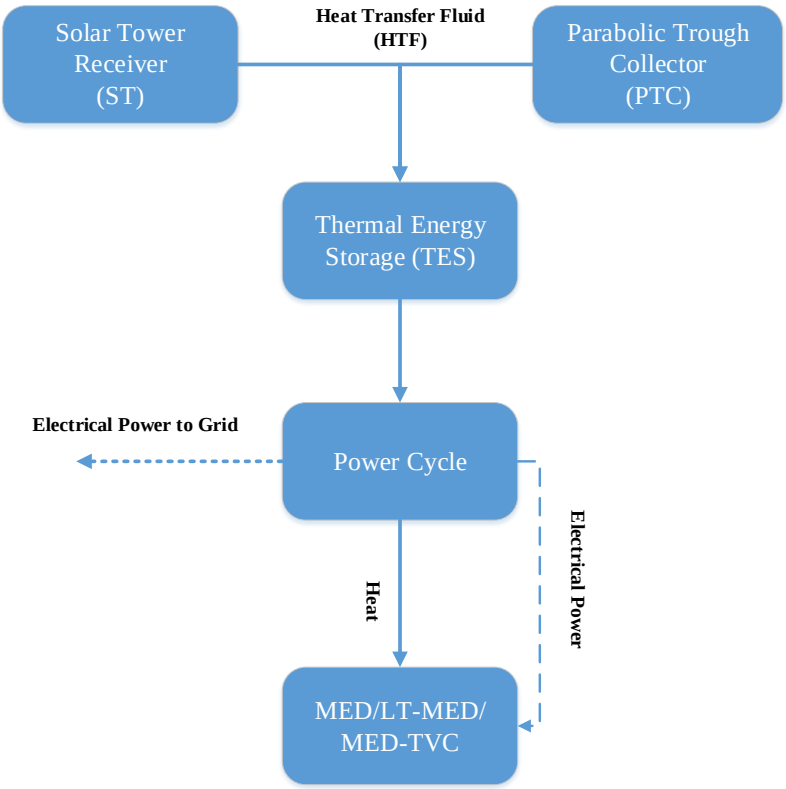

Figure 14 Solar-co-generation plant combination with MED.

Solar steam Rankine cycle (SRC) in the temperature range of 370°C – 700°C was considered in many research studies. Low pressure steam from the turbine exhaust operates the MED/MED-TVC, and the MED becomes the condenser of the Rankine cycle. Palenzuela et al.

[28,29,68] analyzed different configurations for CSP-MED. The steam Rankine cycle proposed operated at 370 °C and 100 bar. Three configurations were analyzed: low pressure steam at 70°C entering the 1st effect of LT-MED as a motive steam, high pressure steam entering TVC as the motive steam in MED-TVC, and low pressure steam entering the TVC as an entrained vapor. The configuration of CSP-LT-MED replacing the condenser had the lowest cost and the overall efficiency was decreased from 24% to 20% when the pressure of motive steam entering TVC was increased from 2 bar to 7 bar.

A solar organic Rankine cycle that could be operated at temperatures less than 300 °C was considered by Sharaf et al. [43] using the 1st effect of LT-MED with different arrangements as a condenser of the ORC where Toluene was used as the working fluid. The specific thermal energy consumption for MED-FFH and MED-PF was 43.7 kWh_{th}/m^3 and 33.7 kWh_{th}/m^3 respectively.

Solar supercritical-CO_2 Brayton cycles that could be operated at high temperatures was considered by Kouta et al. [69]. Two sCO_2 Brayton cycles (regeneration and recompression) powered by solar tower coupled with MED-TVC and thermal energy storage (TES) were analyzed. The incoming feed was preheated by the condenser of the power cycle and the motive steam entering TVC at a pressure of 2.5 bar was heated from TES. The specific cost of unit produced was about 1.2 $\$/m^3$.

Table 7 shows the specific thermal energy consumption and cost of unit water produced for solar-co-generation plants.

Table 6 Summary of solar assisted MED-MVC.

Author	Model or Exp.	Solar System	Number of Effects	Desalination Capacity (m^3/day)	Salinity of the Feed (ppm)	Motive Steam Temp. (°C)	Cost of Unit Produced ($/$m^3$)	Specific thermal energy Consumption (kWh_{th}/m^3)
Helal and Al-Malik [41]	Exp.	PV	1	120	45,000	59	-	~ 45[1]
Sharaf et al.[66]	Model	PTC-ORC	16	4545	46,000	60	0.94	~ 12.54[1]

Table 7 Summary of solar assisted co-generation coupled with MED.

Author	Model or Exp.	Solar System	Desalination System	Power Cycle	Working Fluid	Top Cycle Temp. (°C)	Cost of Unit Produced ($/$m^3$)	Specific thermal energy Consumption (kWh_{th}/m^3)
Palenzuela et al. [28,29,68]	Model	PTC	LT-MED	SRC	Steam	370	~0.8	78.8
			MED-TVC					37
			MED-TVC					37-45
Sharaf et al.[43]	Model	PTC	MED-PF	ORC	Toluene	300	5.057	33.7
			MED-FFH				5.132	43.7
			MED-FF				13.75	143.5
			MED-BF				8.031	71.13
Kouta et al. [69]	Model	ST	MED-TVC	sCO_2 Bryton Recompression	CO_2	450-570	0.9-1.2	-
				sCO_2 Bryton Regeneration				-

[1] Convert from electrical to thermal based on efficiency 33.33%

2.6 Discussions

The cost of unit water produced and specific thermal consumption in solar-MED configuration depends on the type of solar collector that was used and the combination of MED as standalone or assisted by vapor compressor. Other factors that impact the cost and thermal consumption include the salinity, feed arrangement of MED, and temperature of the motive steam.

Since the cost of solar subsystem contributes about 60% to the total cost of unit produced, selection of type solar collector is important. Based on our survey and as shown in Figure 15, solar tower (ST) and parabolic troughs collector (PTC) are the lowest cost (<1$/m^3) compared to other solar types.

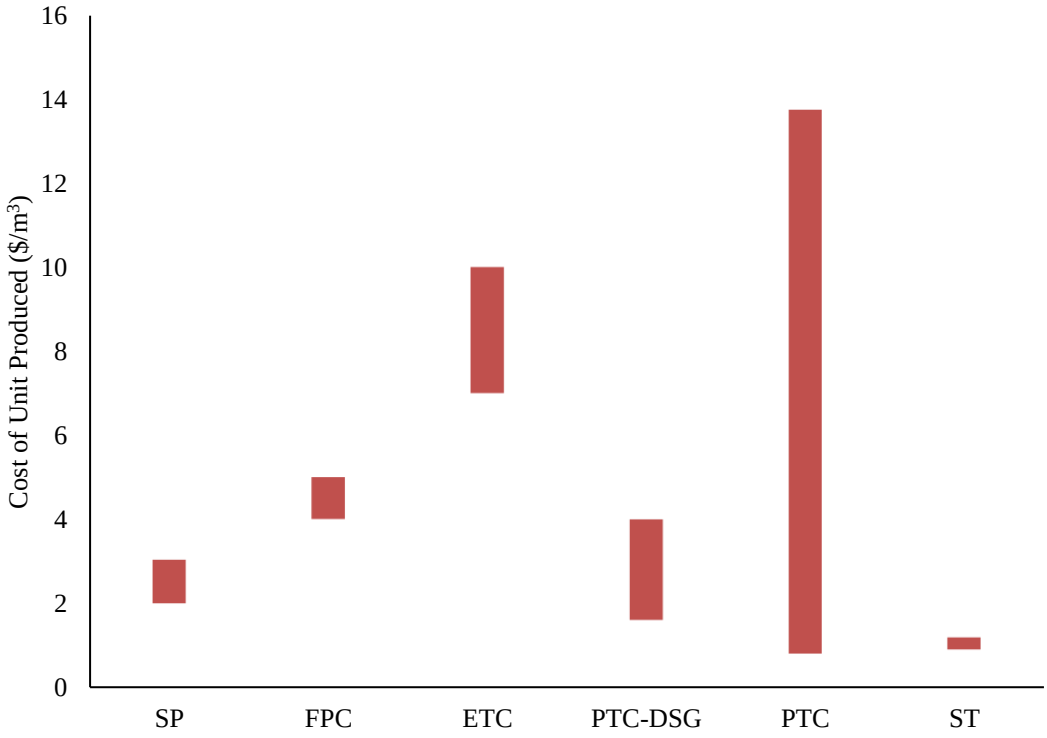

Figure 15 Cost of unit produced based on the type of solar collector used in solar-MED.

The specific thermal energy consumption for each MED depends on the number of effects, and the motive steam temperature. Based on Figure 16, the combination of solar-MED-MVC is the lowest compared with solar-MED and solar-MED-TVC.

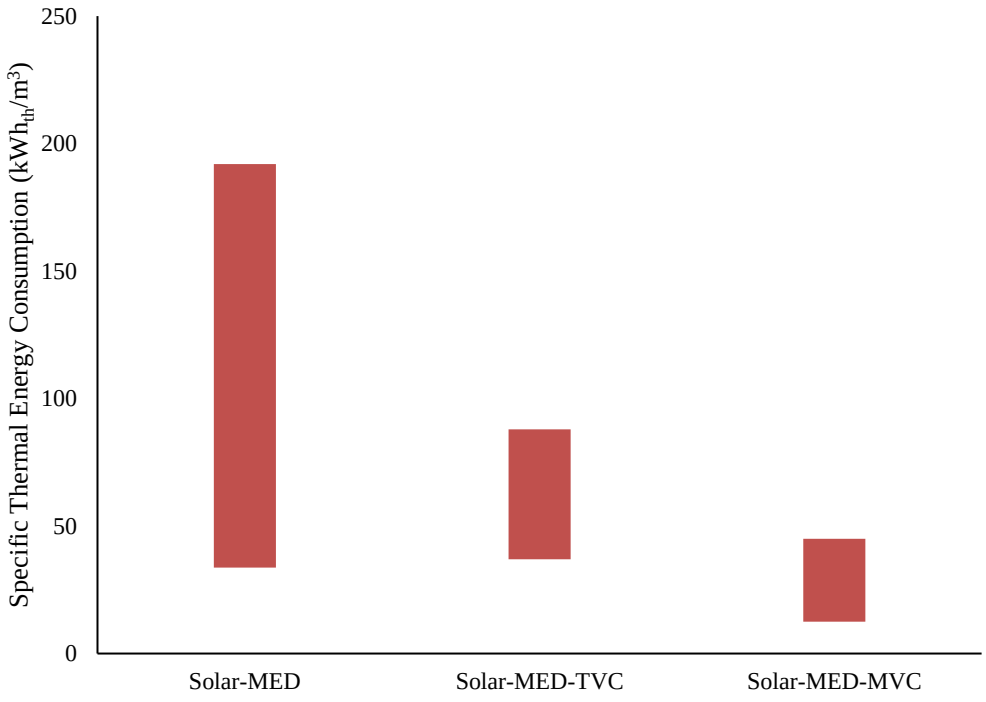

Figure 16 Specific thermal consumption based on MED combination.

The advantage of using co-generation plants is very clear in the cost of unit produced as shown in Figure 17. However, using the MED subsystem as a condenser in the ORC increased the cost of unit produced and specific thermal energy consumption. MED-TVC performance was superior in CSP+D.

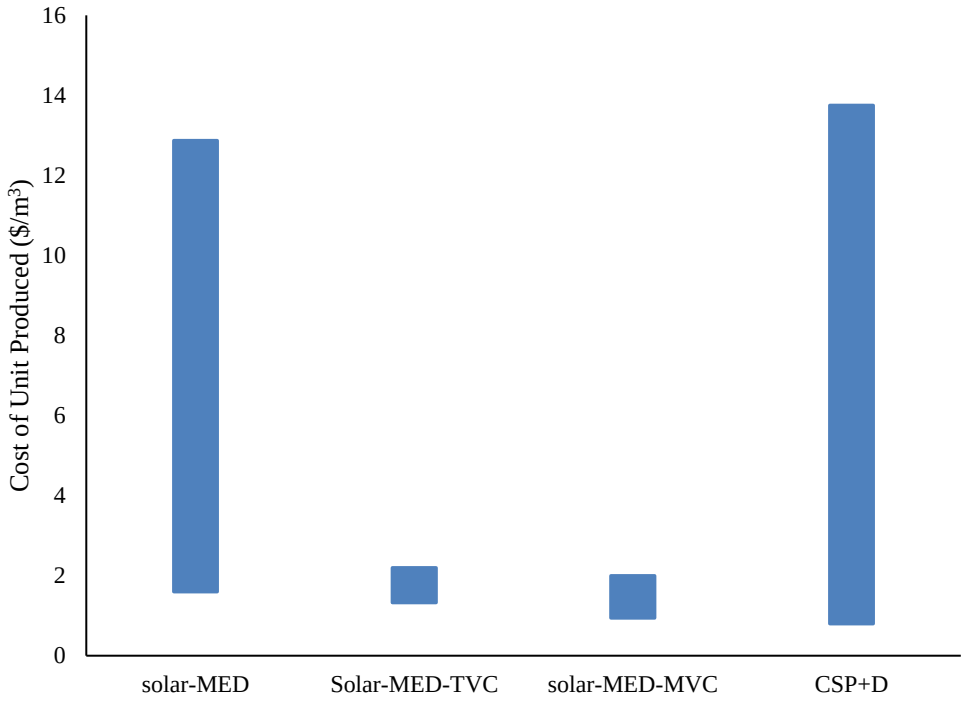

Figure 17 Cost of unit produced based on different system combination.

To give a clearer view of the performance of all of the systems that have been discussed in section 2.2 to 2.5, they have been plotted with respect to specific thermal energy consumption and cost of unit produced. Figure 18 shows that the co-generation solar power plants have the lowest cost of unit produced ($/m3) and Figure 19 shows that PTC-ORC-MED-MVC has the lowest specific thermal energy consumption among solar-MED.

In conclusion, the specific thermal energy consumption and cost of unit produced have varied across different combinations in the literature review that require a fair comparison between solar-MED, solar-MED-TVC and solar-MED-MVC with the same assumptions and variables.

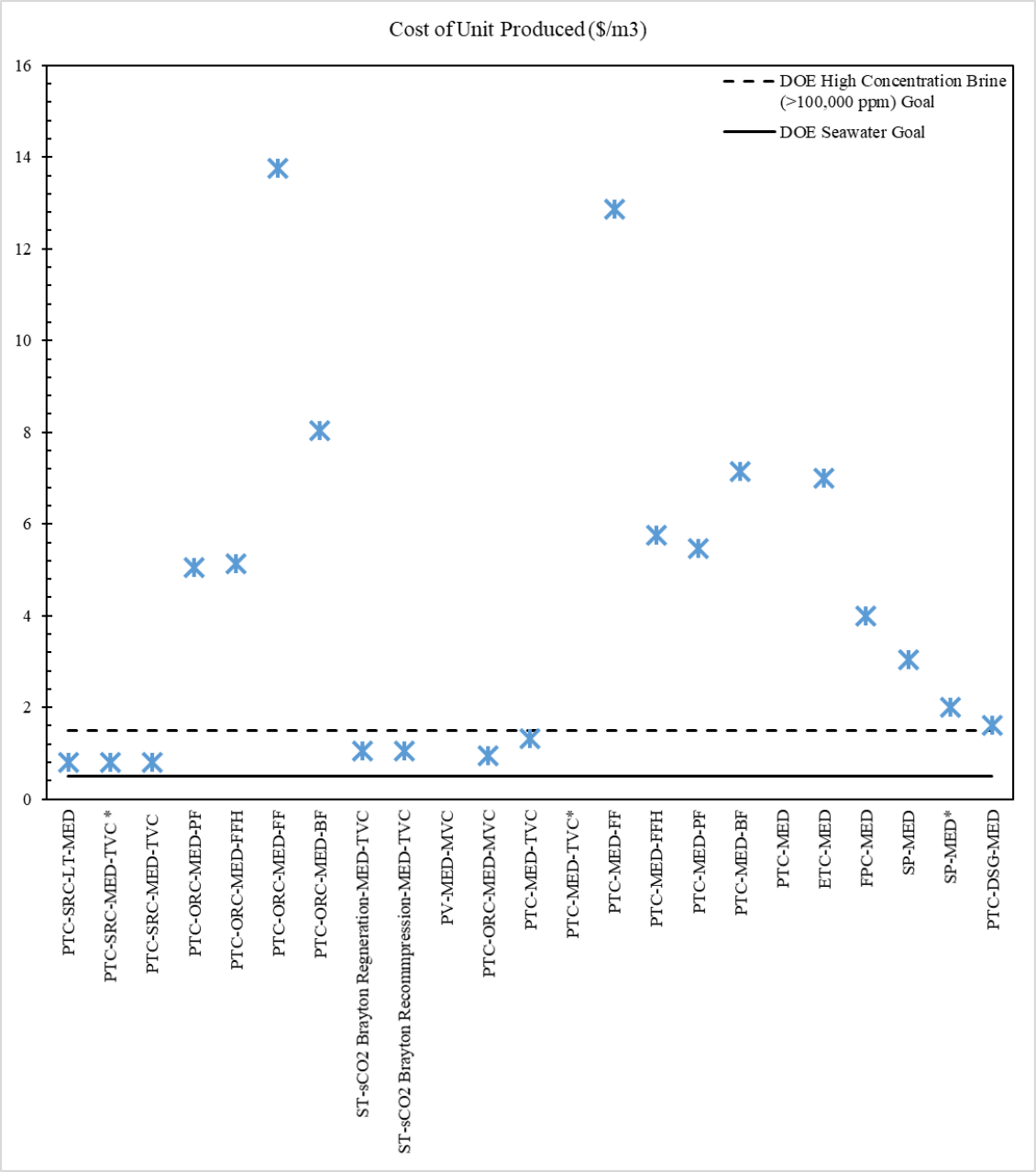

Figure 18 Distribution of specific cost of different solar-MED.

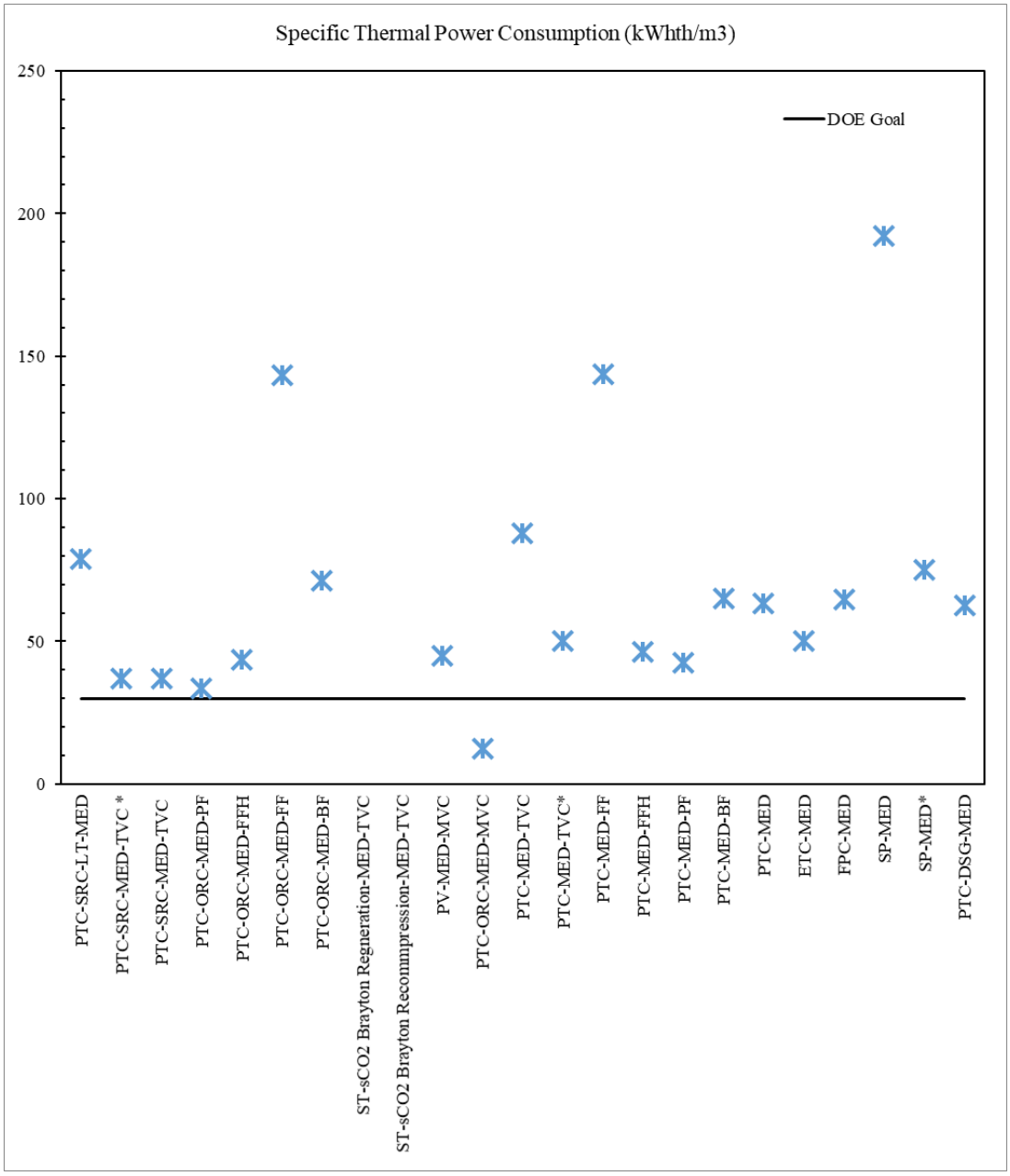

Figure 19 Distribution of specific thermal energy consumption for different solar-MED.

CHAPTER 3: DESIGN OF SOLAR POWERED SUPERCRITICAL ORGANIC RANKINE CYCLE DRIVEN MED-MVC[1]

3.1 Introduction

Use of solar organic Rankine cycle (solar-ORC) in desalination applications has had recent advances in both phase change processes and membrane processes. Solar-ORC powered reverse osmosis (RO) has more attention in recent research. Li et al. proposed a co-generation system including solar parabolic troughs, a supercritical organic Rankine cycle (ORC), and reverse osmosis (RO) desalination [70]. A system efficiency of 21% was achieved when the high temperature of the power cycle was 400°C [70]. Palenzuela et al. studied three co-generation systems: a steam regenerative Rankine cycle at a temperature of 400 °C coupled with RO, a low temperature multiple effect desalination (LT-MED), and an LT-MED coupled with thermal vapor compressor (TVC), or LT-MED-TVC, where the exhaust steam from the high or low pressure turbine was used in the LT-MED. The specific energy consumption for using RO was 5.6 kwh/m^3 as compared to 2.5 kWh/m^3 for LT-MED and LT-MED-TVC [68]. Sharaf et al. analyzed a model coupling multiple effect desalination (MED) with an ORC using solar parabolic troughs and toluene as the working fluid. The system of 16 effects utilized the first effect as the condenser for the ORC. The specific energy consumption was about 11.1 kWh/m^3 for preheated forward feed and parallel feed configurations when the motive steam temperature was set at 88 °C and the

[1] The material in this chapter has been previously published in the following paper: Almatrafi, E., Moloney, F., and Goswami, D. Y., 2017, Multi-Effects Desalination-Mechanical Vapor Compression Powered by Low Temperature Supercritical Organic Rankine Cycle, IMECE 2017: Proceedings of the ASME's International Mechanical Engineering Congress and Exposition (IMECE); 2017 Nov 3-9; Tampa, USA, Volume 6: Energy, ASME, p. V006T08A020

salinity of the feed was 42,000 ppm [43]. Sharaf et al. analyzed a model of an MED system with 16 effects in parallel feed configuration assisted by mechanical vapor compression (MVC) powered by an ORC where the feed was preheated in the condenser of the power cycle. The specific energy consumption was about 4 kWh/m^3, when the motive steam temperature was 60 ^{o}C and the salinity of the feed was 46,000 ppm [66]. For low temperature heat sources at 80 to 170 ^{o}C using solar evacuated tube collectors, geothermal or waste heat, Li et al. presented a model for a combined system to treat high concentration brine by coupling an MED-ejector with a supercritical ORC. The working fluid of the supercritical ORC-ejector condensed in the first effect. The power cycle efficiency was about 5%, the ejector efficiency was 47.5% and the concentration feed was 40,000 ppm for 14 forward feed MED effects. When the salinity of the feed increased to 55,000 ppm, the system consumed all of the work generated by the power cycle [71]. Table 8 has listed some selected solar powered ORC driven desalination systems for low-medium temperature heat sources.

Table 8 Selected solar-ORC powered desalination systems.

Author	Model or Exp.	Solar System	DNI (W/m^2)	Desalination System	ORC Configuration	Working Fluid	Max. Operating Temp. (°C)	Spc. energy Cons. (kW$_h$/m^3)
Delgado-Torres [72,73]	Model	PTC	850	RO	Single	Toluene	380	2.38[1]
Nafey [74]	Model	FPC	850	RO	Single	Butane	100	6.84
		CPC				Hexane	150	7.231
		PTC				Toluene	320	7.679
Beñate [75]	Model	PTC	850	RO	Cascade Upper	MM	350	2.99
					Cascade Bottom	Isopentane	150	
Sharaf [43]	Model	PTC	252	MED-MVC	ORC with Recuperator	Toluene	350	4.18

[1] Calculated based on DNI and efficiency of ORC and fresh water production.

In this chapter, a design of a solar assisted supercritical-ORC driven MED-MVC is presented. The proposed system is composed of four subsystems; solar subsystem which is represented by evacuated tube collectors providing a low temperature heat source, a supercritical ORC subsystem, a low temperature multi effect desalination (LT-MED) subsystem, and a mechanical vapor compressor (MVC) subsystem. The advantage of using a supercritical ORC as opposed to a subcritical ORC is that the heating process does not go through the two phase region, creating a better thermal match in the heat exchanger with less exergy destruction and ultimately a higher cycle efficiency [76]. LT-MED, where the top boiling temperature is less than 90^{o}C, reduces fouling and scaling in the effects common in standard MED systems [77]. MVC has a high efficiency and is more reliable when compared with other vapor compressors [78–80]. The proposed innovative design has the potential to desalinate water of high salt concentrations with low energy consumption and high efficiency when compared with the previously discussed systems. The impact of number of effects of an MED subsystem on the specific energy consumption of the proposed system and the performance of the MED subsystem has been analyzed.

3.2 Methodology

A steady state numerical model was developed in MATLAB to analyze the proposed system. The system has four main components, as shown in Figure 20, which are the solar field, the supercritical ORC, the multi-effect desalination (MED), and the mechanical vapor compressor (MVC). A solar field of evacuated tubes collects the heat used in the power cycle. The supercritical ORC serves two purposes: to run the MVC by the turbine and to heat the feed (M_f) by rejected heat through the condenser. The saturated vapor formed in last effect (M_n) in MED subsystem is mechanically compressed by the MVC subsystem resulting in superheated steam at the same

pressure as in the first effect. Then it mixes with some of the saturated liquid product from the first effect ($M_s - M_n$) to balance the mass flow rate, which has been omitted from Figure 20 for the sake of clarity, and de-superheat the stream before proceeding to the first effect as a motive steam at saturation temperature (T_s). The motive steam passes through the first effect while the preheated feed fluid is sprayed into the first effect at T_f. Some desalinated water from the feed fluid evaporates out using the latent heat condensation of the motive steam (λ_s). The vapor formed in the first effect (M_1) moves to the feed pre-heater to elevate the temperature of the feed by condensing a small amount of the vapor before the second effect to work as the motive steam and heat source at (T_{v1}) which is less than the temperature of the brine by boiling point elevation (BPE) and so on. The brine enters the next effect at a lower pressure, flashing a small amount of vapor, and gains heat from the new motive steam, producing boiling vapor. The produced vapor passes through the feed preheater and acts as motive steam in the next effect. At the last effect, the vapor formed ($\dot{M}_n$) is sent to the MVC to continue the cycle.

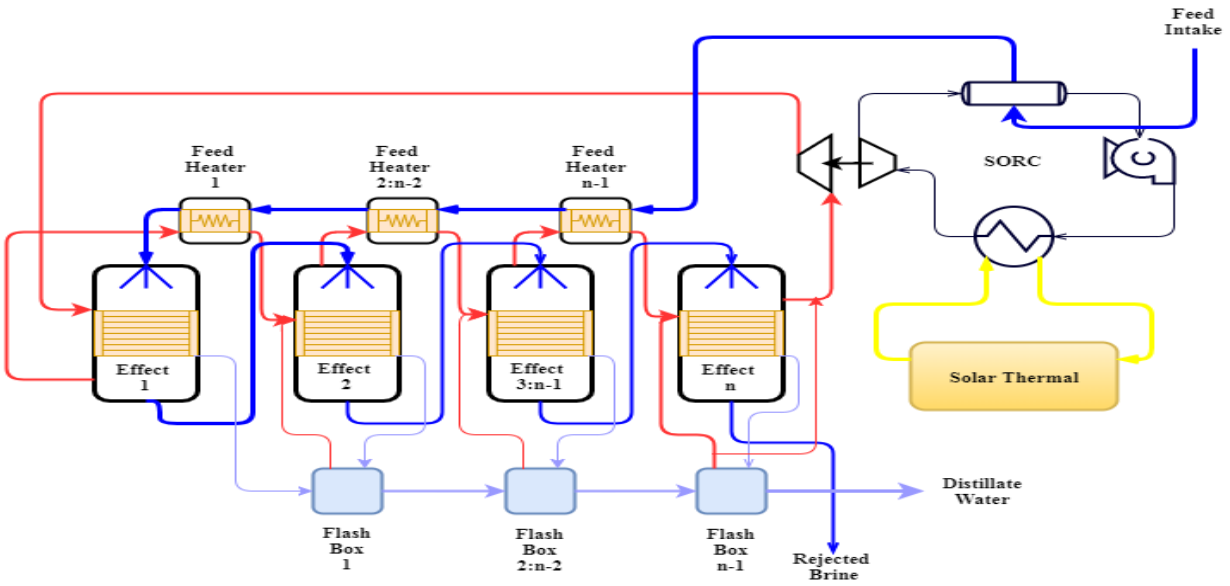

Figure 20 A schematic diagram of the proposed system showing (1) solar subsystem, (2) supercritical-ORC subsystem, (3) MVC subsystem, (4) LT-MED subsystem and different streams HTF (gold), feed (blue), working fluid (black), steam (red) and water (light blue).

3.3 Solar Field

The solar field is the heat source for the proposed system. The maximum temperature is 150°C that enters the heat exchanger of the power cycle and exits at 105°C. The thermal power output from the solar field is the heat input of the cycle divided by the effectiveness of the heat exchanger as shown in (Eq. 1). After specifying the total mass flow rate of the heat transfer fluid (HTF) required to deliver the thermal power and calculating the efficiency of the collector using Eq. 2, the solar area is calculated based on Eq.4. The values used for the solar subsystem are shown in Table 9.

$$\dot{Q}_{Solar} = \frac{\dot{Q}_{in}}{\varepsilon} = \dot{M}_{HTF} * c_{p_{HTF}}(T_{out_{col}} - T_{in_{col}}) \quad (1)$$

$$\eta_{col} = \eta_{optical} - a_1\left(\frac{T_{avg}-T_a}{G}\right) - a_2\left(\frac{(T_{avg}-T_a)^2}{G}\right) \quad (2)$$

$$T_{avg} = \frac{\left(T_{out_{col}}+T_{in_{col}}\right)}{2} \quad (3)$$

$$A_{solar} = \frac{\dot{Q}_{\text{Solar}}}{G * \eta_{col}} \quad (4)$$

Table 9 Preliminary design parameters for solar field subsystem.

Parameter	Value
Solar Subsystem	
Designed solar insolation, G, W/m^2	1000
Ambient temperature, T_a, °C	25
ETC model specifications[81]	
Area of the collector, $A_{collector}$, m^2	3
Designed mass flow rate in a collector, $M_{htf\text{-}c}$, l/min	6
The optical efficiency of solar collector, $\eta_{optical}$	64.4
Heat transmission coefficient, a1	0.89
Heat transmission coefficient, a2,	0.001
Heat transfer fluid (HTF) Tyfocor Ls[82]	
Designed high HTF temperature, T_{out}, °C	150
Designed low HTF temperature, T_{in}, °C	105
Specific heat capacity of HTF at T_{avg}, kJ/kg. °C	3.97[82]

3.4 Supercritical Organic Rankine Cycle

For low-temperature heat sources (below 170°C), using organic fluids in a Rankine cycle as working fluids instead of steam is more economical[83]. Organic Rankine cycles (ORC) have the same processes of a conventional Rankine cycle, however an organic fluid is used. A schematic of a solar-ORC has been shown in Figure 21. The working fluid in the supercritical ORC is R152a which performs well at the proposed temperatures of a supercritical ORC [76]. The temperature-specific entropy diagram of R152a is shown in Figure 22 with the states for a supercritical cycle. R152a has a critical point of 113°C and 4.52 MPa. Heat input from the solar field heats the R152a beyond its critical temperature via the heat exchanger as modeled in Eq. 5. As the condenser is used to heat the feed of the desalination system defined in Eq. 6, the working fluid needs to remain at a higher temperature throughout the condenser to ensure heat transfer. The pinch point in the primary heat exchanger (boiler) was set to 5˚C and 2˚C for the condenser. The effectiveness of the boiler and the condenser was set at 0.95 each, and the design parameters of the supercritical ORC are listed in Table 10. The net power of the cycle is defined as the difference between the turbine

output and the pump input work and equals the total work required by the desalination system for the MVC work and the feed pump work (Eq. 7).

$$\dot{Q}_{in} = \dot{m}_{WF}(h_1 - h_4) = \varepsilon * \dot{M}_{HTF} * c_{p_{HTF}}(T_{out_{col}} - T_{in_{col}}) \quad (5)$$

$$\dot{Q}_{out} = \dot{m}_{WF}(h_2 - h_3) = \varepsilon * \dot{M}_F * c_{p_F}\Delta T_F \quad (6)$$

$$\dot{W}_{net} = \dot{W}_t - \dot{W}_p = \dot{m}_{WF}[(h_2 - h_1) - (h_3 - h_4)] \quad (7)$$

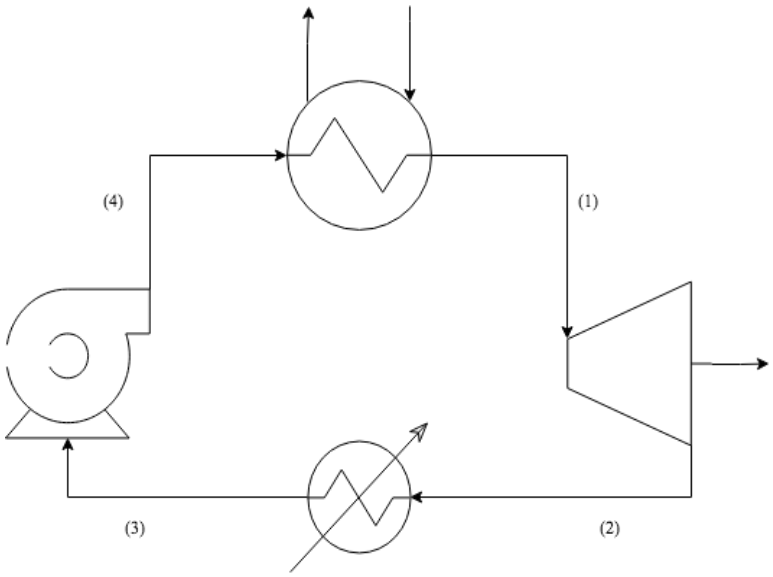

Figure 21 A schematic of ORC cycle.

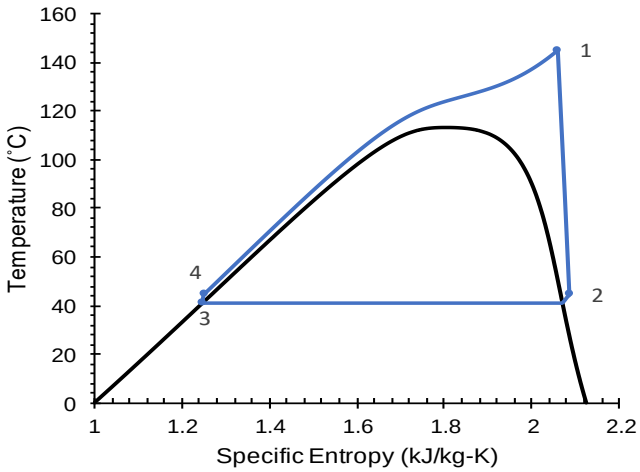

Figure 22 Basic supercritical organic Rankine cycle with R152a T-s diagram.

Table 10 Preliminary design parameters for supercritical-ORC subsystem.

Parameter	Value
Effectiveness of heat exchanger boiler and condenser, %	95
Designed pinch in heat exchanger boiler, °C	5
Designed pinch in the condenser, °C	2
High pressure cycle, P, MPa	5
Efficiency of turbine and pump, %	85
Condensation temperature, T_{cond}, °C	41

3.5 Multi Effect Desalination (MED)

Preheated forward feed LT-MED consists of a series of evaporators, preheaters and flash boxes where the feed and the formed vapor move in the same direction through the effects, as shown in Figure 23. The feed is moving from one effect to another due to the difference in pressure and the vapor is condensed in each effect at a pressure higher than the pressure set in the effect. After compressing the vapor formed in last effect, the fluid has a high temperature and pressure and is known as motive steam. The motive steam entering the first effect condenses and part of the mass of feed that is sprayed and evaporated by the latent heat of the motive steam. Then this vapor will be a motive steam for the following effect. The first effect is further detailed in Figure 24.

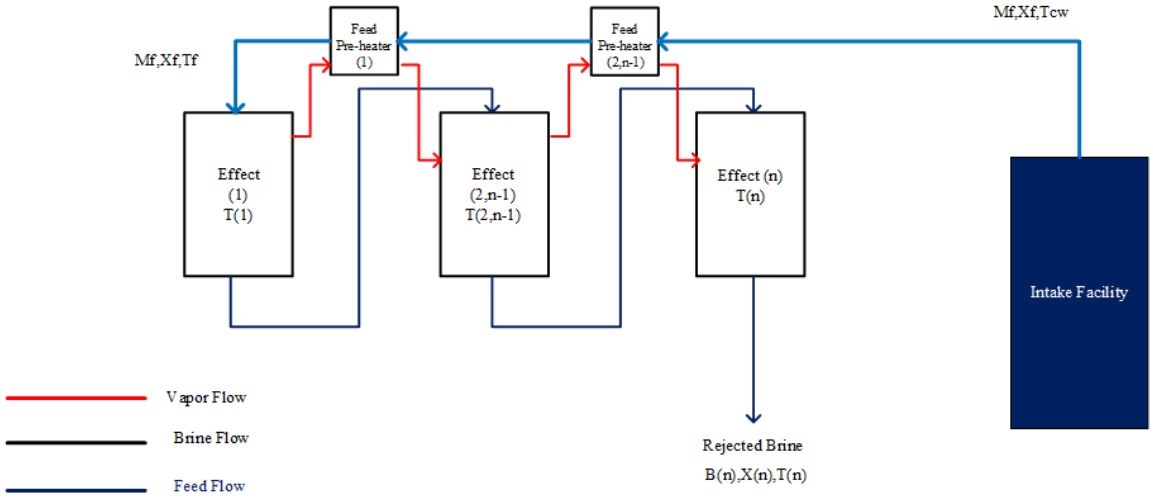

Figure 23 Feed flow arrangement in MED subsystem.

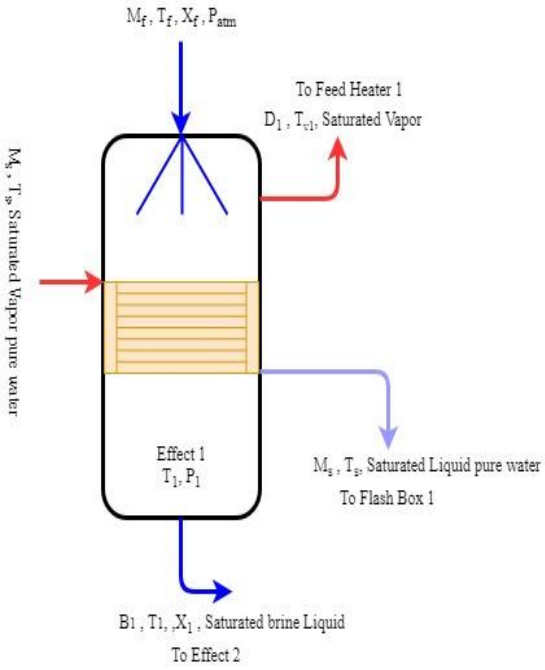

Figure 24 First effect of MED schematic.

Considering the energy balance, mass balance and material balance in the system a detailed model of MED was developed in MATLAB. The preliminary design parameters are shown in Table 11. The following assumptions were used in the model:

- Steady state
- Thermal losses and vapor leaks to the environment are negligible
- The vapor formed in the effects contains no salt
- The effect of demister in pressure drop is negligible
- The brine, feed, and distillate are in the saturated liquid phase in each effect
- No pressure drop in the effects

Table 11 Preliminary design parameters for LT-MED subsystem.

Parameter	Value
LT-MED Subsystem	
Intake seawater temperature, T_{intake}, °C	30
Rejected brine temperature, T_{brine}, °C	40
Motive Steam temperature, T_s, °C	60
Temperature in the last effect, T_n, °C	40
The distillated flow rate, $\dot{m}_d$, kg/s	11.04
Salinity of the intake seawater, X_f, ppm	42,000
Salinity of the rejected brine in last effect, X_n, ppm	84,000
MVC Subsystem	
Efficiency of MVC, η_{MVC}, %	85

3.5.1 Mathematical Model of the Effects

For the 1st effect, the energy, mass and material balance are defined in Eq. 8-10:

$$\dot{m}_s * \lambda_s = \dot{M}_f * c_{p_f} * (T_1 - T_f) + \dot{m}_1 * \lambda_1 \quad (8)$$

$$\dot{M}_f = \dot{m}_1 + B_1 \quad (9)$$

$$\dot{M}_f * X_f = B_1 * X_1 \quad (10)$$

For 2nd– nth effect, the energy, mass and material balance are defined in Eq. 11-13, where i = 2.. n:

$$\dot{Q}_e = \dot{m}_{i-1} * \lambda_{i-1} = \dot{m}_i * \lambda_i \quad (11)$$

$$B_{i-1} = \dot{m}_i + B_i \quad (12)$$

$$B_i * X_i = B_{i-1} * X_{i-1} \quad (13)$$

For MED system, the mass and material balance are defined in Eq. 14-15:

$$\dot{M}_f = \dot{m}_d + B_n \quad (14)$$

$$\dot{M}_f * X_f = B_n * X_n \quad (15)$$

Since the thermal load in each effect is equal, the area of each effect is calculated by Eq. 16, where i= 1 …n:

$$A_1 = A_i = \frac{Q_e}{U_i*(T_{vi}-T_{i+1})} \quad (16)$$

The correlation developed by El-Dessouky et al. was used to calculate the overall heat transfer coefficient for each effect [84] that is defined in Eq.17.

$$U_i = 1.9394 + 1.40562 * 10^{-3} * T_i - 2.0752 * 10^{-4} * T_i^2 + 2.3186 * 10^{-6} * T_i^3 \quad (17)$$

3.5.2 Design Feed Preheater

The main purpose of the feed preheaters (Figure 25) is to increase the temperature of the seawater intake (T_{intake} to T_f), reducing the energy required to deliver in the first effect by the motive steam. In this proposed system, the number of feed preheaters is one less than the number of effects. The feed gains the heat from a part of the vapor formed in previous effects. The vapor flashed in each effect will be condensed in the feed preheater as shown in Eq. 18. The heat balance across one feed preheater is defined as Eq. 19 and the area of feed preheater is illustrated in Eq. 20 where the overall heat transfer coefficient is defined in Eq.21 [85].

$$\dot{m}_{fl} = \frac{(B_n*c_{p_n}*(T_{n-1}-T_n))}{\lambda_i} \quad (18)$$

$$\dot{M}_f * c_{p_f} * \left(T_{f_n} - T_{f_{n-1}}\right) = \dot{m}_{fl} * \lambda_i \tag{19}$$

$$\dot{m}_{fl} * \lambda_i = A_{fh} * U_{fh} * \frac{T_{Mf}^{in} - T_{Mf}^{out}}{\ln \frac{T_{f\_n} - T_{Mf}^{out}}{T_{f\_n} - T_{Mf}^{in}}} \tag{20}$$

$$U_{fh} = 1.6175 + 0.1537 * 10^{-3} * T_i - 0.1825 * {T_i}^2 - 80.26 * 10^{-6} * {T_i}^3 \tag{21}$$

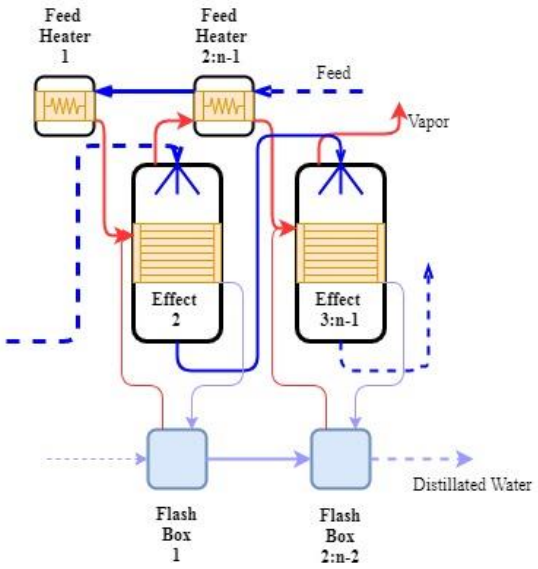

Figure 25 Schematic design of MED with feed preheaters.

The thermophysical properties of the working fluid and pure water such as the enthalpy, latent heat, and entropy were analyzed by REFPROP software that is developed by NIST [86]. The properties of saline water were calculated based on the seawater thermophysical properties library developed by Al-Sharqawi et al.[87,88]. Boiling point elevation (BPE), which represents the difference in the temperature between fresh water and saline water due to salinity, and the constant specific heat of the saline water was calculated accounting for salinity and temperature.

3.6 Mechanical Vapor Compressor (MVC)

The mechanical vapor compression (MVC) is a standalone desalination technology. Combining the MED and MVC increases the thermal performance of the desalination process and makes it suitable for small desalination plants. More than that, it requires less pretreatment process. The MVC assists MED by compressing the vapor formed in the last effect at (T_n) and P_n to the pressure P_s and T_{vs} which is greater than the temperatures of the steam (T_s) as shown in Figure 26. Compressed vapor is entering the first effect of MED subsystem and heating the feed by its latent heat. Small amount of vapor is formed in the first effect as a result of condensation of the motive steam and drives the second effect. The work done by MVC is defined in Eq. 22 where the isentropic constant of the steam (k) is 1.3. Since the steam exits from MVC as superheated, it is de-superheated by mixing a small stream of liquid from the first effect as explained in Figure 27. The energy balance after mixing is defined in Eq.23 and the enthalpy after mixing is defined as saturated vapor at T_s.

$$\dot{W}_{MVC} = \dot{m}_n * \left\{ \frac{\frac{k}{k-1} p_n v_n \left[\left(\frac{p_s}{p_n} \right)^{\frac{k-1}{k}} - 1 \right]}{\eta_{MVC}} \right\} = \dot{m}_n * (h_{ss} - h_{vn}) \quad (22)$$

$$\dot{m}_s * h_{vs} = \dot{m}_n * h_{ss} + (\dot{m}_s - \dot{m}_n) * h_{fs} \quad (23)$$

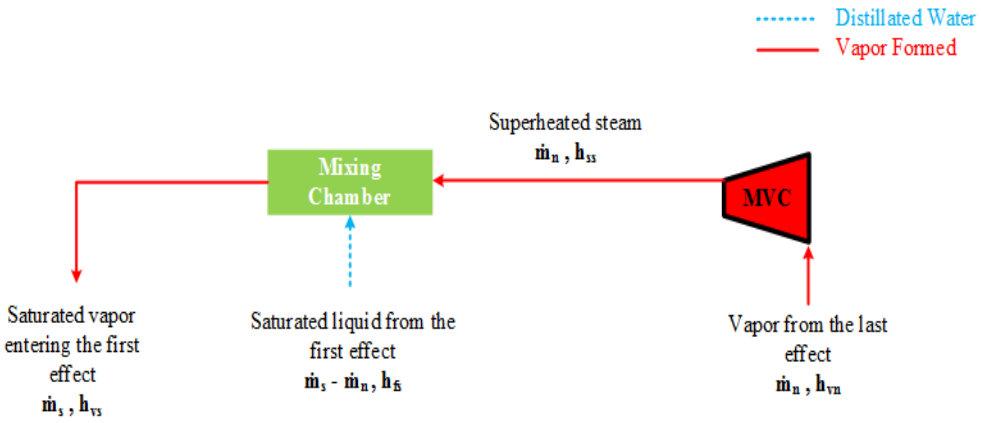

Figure 26 Schematic design of MVC and mixing chamber.

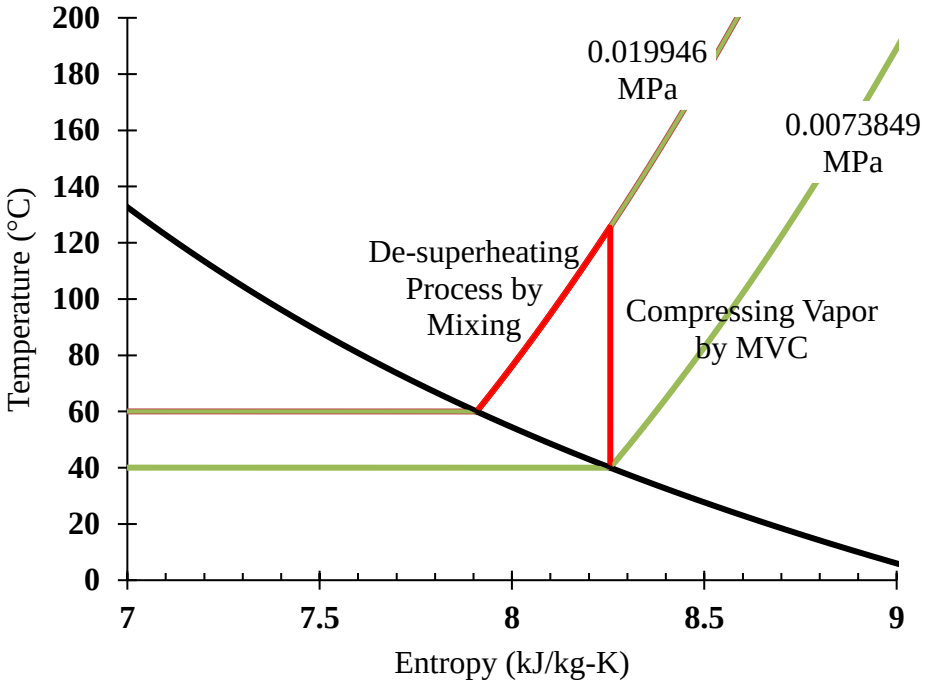

Figure 27 T-s diagram of water in MVC subsystem.

3.7 System Model Validation

Since there is no such system in the literature to compare with, the major subsystems were validated first. The supercritical ORC was validated with the modeled results by Le et al [89]. The MED subsystem was validated with the experimental and modeled data found in the literature. The

experimental data was for a system with 14 effects and motive steam temperature between 57 and 74°C and a final effect vapor temperature of 35°C [90]. The thermal load input, performance and distillated mass flow rate and the results of the model from Li et al. using the Engineering Equation Solver (EES) software are listed in Table 12 [71]. The temperature profile (Figure 28), mass flow rate for the brine (Figure 29) and the brine concentration (Figure 30) were found to be within 3% of the Li's model based on the design parameters shown in Table 13.

Table 12 Model validation with experimental data and Li's model for 14 effect and mass flow for feed 2.22 kg/s.

Motive Steam Temperature (°C)	Performance Ratio	Recovery Rate			Thermal Power Input (kW)			Distillation Product (kg/s)		
		Exp.	Chennan's Model	Model	Exp.	Chennan's Model	Model	Exp.	Chennan's Model	Model
57.00	8.90	0.24	0.24	0.24	137.00	135.60	140.34	0.53	0.53	0.53
60.00	9.10	0.28	0.28	0.27	153.00	153.50	158.39	0.61	0.61	0.61
63.00	9.30	0.30	0.30	0.30	166.00	163.90	168.65	0.67	0.67	0.67
65.00	9.00	0.34	0.34	0.34	191.00	190.50	195.54	0.75	0.75	0.75
68.00	10.00	0.36	0.38	0.36	182.00	184.20	188.52	0.80	0.83	0.81
70.00	9.50	0.36	0.36	0.36	195.00	193.90	198.02	0.80	0.80	0.81
72.00	9.40	0.38	0.38	0.37	203.00	202.70	206.38	0.83	0.83	0.83
74.00	9.30	0.38	0.38	0.37	207.00	204.90	208.14	0.83	0.83	0.83

Table 13 Design parameters used in Li's model.

Parameter	**Value**
Number of effects, n	14
Mass of water production, M_d (kg/s)	0.748
Motive steam Temperature, T_s (°C)	65
Temperature of Vapor in last effect, T_n (°C)	35
The intake seawater temperature, T_{cw} (°C)	25
Feed seawater mass flow rate, m_f, (kg/s)	2.215
Salt concentration of intake seawater, X_{cw} (ppm)	55000
MED performance ratio	9

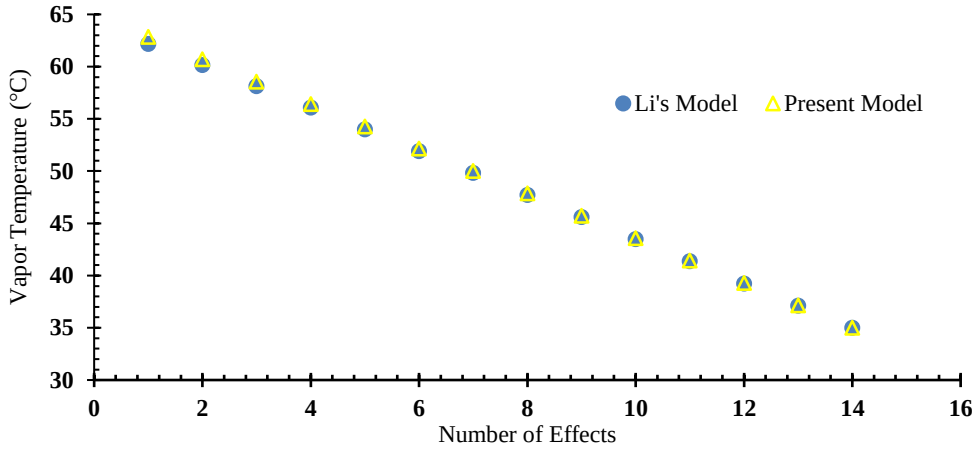

Figure 28 Validation of temperature of vapor in each effect.

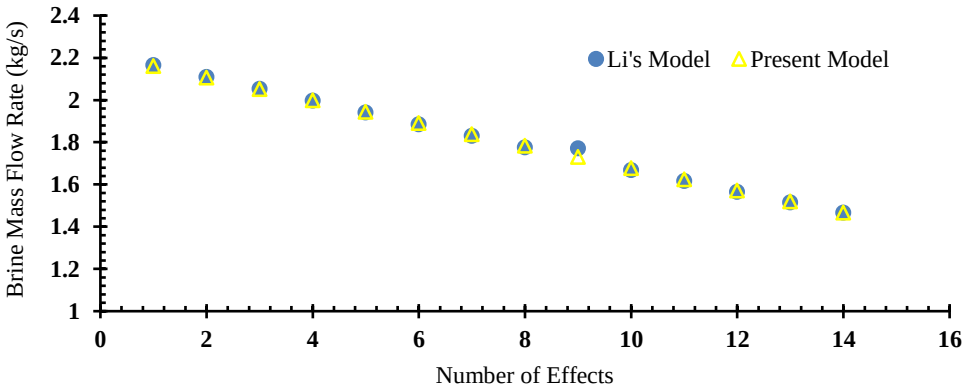

Figure 29 Validation of brine mass flow rate in each effect.

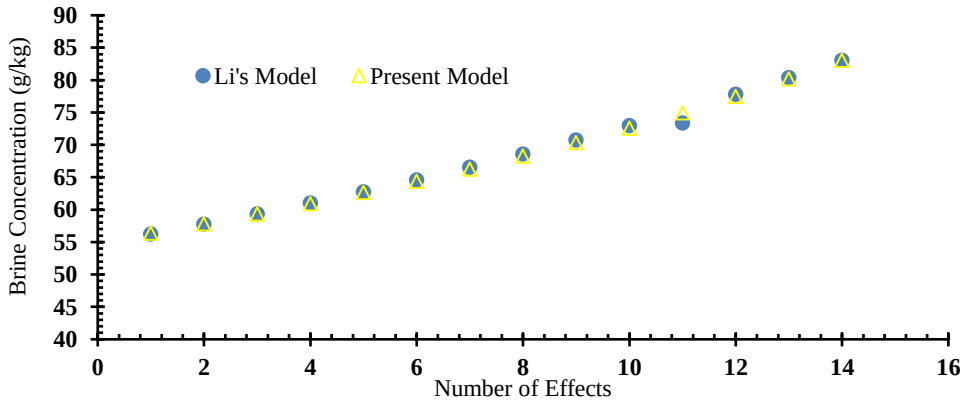

Figure 30 Validation of brine concentration in each effect.

3.8 Performance Parameters

The following parameters were considered in order to evaluate the performance of the proposed system (solar-supercritical ORC-LT-MED-MVC) described above, when the number of effects is increased from 4 to 14.

Performance Ratio (PR) is the ratio of the mass flow rates of distillate water production to motive steam (Eq. 24). The specific energy consumption (w_{spc}), describes the energy delivered by MVC in kWh over the total volumetric production of purified water in one hour (Eq. 25).

$$PR = \frac{\dot{m}_d}{\dot{m}_s} \tag{24}$$

$$w_{spc} = \frac{W_{MVC}}{V_h} \tag{25}$$

3.9 Results and Discussion

The number of effects had a major impact on the performance of the MED subsystem; the performance ratio increased when the number of effects increased, as shown in Figure 31. The performance ratio as defined in Eq. 22 has two factors; mass flow rate of distillated product, and mass flow rate of the motive steam. Since the distillated mass flow rate was held constant in the model, mass flow rate of the motive steam had the main effect on the performance ratio of MED. However, the motive steam mass flow is affected by the temperature and mass flow rate of the vapor formed in the first effect and the preheated feed temperature based on Eq. 8. As a result, as the number of effects increased from 4 to 14, the performance ratio was increased from 3.5 to about 9 as a result of decreasing the mass flow rate of the motive steam from 3.17 kg/s to 1.21 kg/s.

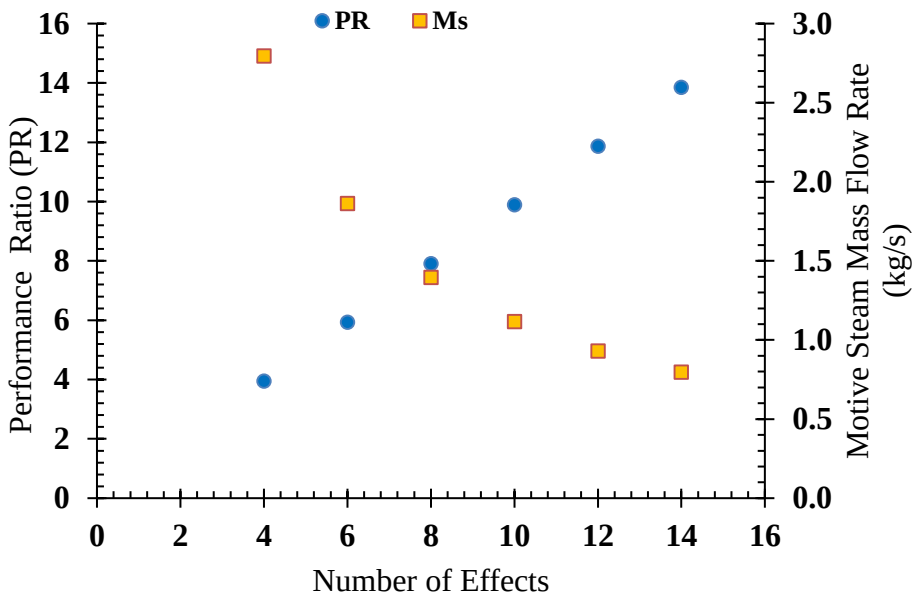

Figure 31 Results for different number of MED effects and performance ratio (PR).

The specific energy consumption decreased by about 250% as shown in Figure 32 when the number of effects was increased from 4 to 14. The mass flow of the vapor formed in the last effect had the largest effect as the temperature of the last effect and the motive steam were held constant. This reduced the mass flow of the motive steam, causing the MVC to perform less work as the number of effects increased.

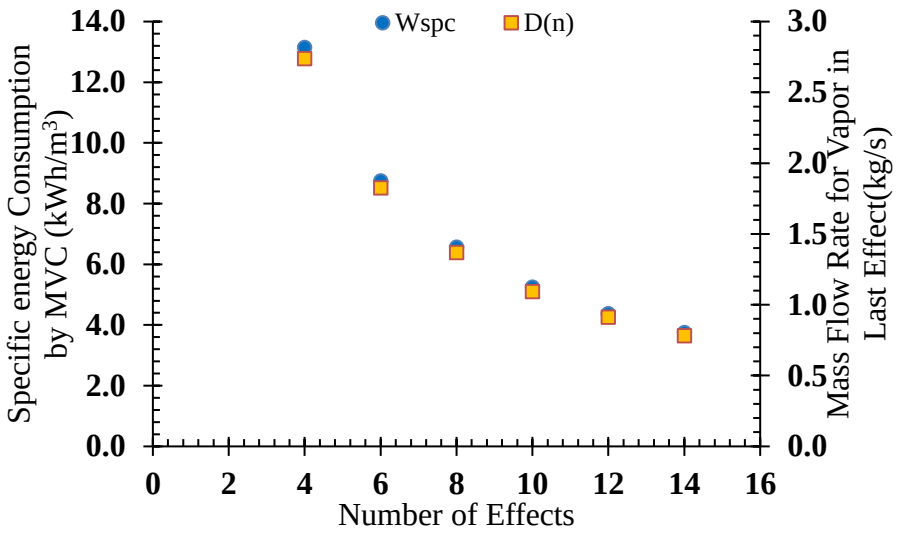

Figure 32 Results for different number of MED effects and specific energy consumption by MVC subsystem.

3.10 Conclusion and Recommendations

In this chapter, an innovative desalination system is proposed and analyzed. This proposed system could be operated as a combined power and desalination system that utilizes a low-grade heat source powered supercritical-ORC drive MED-MVC thermal desalination. Parameters such as performance ratio and specific energy consumption were analyzed for the proposed solar-supercritical ORC-LT-MED-MVC system while increasing the number of effects from 4 to 14. The best performance was found for a system of 14 effects where the system efficiency was about 16% with a performance ratio of MED greater than 9 and a specific energy consumption of 3.9 kWh/m^3. Analysis of other factors such as the salinity of the feed, motive steam temperature, difference temperature of HTF and pressure of ORC cycle for the system, will be discussed in next chapters.

CHAPTER 4: PERFORMANCE ANALYSIS OF SORC ASSISTED LT-MED COUPLED WITH MECHANICAL VAPOR COMPRESSION[1]

4.1 Introduction

In this chapter, the feasibility and performance of a solar-supercritical ORC-LT-MED-MVC are analyzed for the high concentration brine feed (100,000 ppm) in an effort to reduce the energy consumption of a desalination system. The impact of the number of MED effects has been analyzed as a design point on the solar collector area, specific energy consumption by MVC, the efficiency of system, specific thermal energy consumption and the specific area of MED. Also, the impact of varying the motive steam temperature, the pressure of the power cycle and the salinity of the feed has been investigated on the proposed system at 14 effects.

4.2 Methodology

A steady state numerical model was developed in MATLAB to analyze the proposed system. The system has four main components: the solar field, the supercritical ORC, the multi-effect desalination (MED), and the mechanical vapor compressor (MVC). The process description has been introduced in chapter 3 section 3.2. The preliminary design parameters are listed in Table 14.

[1] The material in this chapter has been previously published in the following paper: Almatrafi, E., Moloney, F., and Goswami, D. Y., 2018, Performance Analysis of Solar Thermal Powered Supercritical Organic Rankine Cycle Assisted Low-Temperature Multi Effect Desalination Coupled with Mechanical Vapor Compression, ASME. Paper presented at the ASME Power Conference, Lake Buena Vista, FL, USA

Table 14 Preliminary design parameters for proposed system.

Parameter	Value
Solar Subsystem	
Designed solar insolation, G, W/m^2	1000
Ambient temperature, T_a, °C	25
ETC model ESC V18 specifications[81]	
The optical efficiency of solar collector, η_{op}%	64.2
Heat transmission coefficient, a_1, $W/m^2.K$	0.89
Heat transmission coefficient, a_2, $W/m^2.K^2$	0.001
Area of the collector, $A_{collector}$, m^2	3
Designed mass flow rate in a collector, $M_{htf\text{-}c}$, l/min	6
Heat transfer fluid, HTF Tyfocor Ls[82]	
Designed high HTF temperature, T_{out}, °C	150
Designed low HTF temperature, T_{in}, °C	105
Specific heat capacity of HTF at T_{avg}, kJ/kg.°C[82]	3.97
Supercritical ORC Subsystem	
Effectiveness of heat exchanger boiler and condenser, %	95
Designed pinch in heat exchanger boiler and condenser, °C	5
High pressure cycle, P, MPa	5
Efficiency of turbine and pump, %	85
Condensation temperature, T_{cond}, °C	41
LT-MED Subsystem	
Intake seawater temperature, T_{cw}, °C	30
Rejected brine temperature, T_{br}, °C	40
Motive Steam temperature, T_s, °C	60
Temperature in the last effect, T_n, °C	40
The distillated flow rate, $\dot{m}_d$, kg/s	11.04
Salinity of the intake seawater, X_f, ppm	100,000
Salinity of the rejected brine in last effect, X_n, ppm	200,000
MVC Subsystem	
Efficiency of MVC, η_{MVC}, %	85

Since the feed has a higher salinity than 100,000 ppm, the sea water package library developed by Sharqawi et. al could not be used to determine the properties of the seawater and brine, accounting for salinity and temperature [87,88]. So, the BPE, which represents the difference in temperature between fresh water and saline water due to salinity, and the constant specific heat of the saline water was calculated by Eq. 26 and Eq. 27.

$$BPE = 0.33 * exp(4X), where\ X\ in\ \% \quad (26)$$

$$c_{p_f} = 4.187 * \left(1 - X\left(0.57 - 0.0018(T_{sat} - 20)\right)\right), T_{sat} \text{in } ℃ \quad (27)$$

4.3 Performance Parameters

The following parameters were considered in order to evaluate the performance of the proposed SORC-LT-MED-MVC system when the number of effects is increased from 4 to 16 for the conditions shown in the preliminary tables. Also, the effects of varying the upper pressure of the ORC from 4 MPa to 6 MPa, the salinity of the feed from 50,000 to 120,000 ppm, and the temperature of motive steam for 14 effects were analyzed.

The specific heat transfer area (sA) is described in Eq. 28 as the total area of the effects and feed pre-heater per unit mass of the distillated water production (m^2-s/kg) as defined in chapter 3. The specific energy consumption (w_{spc}), describes the energy consumed by MVC in kWh over the total volumetric production of purified water in one hour (Eq. 29). The solar collector area is defined in Eq. 30. The system efficiency is the net power out of the system over the heat into the system (Eq. 31). The specific thermal energy is the heat delivered by solar system in kWh over the total volumetric production of fresh water in hour (Eq. 32).

$$sA = \frac{\sum_{i=1}^{n} A_i + A_{fh}}{\dot{m}_d} \quad (28)$$

$$W_{spc_{power}} = \frac{W_{MVC}}{V_h} \quad (29)$$

$$A_{solar} = \frac{\dot{Q}_{Solar}}{G * \eta_{col}} \quad (30)$$

$$\eta = \frac{\dot{W}_{net}}{\dot{Q}_{in}} \quad (31)$$

$$W_{spc_{th}} = \frac{Q_{solar}}{V_h} \quad (32)$$

4.4 Results and Discussions

As shown in Figure 33, the number of effects has a large impact on the solar collector area. As the number of effects increased from 4 to 16, the solar collector area decreased by about 75% since the heat required from supercritical-ORC subsystem is decreased due to less work required my MVC subsystem. The total specific thermal energy delivered by the solar field, as defined by Eq. 30, was also decreased by the same percentage, decreasing the size and thereby the costs of the solar field, the heat exchanger boiler, and the pump of the HTF.

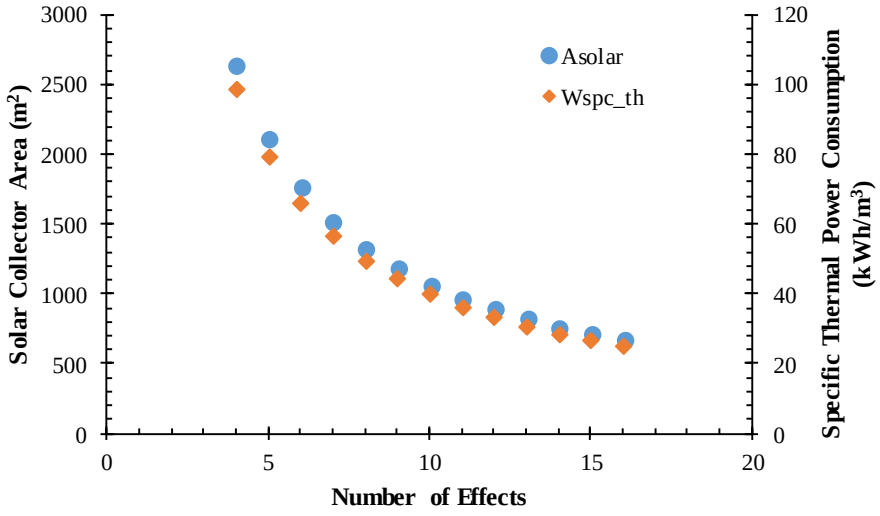

Figure 33 Results for different number of MED effects solar collector area and specific thermal energy consumption

The specific area of the MED system, which is defined in Eq. 26, is related to the number of effects in the system. As shown in Figure 34, the specific area increases from about 165 m^2-s/kg for 4 effects to about 1200 m^2-s/kg for 16 effects. This change is a result of the decreasing temperature difference between the motive steam and the vapor formed in the effect since the thermal load in each effect is considered constant in the model.

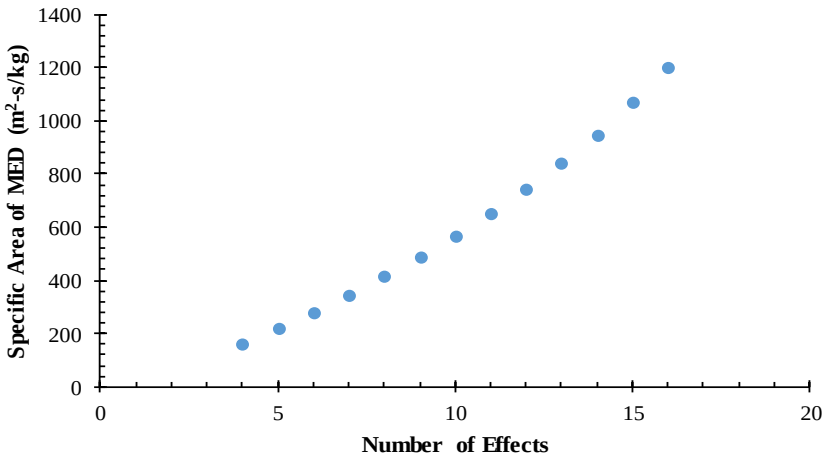

Figure 34 Results for different number of MED effects on specific area of MED subsystem.

The specific energy consumption decreased by about 75% when the number of effects was increased from 4 to 16 as shown in Figure 35. The reduced mass flow of the vapor formed in the last effect, caused the MVC to perform less work as the number of effects increased, where the specific energy consumption is about 3 kWh/m^3 at 16 effects.

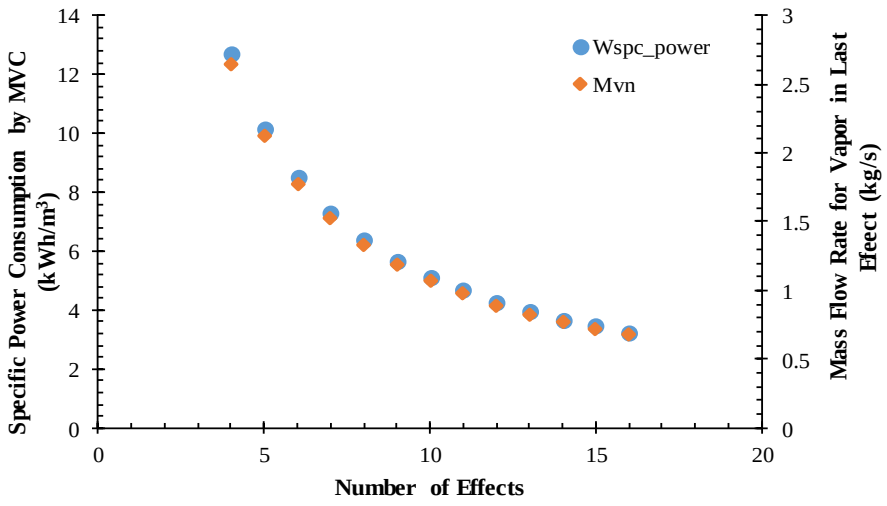

Figure 35 Results for different number of MED effects on specific energy consumption for MVC subsystem.

The number of effects was set to 14 effects and the pressure of the power cycle was varied from 4 MPa to 6 MPa, as shown in Figure 36. Since the critical pressure of R152a is 4.52 MPa, the efficiency increased as the pressure of the cycle increased. In the supercritical region, the efficiency was increased by more than 8%. However, the optimum pressure was about 5.7 MPa and the efficiency, which is defined in Eq.29 is 13.55%. For pressures higher than 5.7 MPa, the increasing work of the pump in ORC was greater than the added work produced in the turbine. As the net power is increased as a result of the increase in the efficiency of the supercritical ORC, the total specific thermal energy, and solar area were decreased by about 9%, reducing the size of the solar system and power cycle as shown as superimposed lines in Figure 36. The pressure of the ORC and subsequently the efficiency of the cycle had no impact on the specific area of the MED and specific energy by MVC.

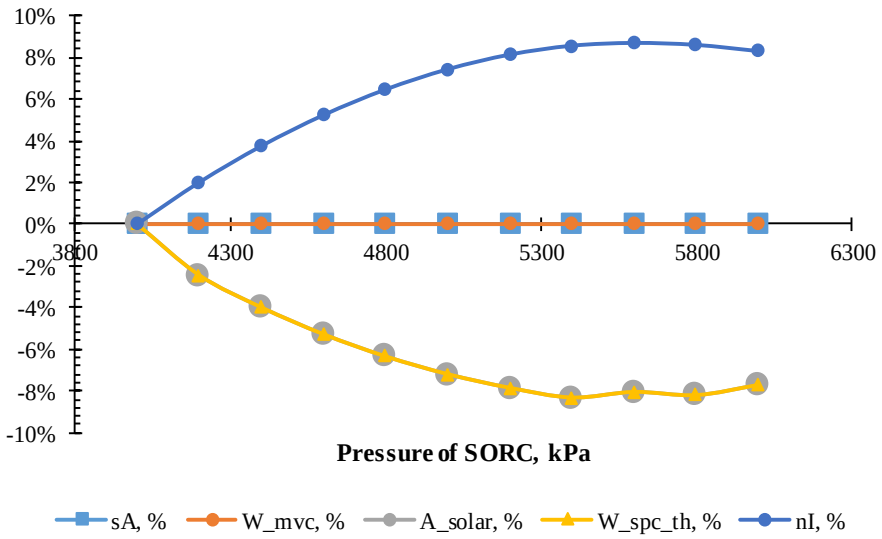

Figure 36 Pressure of ORC vs. performance parameters as a percent difference from the 4 MPa case.

When the salinity of feed changed from 50,000-120,000 ppm, the only impact was on the specific area of MED system which increased by about 25% as illustrated in Figure 37. That

increase was a result of increasing the boiling point elevation (BPE) in Eq. 24, which decreased the temperature difference in each effect, requiring more area to process the heat transfer. The salinity has no effect on the other parameters such as the specific energy consumption as shown in Figure 37. In contrast, modeling RO in ROSA software that was developed by DOW water and process solutions studying the effect of increasing the salinity of the feed on the performance of RO. The results show the specific energy consumption is increased by more than 250% when the salinity feed is increased to 100,000 ppm as shown in Figure 38. That means RO is more sensitive to the salinity of the feed from energy point than the proposed system.

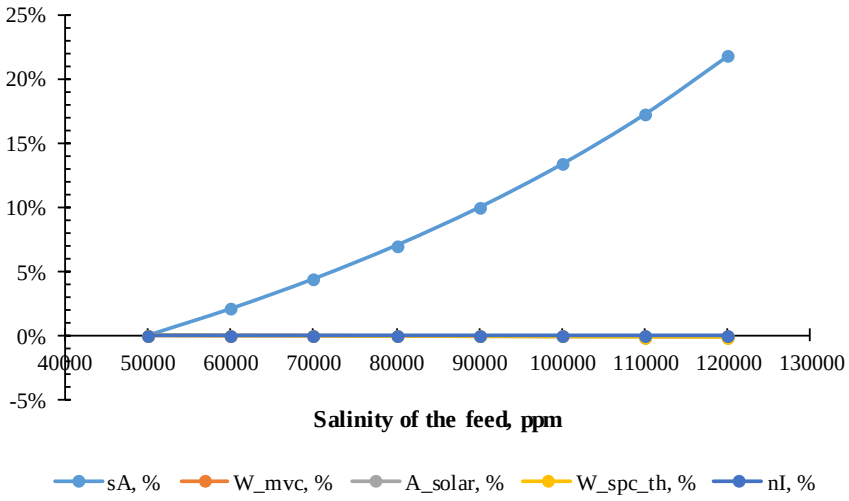

Figure 37 Salinity of the feed vs. performance parameters as a percent difference from the 50,000 ppm case.

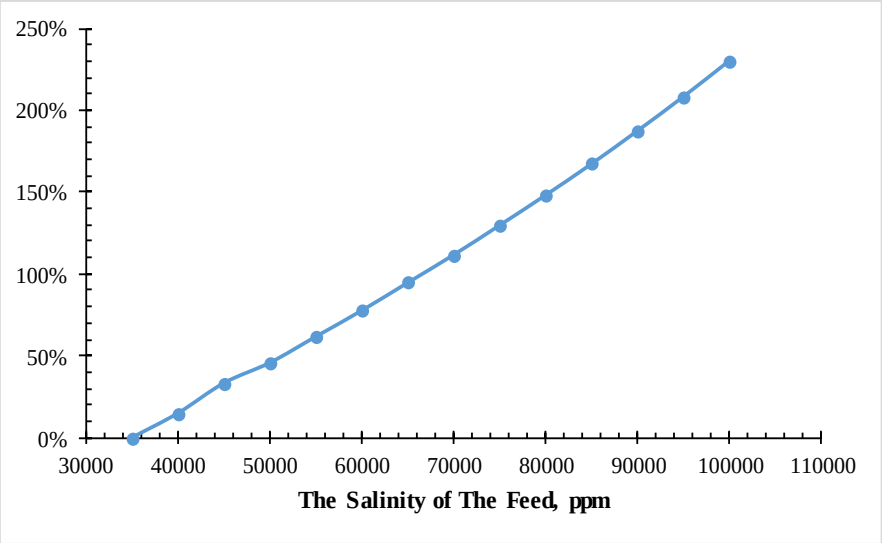

Figure 38 Salinity of the feed vs. specific energy consumption for RO.

Varying the motive steam temperature from 58°C to 72°C by increasing the work of MVC that defined in Eq.27, representing a LT-MED (<90°C) system, had an impact on the specific area of the MED system, the specific thermal energy consumption, the specific energy consumption by MVC, and the solar field area as presented in Figure 39. It had no impact on the efficiency of the system. The specific area of the MED decreased by almost 60% due to increasing the difference in temperature of the effect. However, the solar field area, specific thermal energy consumption and specific energy consumption by the MVC were increased by about 80% due to increasing the compression ratio which increased the power required by the MVC.

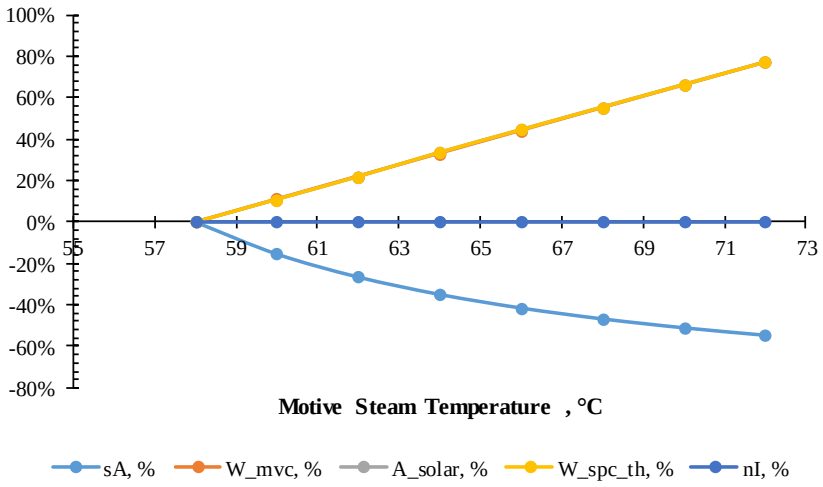

Figure 39 Motive steam temperature vs. performance parameters as a percent difference from the motive steam temperature of 58°C case.

4.5 Conclusion and Recommendations

In this chapter, parameters such as the solar collector area, specific area of MED, specific energy consumption, specific thermal energy consumption and system efficiency were analyzed for the proposed solar-supercritical ORC-LT-MED-MVC system while increasing the number of effects from 4 to 14. Also, the impact of varying of the salinity of feed, motive steam temperature and pressure of ORC have been investigated on 14 effects. The best performance was found for a system of 14 effects where the system efficiency was about 13.55% with a specific energy consumption of 3.6 kWh/m^3. Exergy analysis for the system, will be discussed in following chapter.

CHAPTER 5: EXERGY ANALYSIS OF SOLAR POWERED SUPERCRITICAL ORGANIC RANKINE CYCLE ASSISTED MULTI-EFFECT DESALINATION COUPLED WITH MECHANICAL VAPOR COMPRESSOR[1]

5.1 Introduction

Based on our own literature survey, no system has been investigated that uses supercritical ORC powered MED-MVC for low and medium temperature heat sources. The advantage of using a supercritical ORC as opposed to a subcritical ORC is that the heating process does not go through the two phase region, creating a better thermal match in the heat exchanger with less exergy destruction and ultimately a higher cycle efficiency for wet organic fluids. Due to the availability of low and medium temperature heat sources such as waste heat, solar or geothermal source, we have proposed a MED-MVC desalination powered by supercritical-ORC.

In this chapter, an exergy analysis is presented for a novel system that couples a solar energy system and a supercritical organic Rankine cycle with low-temperature multi-effect desalination assisted by mechanical vapor compressor (solar-supercritical ORC-LT-MED-MVC) for the treatment of high salinity concentration feed. The effect of the motive steam temperature, pressure of the power cycle, the salinity of feed, and the number of effects on the exergy destruction are analyzed.

[1] The material in this chapter has been previously published in the following paper: Almatrafi, E., Moloney, F., and Goswami, D. Y., (2018). Exergy Analysis of Solar Powered Supercritical Organic Rankine Cycle Assisted Multi-Effect Desalination Coupled with Mechanical Vapor Compressor. In U. do M. D. de E. Mecânica (Ed.), Proceedings of ECOS 2018 - The 31st International Conference on Efficiency, Cost, Optimization, Simulation and Environmental Impact of Energy Systems (pp. 1–12). Guimarães. ISBN: 978-972-99596-4-6

5.2 Methodology

The innovative desalination system design, as shown in Figure 20, is composed of the following components:

- Evacuated solar tube collectors supplies the heat source of the proposed system
- A supercritical organic Rankine cycle (supercritical ORC) with R152a as the working fluid, where the working fluid is compressed by the pump to a supercritical pressure and is heated by the heat exchanger boiler to a supercritical temperature
- A mechanical vapor compressor (MVC) that compresses the vapor formed in last effect of the MED subsystem
- Low temperature multi effect desalination (LT-MED), which is a series of evaporators, feed pre-heaters and flash boxes where the temperature of the motive steam entering the first effect is less than 90°C.

A numerical model was created in MATLAB for the proposed desalination system and its four main components. The solar heat absorbed by the evacuated tube collector subsystem is transferred by the HTF to the supercritical ORC via the heat exchanger boiler (HXB) as represented in Figure 20 as the process 1-2. The maximum temperature of the heat transfer fluid (HTF) was 150 °C. The supercritical ORC serves two purposes: to produce work to run the MVC subsystem and to heat the feed ($\dot{M}_{HTF}$) entering the first effect of MED.

The vapor formed in the last effect of MED subsystem ($\dot{M}_{v_n}$) is mechanically compressed by the MVC subsystem to pressurize the motive steam and raise its temperature. The motive steam at saturation temperature (T_s) is then passed through the first effect while the preheated feed fluid is sprayed into the first effect. The processes of condensation and vaporization continue through the effects in the MED subsystem producing the required product of fresh water ($\dot{M}_D$). At the last

effect, the vapor formed ($\dot{M}_{v_n}$) is sent to the MVC subsystem to continue the cycle and the brine ($\dot{M}_B$) is removed.

5.3 Exergy Analysis for Solar-supercritical ORC-MVC-LT-MED System

Exergy analysis is a powerful tool that combines the mass and energy conservation with the second law of thermodynamics to design a system that operates at the optimum performance. Whereas the energy for any system is conserved based on the first law of thermodynamics, the exergy is not. Exergy, or the useful energy, can be destroyed through a process. Therefore, quantifying the exergy loss has a valuable meaning in economics to minimize the losses or manage them.

An exergy analysis considers the mass, work and heat inputs and outputs of a specified system. For a steady state system control volume, the exergy balance equation and exergy efficiency are defined as:

$$\Sigma \dot{E}_{x_{in}} - \Sigma \dot{E}_{x_{out}} = \dot{E}_{x_d} \tag{33}$$

$$\eta_{ex} = \frac{\Sigma \dot{E}_{x_{out}}}{\Sigma \dot{E}_{x_{in}}} = 1 - \frac{\Sigma \dot{E}_{x_d}}{\Sigma \dot{E}_{x_{in}}} \tag{34}$$

For the solar-supercritical ORC-MVC-LT-MED system, there are four subsystems and five streams which are the heat transfer fluid (HTF), working fluid (WF), feed saline water (F), rejected brine (B), and distillate product (D).

5.3.1 Exergy Analysis for the Solar Subsystem

The exergy efficiency for solar thermal collectors is low as the solar radiation is not completely absorbed by the solar collectors and the energy losses from the surface of the collectors. Petela performed extensive exergy studies of thermal radiation for solar power utilization and proposed an expression representing the maximum relative potential of available solar radiation

energy [91–93]. This term, which is known as the exergy efficiency term and calculated in (Eq.35), is based on the relation of the temperature of the sun, which is calculated in [94] as 5760 K, and the temperature of the environment in Kelvin. Multiplying the solar radiation by the exergy efficiency term and the total area of collectors represent the exergy of the solar energy as Eq.36. The area of the collectors needed to provide the heat input to the supercritical ORC, is calculated using equation Eq.39 which uses the efficiency of the collectors as shown in Eq.37. The exergy destruction of the solar field is calculated in Eq.41 and the exergy efficiency in Eq.42. All parameters of the solar subsystem and reference temperature are listed in Table 15.

$$\Psi = [\,1 + \left(\frac{1}{3}\right)\left(\frac{T_a}{T_{sun}}\right)^4 - \left(\frac{4}{3}\right)\left(\frac{T_a}{T_{sun}}\right)\,] \tag{35}$$

$$\dot{E}_{x_{sun}} = G * A_{solar} * \left[\,1 + \left(\frac{1}{3}\right)\left(\frac{T_a}{T_{sun}}\right)^4 - \left(\frac{4}{3}\right)\left(\frac{T_a}{T_{sun}}\right)\,\right] \tag{36}$$

$$\eta_{collector} = \eta_{optical} - a_1\left(\frac{T_{avg}-T_a}{G}\right) - a_2\left(\frac{(T_{avg}-T_a)^2}{G}\right) \tag{37}$$

$$T_{avg} = \frac{\left(T_{out_{col}}+T_{in_{col}}\right)}{2} \tag{38}$$

$$A_{solar} = \frac{\dot{Q}_{in_{SORC}}}{G*\varepsilon*\eta_{col}} \tag{39}$$

$$\dot{Q}_{in_{SORC}} = \varepsilon * \dot{M}_{HTF} * c_{p_{HTF}}\left(T_{out_{col}} - T_{in_{col}}\right) \tag{40}$$

$$\dot{E}_{x_{d_{solar}}} = \dot{E}_{x_{sun}} - \dot{M}_{HTF} * c_{p_{HTF}}(T_{out_{col}} - T_{in_{col}} - T_a * \ln\frac{T_{out_{col}}}{T_{in_{col}}}) \tag{41}$$

$$\eta_{II_{solar}} = \frac{\dot{E}_{x_{out}}}{\dot{E}_{x_{sun}}} = \frac{\dot{M}_{HTF}*c_{p_{HTF}}(T_{out_{col}}-T_{in_{col}}- T_a*\ln\frac{T_{out_{col}}}{T_{in_{col}}})}{\dot{E}_{x_{sun}}} = 1 - \frac{\dot{E}_{x_{d_{solar}}}}{\dot{E}_{x_{sun}}} \tag{42}$$

Table 15 Preliminary design parameters for solar field subsystem.

Parameter	Value
Solar Subsystem	
Designed solar insolation, G, W/m^2	1000
Ambient temperature, T_a, ^{o}C	30
Temperature of the sun, K	5760
ETC model ESC V18 specifications	
Area of the collector, $A_{collector}$, m^2	3
The optical efficiency of solar collector, $\eta_{optical}$%	64.2
Heat transmission coefficient, a_1, W/m^2.K	0.89
Heat transmission coefficient, a_2, W/m^2.K^2	0.001
Heat transfer fluid, HTF Tyfocor Ls	
Designed high HTF temperature, $T_{out_{col}}$, ^{o}C	150
Specific heat capacity of HTF at T_{avg}, kJ/kg.K	3.97

5.3.2 Exergy Analysis for Supercritical-ORC Subsystem

While the role of the solar subsystem is to deliver the heat required to run the supercritical-ORC subsystem, the two main roles of the supercritical-ORC subsystem are to provide the work required by the MVC subsystem through the turbine and pre-heating the feed that enters the first effect in the MED subsystem through the condenser. This role requires more attention since it's interlacing the main three streams in the proposed system, which are heat transfer fluid, working fluid and feed. Thus, a detailed exergy analysis for each component in supercritical-ORC subsystem is presented in Eq. 43-46 and the exergy destruction in Eq.47. The properties of the three streams, the dead states and the preliminary design of the supercritical-ORC subsystem are listed in Table 16.

$$\dot{E}_{x_{d_{HXB}}} = \dot{M}_{HTF} c_{p_{HTF}} \left(T_{out_{col}} - T_{in_{col}} - T_a \ln \frac{T_{out_{col}}}{T_{in_{col}}} \right) + \dot{M}_{WF} (\Delta h_{3-4} - T_a \Delta s_{3-4}) \quad (43)$$

$$\dot{E}_{x_{d_{TURBINE}}} = \dot{M}_{WF} (\Delta h_{4-5} - T_a \Delta s_{4-5}) - \dot{W}_{TURBINE} = \dot{M}_{WF} * T_a \Delta s_{5-4} \quad (44)$$

$$\dot{E}_{x_{d_{CONDENSOR}}} = \dot{M}_{WF} (\Delta h_{5-6} - T_a \Delta s_{5-6}) + \dot{M}_F \left(\psi_{F_{in}} - \psi_{F_{out}} \right) \quad (45)$$

$$\dot{E}_{x_{d_{PUMP}}} = \dot{M}_{WF} (\Delta h_{6-3} - T_a \Delta s_{6-3}) + \dot{W}_{PUMP} = \dot{M}_{WF} * T_a \Delta s_{3-6} \quad (46)$$

$$\dot{E}_{x_{d_{SORC}}} = \dot{E}_{x_{d_{HXB}}} + \dot{E}_{x_{d_{TURBINE}}} + \dot{E}_{x_{d_{CONDENSOR}}} + \dot{E}_{x_{d_{PUMP}}} \quad (47)$$

$$\eta_{II_{SORC}} = \frac{\dot{E}_{x_{out}}}{\dot{E}_{x_{in_{SORC}}}} = 1 - \frac{\dot{E}_{x_{d_{SORC}}}}{\dot{E}_{x_{in_{SORC}}}} \quad (48)$$

$$\dot{E}_{x_{in_{SORC}}} = \dot{M}_{HTF} c_{p_{HTF}} \left(T_{out_{col}} - T_{in_{col}} - T_a \ln \frac{T_{out_{col}}}{T_{in_{col}}} \right) \quad (49)$$

Table 16 Preliminary design parameters for supercritical- ORC subsystem.

Parameter	Value
Effectiveness of heat exchanger boiler and condenser, ε, %	95
Designed pinch in heat exchanger boiler, °C	5
Designed pinch in the condenser, °C	4
Efficiency of turbine and pump, %	85
Condensation temperature, T_{cond}, °C	41
Temperature of the feed intake, T_{intake}, °C	30
Salinity reference of the feed, X_o, ppm	42,000

5.3.3 Exergy Analysis for MVC Subsystem

The turbine output work is used to drive the MVC subsystem to compress the saturated vapor formed in the last effect of the MED subsystem. The exergy destruction for this process is described in Eq.50 and the exergy efficiency in Eq.51. Using MVC subsystem avoids major exergy destruction in MED technology by eliminating the down condenser which contributes the most to exergy destruction though it reclaims the waste heat from the vapor formed. The MVC subsystem has one stream which is the saturated vapor entering at low pressure (P_n) and exiting at pressure (P_s), the saturation pressure of the design motive steam temperature (T_s). The properties of the MVC subsystem are listed in Table 17.

$$\dot{E}_{x_{d_{MVC}}} = \dot{M}_{v_n}(\Delta h_{11-12} - T_a \Delta s_{11-12}) + \dot{W}_{MVC} = \dot{M}_{v_n} T_a \Delta s_{12-11} \quad (50)$$

$$\eta_{II_{MVC}} = \frac{\dot{E}_{x_{out}}}{\dot{E}_{x_{in_{MVC}}}} = 1 - \frac{\dot{E}_{x_{d_{MVC}}}}{\dot{E}_{x_{in_{MVC}}}} \quad (51)$$

Table 17 Preliminary design parameters for MVC subsystem.

Parameter	Value
MVC subsystem	
Efficiency of MVC, η_{MVC}, %	85
Temperature of the saturated vapor in last effect, T_n, °C	40
Saturated pressure of the vapor in the last effect, P_n, kPa	7.385

5.3.4 Exergy Analysis for LT-MED Subsystem

For the MED subsystem, there is no work or heat crossing the boundaries except the mass transfer of the feed, distillate water and rejected brine. The flow exergy of the distillate water stream is defined as that of pure water; however, the feed and the rejected brine are considered as the sum of the chemical and physical exergies that depend on the salinity and the temperature of the stream. The software package of thermophysical seawater properties was used for salinity less than 120,000 ppm and temperature of the stream less than 100 °C. The rate of exergy flow related to the stream is defined in Eq.50 and the flow exergy for feed and brine is shown in Eq.53. Table 18 shows the dead states for the streams and the exergy destruction of MED subsystem is represented in Eq.56.

$$\dot{E}_{x_{stream}} = \dot{M}\psi = \dot{M}[h - h_o - T_a(s - s_o)] \quad (52)$$

$$\dot{E}_{x_{feed/brine}} = \dot{M}\psi = \dot{E}_{x_{ph}} + \dot{E}_{x_{ch}} \quad (53)$$

$$\dot{E}_{x_{ph}} = \dot{M}[C_p(T,X) * (T - T_a) - T_a * C_p(T,X) * log\frac{T}{T_a}] \quad (54)$$

$$\dot{E}_{x_{ch}} = \dot{M}[N_{mol}\frac{(X,M_W,M_S)}{1000} * 8.314 * T_a * (-w_W * logw_W - w_S * logw_S)] \quad (55)$$

$$\dot{E}_{x_{d_{MED}}} = \dot{M}_{v_n}(\Delta h_{12-11} - T_a\Delta s_{12-11}) + \dot{M}_F\psi - \dot{M}_B\psi - \dot{M}_D\psi \quad (56)$$

$$\eta_{II_{MED}} = \frac{\dot{E}_{x_{out}}}{\dot{E}_{x_{in_{MVC}}}} = 1 - \frac{\dot{E}_{x_{d_{MED}}}}{\dot{E}_{x_{in_{MED}}}} \quad (57)$$

Table 18 Preliminary design parameters for LT-MED subsystem.

Parameter	Value
LT-MED Subsystem	
Feed temperature, T_F, °C	37
Rejected brine temperature, T_B, °C	40
Distillate temperature, T_D, °C	40
Temperature in the last effect, T_n, °C	40
The distillate flow rate, $\dot{M}_D$, kg/s	11.04
The rejected brine flow rate, $\dot{M}_B$, kg/s	11.04
Recovery Ratio	0.5

5.4 Parameters of Analysis

The following parameters affect the exergy destruction and exergy efficiency for the solar-supercritical ORC-MVC-LT-MED and were used for parametric analyses:

- Increasing the number of effects in the MED subsystem from 4 – 16 effects
- Varying the temperature of the motive steam entering the first effect in MED subsystem from 58°C to 90°C
- Increasing the salinity of the feed from 40,000 ppm to 60,000 ppm
- Changing the upper pressure of the supercritical ORC from 4 MPa to 6 MPa
- Varying the temperature of the HTF exiting from heat exchanger boiler from 80 °C to 130 °C

While varying one of the parameters, the other variables are held constant at the preliminary design parameters shown in Table 19.

Table 19 Preliminary design parameter of the proposed system.

Parameter	Value
Temperature of HTF existing HXB entering solar field, T_{in_col}, °C	110
Temperature of the motive steam entering 1st effect in MED subsystem, T_s, °C	60
Intake feed salinity, X_F, ppm	42,000
High Pressure of supercritical ORC subsystem, P_3, MPa	5.7

The exergy efficiency of the proposed system is defined as:

$$\eta_{II_{system}} = \frac{\dot{E}_{x_{out}}}{\dot{E}_{x_{sun}}} = 1 - \frac{\Sigma\dot{E}_{x_{d_{system}}}}{\dot{E}_{x_{sun}}}, \quad (58)$$

$$\Sigma\dot{E}_{x_{d_{system}}} = \dot{E}_{x_{d_{solar}}} + \dot{E}_{x_{d_{SORC}}} + \dot{E}_{x_{d_{MVC}}} + \dot{E}_{x_{d_{MED}}}, \quad (59)$$

5.5 Results and Discussion

For the design parameters shown in Table 19 and by increasing the number of effects of the MED subsystem from 4 to 16, the exergy efficiency for the proposed system solar-supercritical ORC-MVC-LT-MED, based on Eq.56, increases by more than 3.5 times as shown in Figure 40. This improvement is a result of the decrease of exergy destruction of MED subsystem. The mass flow rate of the vapor formed in the last effect is decreased by 75% as the number of effects is increased up to 16 effects. However, this improvement leads to an increase in the surface area of the effects since the difference in temperature between the vapor and the feed that drives the series of condensation and vaporization is reduced.

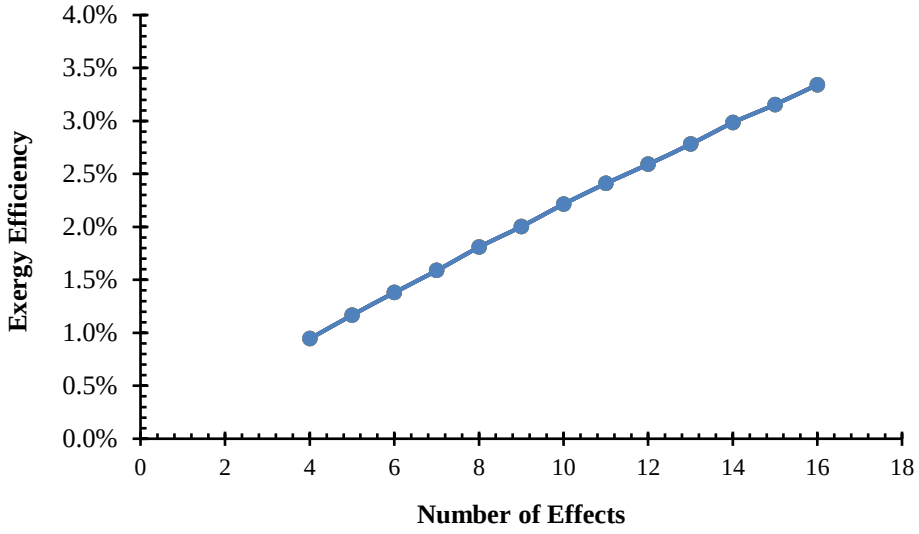

Figure 40 Impact of increasing the number of effects in MED subsystem on exergy efficiency of the system.

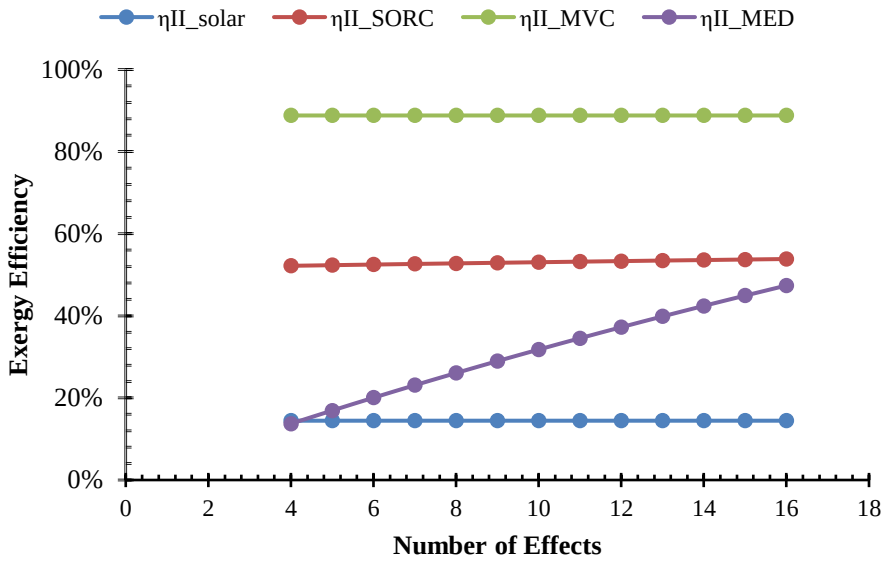

Figure 41 Impact of increasing the number of effects in MED subsystem on exergy efficiency of each subsystems.

The pressure of the ORC working fluid was varied to understand the behaviour of exergy efficiency of ORC subsystem at subcritical, trans-critical and supercritical ORC. The exergy efficiency of the proposed system increases by about 9% when the pressure of the ORC is increased to 5.7 MPa, which is a supercritical condition as shown in Figure 42. Increasing the pressure of the supercritical ORC beyond 5.7 MPa decreases the exergy efficiency of the cycle slightly because of increased exergy destruction of the pump. There is no impact of varying the pressure of supercritical ORC subsystem on other components as Figure 43 and Figure 44.

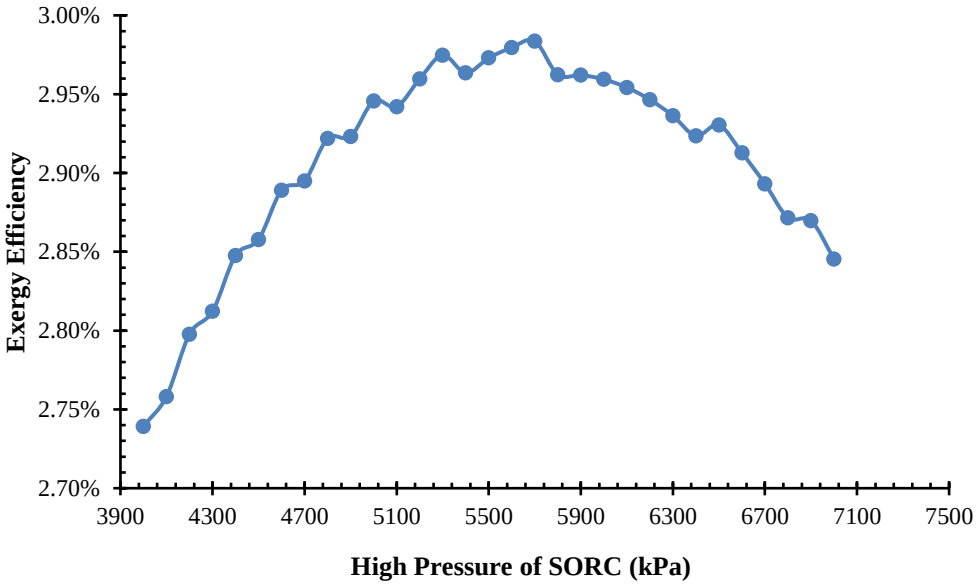

Figure 42 Impact of pressure of the ORC subsystem on exergy efficiency of the proposed system.

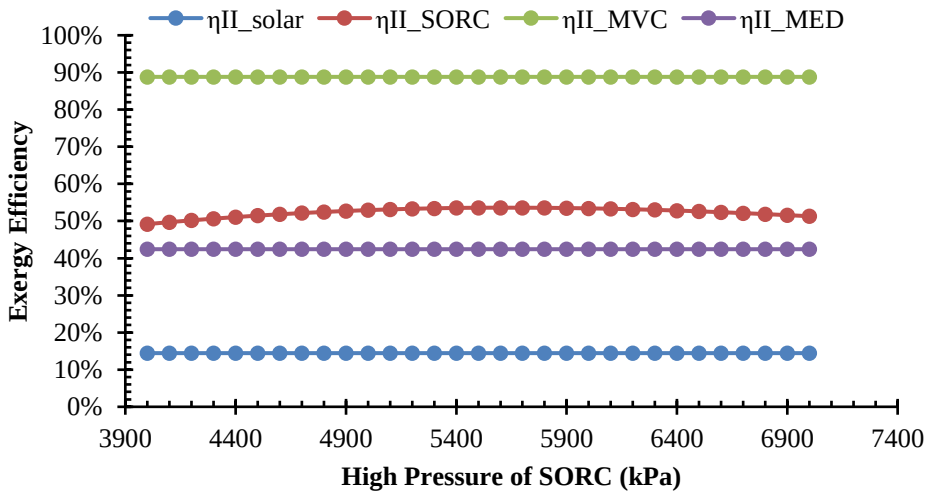

Figure 43 Impact of pressure of the ORC subsystem on exergy efficiency of each subsystem.

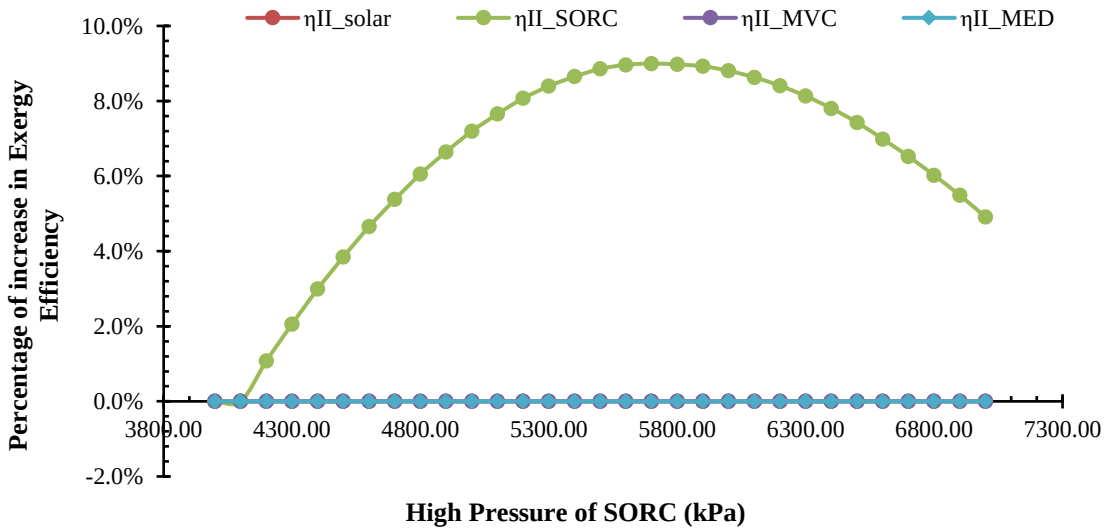

Figure 44 Impact of pressure of the ORC subsystem on percent change in exergy efficiency.

Increasing the motive steam temperature from 58 °C to 90 °C for 14 effects has an impact on the MVC subsystem and MED subsystem. While it increases the exergy efficiency of the MVC subsystem slightly by 3%, it decreases the exergy efficiency of MED subsystem by about 60% due the increase of irreversibility based on Eq.56. That yields to a decrease in the efficiency of the proposed system from about 3.3% at T_s 58°C to 1.22% at T_s 90°C (Figure 45). Thus, the increase of temperature of the motive steam has a major impact on the specific area of MED subsystem. As shown in Figure 46, there is no major impact on the other subsystems.

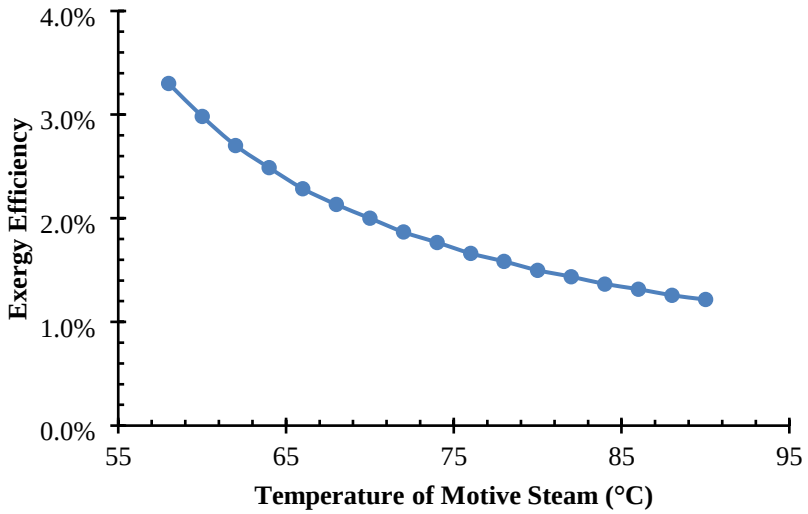

Figure 45 Impact of temperature of the motive steam on exergy efficiency of the system.

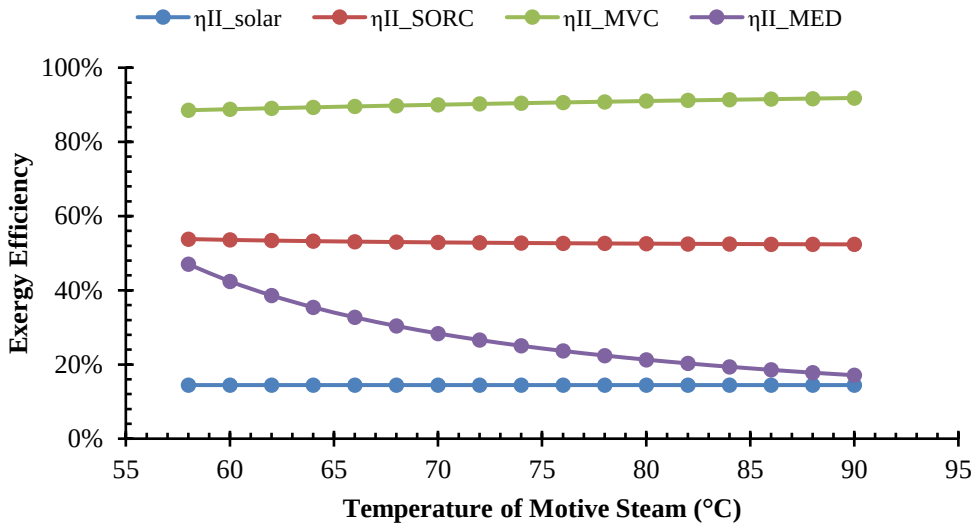

Figure 46 Impact of temperature of the motive steam on exergy efficiency on each subsystem.

For an MED system with 14 effects, increasing the salinity of the feed from 40,000 ppm to 60,000 has a major impact on the MED performance. The exergy efficiency of the proposed system increases by about 45% if the salinity is increased from 40,000 ppm to 60,000 ppm as shown in Figure 47. The exergy efficiency of MED subsystem has been increased by almost 50% with no

major impacts on the other subsystems as shown in Figure 48. The decrease of exergy destruction of the MED subsystem refers to the increase of the exergy flow of the brine as the salinity increases more than the exergy flow of the feed based on Eq.53 with the dead state defined in Table 19.

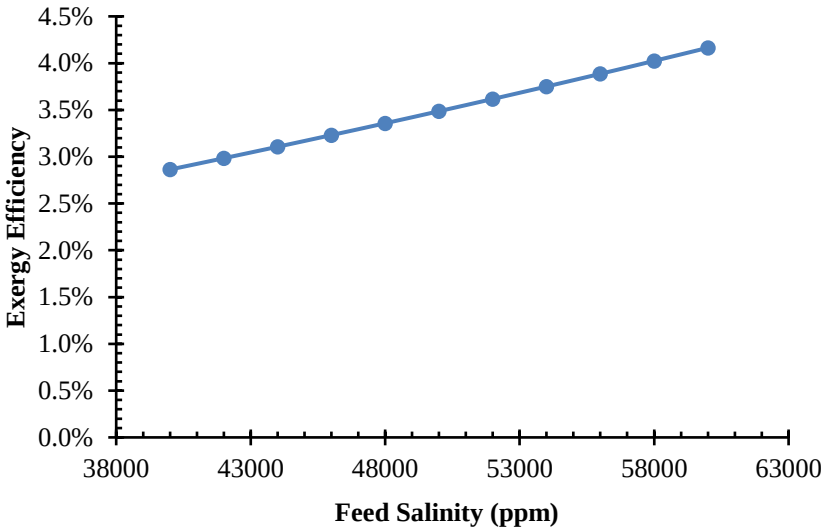

Figure 47 Impact of salinity of the feed on the exergy efficiency of the system.

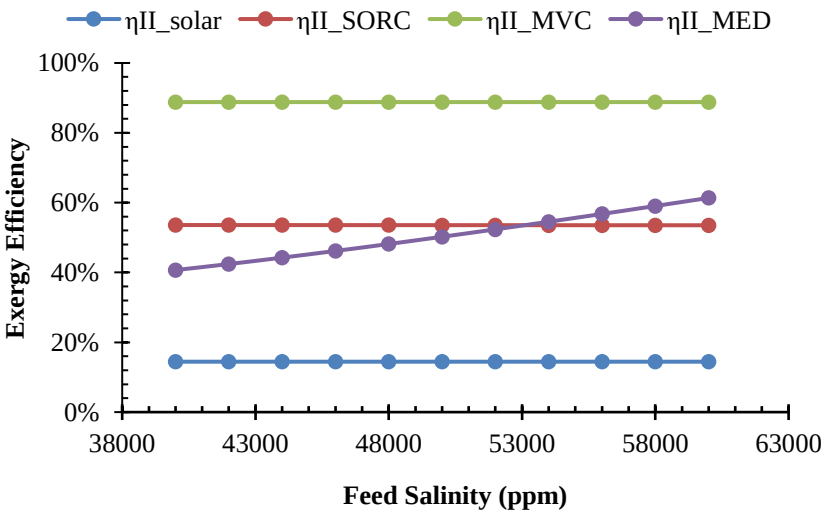

Figure 48 Impact of salinity of the feed on the exergy efficiency of each subsystem.

Varying the temperature of the HTF in the heat exchanger boiler of the supercritical ORC subsystem and entering the solar subsystem has a major impact on the performance of the solar and power cycle subsystems. The exergy efficiency of the proposed system is decreased by about 5% when the temperature of HTF entering the solar subsystem increases from 80 °C to 130°C as in Figure 49. While the exergy efficiency of the supercritical ORC subsystem decreases about 18% as the temperature of the HTF is increased, the exergy efficiency of solar subsystem increases from 13% to about 15% when the HTF temperature is increased from 80°C to 130°C as shown in Figure 50. For the solar field subsystem alone, an increase in the HTF temperature decreases the collector efficiency (Eq.35), increasing the exergy destruction through the solar field. This increases the area of the collectors by 5% to provide the same constant heat to the supercritical ORC (Eq.37). The larger collector area increases the exergy provided by the sun by 2%. However, the exergy output of the solar field is increased by 23%. As the outlet temperature is increased while the heat into the supercritical ORC is held constant, the temperature difference across the collectors decreases, therefore the HTF mass flow has to be increased (Eq.38). This relation between the supercritical ORC and the solar field causes the exergy of the solar field (Eq.40) to increase with an increase in the HTF collector outlet temperature despite a decrease in the collector efficiency.

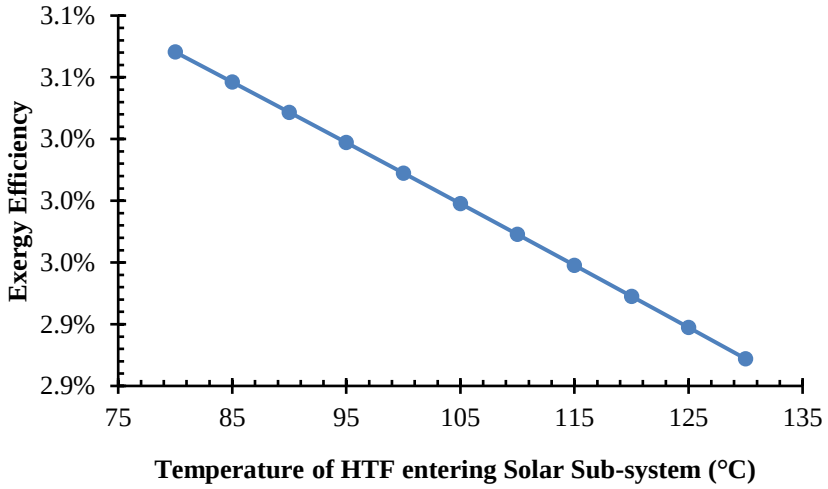

Figure 49 Impact of temperature of HTF on the exergy efficiency of the system.

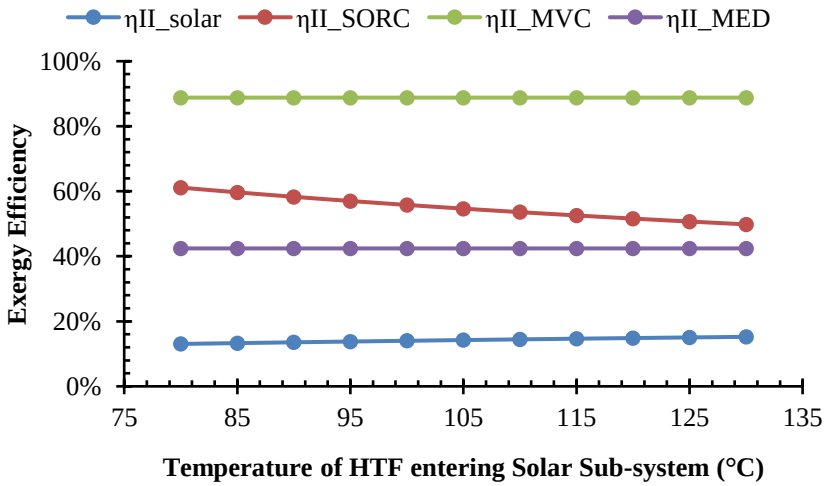

Figure 50 Impact of temperature of HTF on the exergy efficiency of each subsystem.

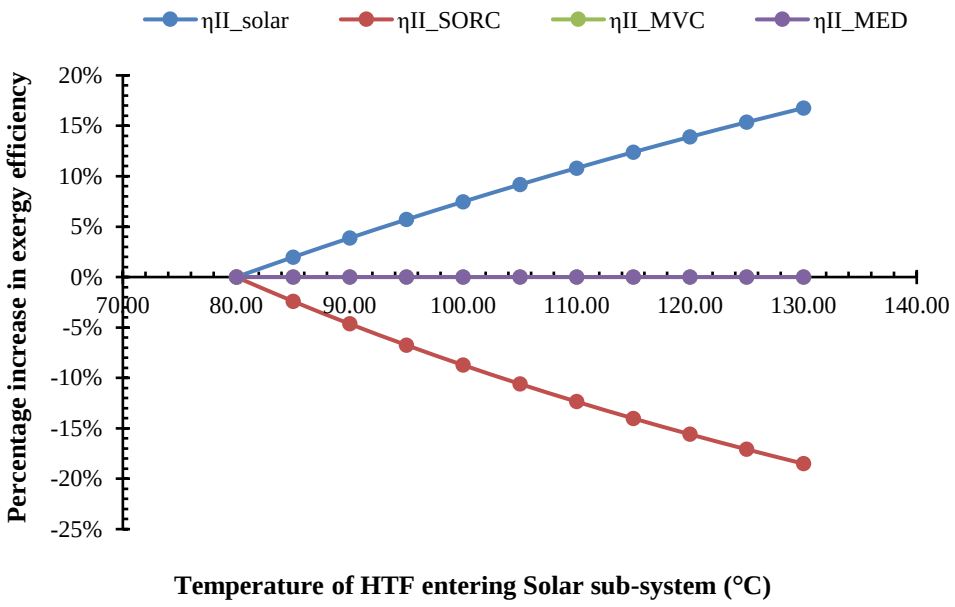

Figure 51 Impact of the temperature of HTF on percent increase in exergy efficiency.

The exergy destruction breakdown by components is shown in Figure 52 for 14 effects in the MED subsystem for the design parameters stated in Table 19. The major exergy destruction is from the solar subsystem that accounts for about 88% of the total exergy destruction. The contribution of the MED subsystem for the total exergy destruction is about 7% and the supercritical ORC subsystem is about 4%. To reduce the system exergy destruction, the solar subsystem performance can be improved by replacing the solar collectors with parabolic troughs or a central receiver where the exergy efficiency is about 25%[95].

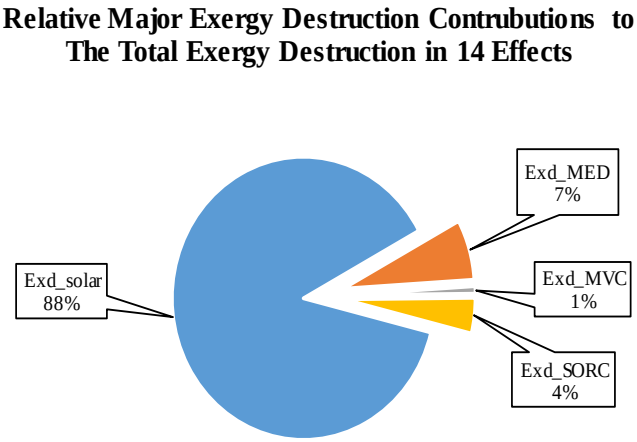

Figure 52 Major exergy destruction contributions of each subsystem in 14 effects.

5.6 Conclusion

In this chapter, a detailed exergy analysis of an innovative proposed system that uses a solar field with a temperature of 150 °C to power a supercritical-ORC driven MVC assisted LT-MED subsystem was conducted. The exergy efficiency of the proposed system is found to be 3% at 14 effects and other parameters are listed in Table 19. The major exergy destruction (88%) was in the solar subsystem. By increasing the number of effects in the MED subsystem from 4 to16, the exergy efficiency of the MED subsystem is increased by about 250%. The pressure of ORC subsystem has a major effect on the exergy efficiency when it increases from 4 to 7 MPa. The optimum pressure was found to be 5.7 MPa, which is in supercritical region. Increasing the temperature of the motive steam (T_s) decreases the exergy efficiency of the MED subsystem while increasing the salinity of the feed entering the first effect increases it. An analysis of major exergy destruction and its contribution to the total exergy destruction was provided in this chapter. In the following chapter, a cost analysis is presented based on the major findings presented in this paper.

CHAPTER 6: ENERGETIC AND ECONOMIC COMPARISON OF SOLAR POWERED MULTI-EFFECTS DESALINATION (MED) WITH DIFFERENT CONFIGURATIONS

6.1 Introduction

Multi effect desalination (MED) may be coupled with solar energy in three configurations; solar-MED, solar-MED assisted by thermal vapor compressor (TVC) and solar-MED coupled with mechanical vapor compressor (MVC). Most of the studies in the literature have focused on solar MED-TVC coupled with a power cycle driven by parabolic trough or central receiver tower system while a few have discussed MED-MVC.

For solar-MED configuration, different combinations with solar collector types have been experimentally tested and numerically modelled. Gerofi et al. [56,96] experimentally tested a system coupling MED with FPC and ETC in Australia for a capacity of 100 m^3/day. The unit cost of water production was \$4/m^3 for FPC and \$5.1/m^3 for ETC. Using PT, Sharaf et al. [43,97] modeled two configurations of an MED system with 16 effects where the motive steam was heated directly from a solar field and a heat exchanger boiler (HXB) or bleeding a stream from the turbine of the organic Rankine cycle (ORC) condensed in the first effect of the MED. For low capacity production (100 m^3/day), the unit cost of water production was \$5.47/m^3 and \$5.05/m^3 for the first and second configurations, respectively. For medium capacity production (5000 m^3/day), the cost dropped to \$1.62/m^3 and \$1.87/m^3 for the first and second configuration, respectively.

In this chapter, three different configurations of MED coupled with a solar field using ETC are investigated. The design of solar-MED, solar-MED-TVC and solar-SORC-MVC-MED systems has been presented. A comparison of the performance of innovative design utilizing

supercritical-ORC powering MED-MVC with conventional solar-MED and solar-MED-TVC is presented for specific thermal energy consumption, solar field area and cost of unit water produced. The impact of the number of MED effects has been analyzed on the solar collector area, specific thermal energy consumption, and the cost of unit water produced.

6.2 Methodology

Multi-effect desalination (MED) can be powered by solar energy in different configurations where the motive steam ($\dot{M}_s$) entering the first effect of the MED subsystem is heated totally or partially or compressed by either a thermal or mechanical vapor compressor resulting in the following systems:

- Solar-MED
- Solar-MED-TVC
- Solar-SORC-MVC-MED

The common input parameters for each three systems are listed in Table 20.

Table 20 Design constraints for MED subsystem.

Parameter	**Value**
Rejected brine temperature, T_{brine}, °C	40
Motive Steam temperature, T_s, °C	60
Temperature in the last effect, T_n, °C	40
The distillated flow rate, $\dot{m}_d$, kg/s	30
Salinity of the intake seawater, X_f, ppm	55,000
Salinity of the rejected brine in last effect, X_n, ppm	110,000

Heat input to each configuration is considered to be the thermal power output from the solar field divided by the effectiveness of the heat exchanger as shown in Eq. 60. The area of the solar field is found from Eq. 61, which uses the efficiency of the collector found from Eq. 62. The parameters of the solar subsystem are listed in Table 21.

$$\dot{Q}_{Solar} = \frac{\dot{Q}_{in}}{\varepsilon} = \dot{M}_{HTF} * c_{p_{HTF}}(T_{out_{col}} - T_{in_{col}}) \quad (60)$$

$$A_{solar} = \frac{\dot{Q}_{\text{Solar}}}{G * \eta_{col}} \quad (61)$$

$$\eta_{col} = \eta_{optical} - a_1\left(\frac{T_{avg} - T_a}{G}\right) - a_2\left(\frac{(T_{avg} - T_a)^2}{G}\right) \quad (62)$$

$$T_{avg} = \frac{\left(T_{out_{col}} + T_{in_{col}}\right)}{2} \quad (63)$$

Table 21 Preliminary design parameters for solar subsystem.

Parameter	Value
Solar Subsystem	
Designed solar insolation, G, W/m^2	800
Ambient temperature, T_a, °C	30
Designed high HTF temperature, T_{out}, °C	150
Designed low HTF temperature, T_{in}, °C	110
Area of the collector, $A_{collector}$, m^2	3
The optical efficiency of solar collector, $\eta_{optical}$	64.4
Heat transmission coefficient, a1	0.89
Heat transmission coefficient, a2,	0.001
Specific heat capacity of HTF at T_{avg}, kJ/kg. °C	3.97

6.3 Solar-MED

In the solar-MED system, the solar and MED subsystems are connected through a heat exchanger boiler (HXB) as shown in Figure 53. The solar heat absorbed by the evacuated tube collectors is transferred by the solar field HTF to the MED subsystem through the HXB. The maximum temperature of the heat transfer fluid (HTF) is 150°C. The motive steam enters the HXB as saturated liquid atT_s. After that, the motive steam enters the first effect of MED as saturated vapor atT_s. The heat input is defined in Eq. 64, where λ_s is the heat of vaporization. The design parameters of the solar-MED configuration are listed in Table 22.

$$\dot{Q}_{in} = \dot{M}_s * \lambda_s \quad (64)$$

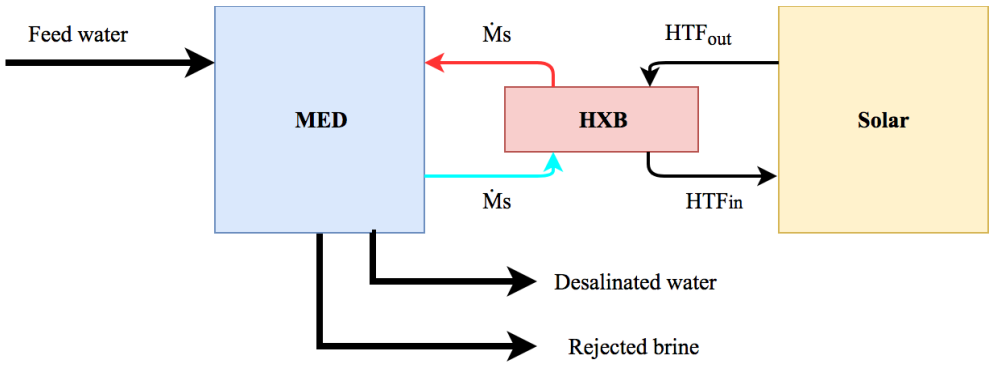

Figure 53 A schematic for solar-MED configuration.

Table 22 Preliminary design parameters for solar-MED configuration.

Parameter	Value
HXB Subsystem	
Effectiveness	0.9
Latent Heat of Vaporization, λ_s, kJ/kg	2357.7

6.4 Solar-MED-TVC

The Solar-MED-TVC system configuration is shown in Figure 54. Coupling a thermal vapor compressor with MED reduces the size of the down condenser in the MED subsystem, reducing the waste heat loss from the entrained part of the vapor formed in the last effect or other effects. To utilize this available latent heat, it is mixed with the high pressure and temperature steam from the HXB through an ejector, where the heat source temperature is 150°C, the pressure of the motive steam (P_m) is 415.68 kPa, the pressure of the entrained vapor is the saturation pressure at the temperature of the last effect (P_n), and the pressure of the compressed steam exiting the ejector is the saturated pressure at the temperature of the first effect (Ps). The ratio of the motive steam to the entrained vapor which is known as the entrainment ratio (ER) is calculated based on a formula developed by Al-Juwayhel [71,98] in Eq. 63; the mass flow rate of the high pressure motive steam of the ejector is calculated in Eq. 64. The heat input through the heat exchanger

boiler is found using Eq. 65. The design parameters of the solar-MED-TVC configuration are listed in Table 23.

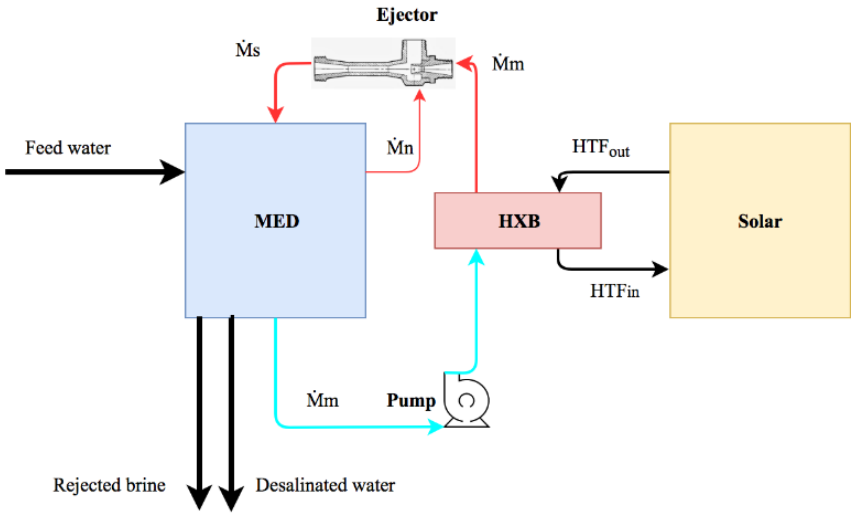

Figure 54 A schematic for solar-MED-TVC configuration.

Table 23 Preliminary design parameters for solar-MED-TVC configuration.

Parameter	Value
HXB Subsystem	
Effectiveness	0.9
Latent Heat of Vaporization, λ_m, kJ/kg	2129.2
Ejector Subsystem	
Motive Steam Pressure, P_m, kPa	415.68
Motive Steam Temperature, T_m, °C	145
Entrained Vapor Pressure, P_n, kPa	7.3851
Entrained Vapor Temperature, T_n, °C	40
Compressed Steam temperature, T_s, °C	60
Compressed Steam Pressure, P_s, kPa	19.947

$$ER = 0.296 * \frac{{P_s}^{1.19}}{{P_n}^{1.04}} * \left(\frac{P_m}{P_n}\right)^{0.015} * \left(\frac{3\times10^{-7}*(P_m)^2-0.0009*P_m+1.6101}{2\times10^{-8}*(T_n)^2-0.0006*T_n+1.0047}\right) \quad (65)$$

$$\dot{M}_m = \dot{M}_s * \left(\frac{ER}{ER+1}\right) \quad (66)$$

$$\dot{Q}_{in} = \dot{M}_m * \lambda_m \quad (67)$$

6.5 Solar-MED-SORC-MVC

In the solar SORC-MVC-MED configuration, the vapor formed in the last effect of the MED subsystem ($\dot{M}_n$) is mechanically compressed by the MVC subsystem. Then, the motive steam at saturation temperature (T_s) is passed through the first effect and the processes of condensation and vaporization continue through the effects in the MED subsystem. The net power of the cycle is defined as the difference between the turbine output and the pump input work and is sized to meet the total work required by the MVC in the desalination system, as defined in Eq. 68. The solar heat is transferred by the HTF to the supercritical ORC via the HXB as represented in Figure 55 as the process 4-1. The maximum temperature of the heat transfer fluid (HTF) was set to 150 °C, as in the prior systems, and the turbine inlet conditions were selected to meet the pinch point criteria and to optimize cycle efficiency at 145°C (T_1) and 5.7 MPa (P_1). The heat input is defined in Eq. 69.

$$\dot{W}_{net} = \dot{W}_t - \dot{W}_p = \dot{m}_{WF}[(h_2 - h_1) - (h_3 - h_4)] \quad (68)$$

$$\dot{Q}_{in} = \dot{m}_{WF}[h_1 - h_4] \quad (69)$$

Table 24 Preliminary design parameters for solar-SORC-MVC-MED configuration.

Parameter	Value
Supercritical ORC Subsystem	
Effectiveness of heat exchanger boiler and condenser, %	90
Designed HXB pinch point, °C	5
Designed condenser pinch point, °C	6
High Pressure of SORC, MPa	5.7
Isentropic efficiency of turbine and pump, %	85
Condensation temperature, T_{cond}, °C	41
WF turbine inlet temperature, T_1, °C	145
WF turbine inlet pressure, P_1, MPa	5.7
Working Fluid	R152a
MVC Subsystem	
MVC efficiency, η_{MVC}, %	85
Motive Steam Pressure, P_s, kPa	19.947
Last Effect Vapor Pressure, P_n, kPa	7.3851

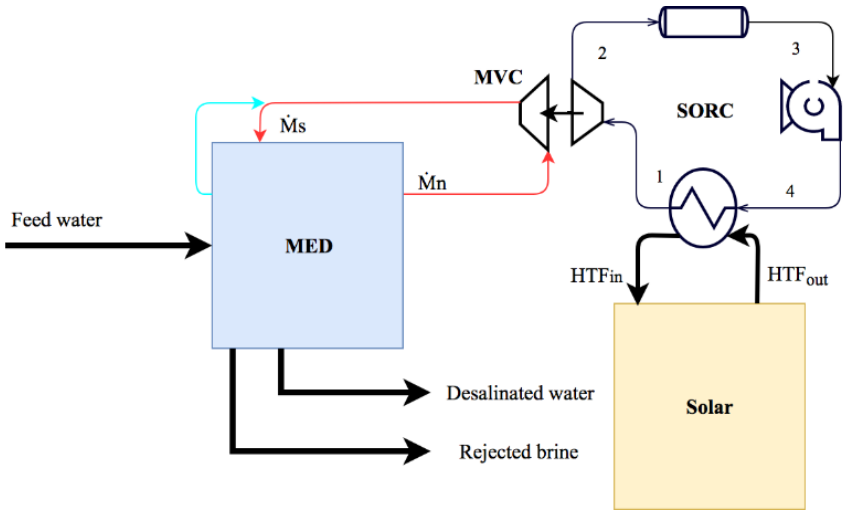

Figure 55 A schematic for solar-MED-SORC-MVC-MED configuration.

6.6 Multi Effect Desalination (MED) Validation

A steady state numerical model was developed in MATLAB to analyze the proposed system. Preheated forward feed LT-MED consists of a series of evaporators, preheaters and flash boxes where the feed and the formed vapor move in the same direction through the effects, as shown in Figure 56. The feed is moving from one effect to another due to the difference in pressure and the vapor is condensed in each effect at a pressure higher than the pressure set in the effect. The MED subsystem was validated in our prior work [99].

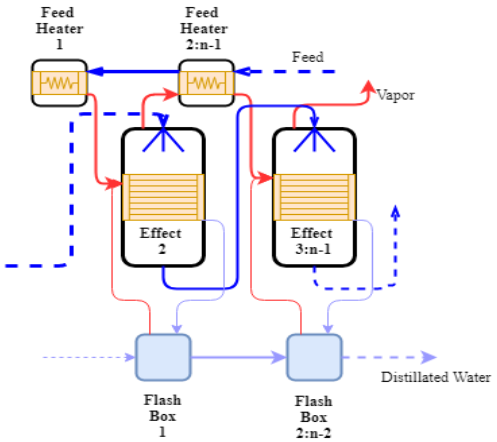

Figure 56 A schematic for MED subsystem.

Considering energy balance, mass balance, and material balance in the system a detailed model of MED was developed in MATLAB. To analyze the thermophysical properties of the working fluid (WF) and pure water, REFPROP was used. For the seawater thermophysical properties, a library developed by Al-Sharqawi et al. [87,88] was used to determine the properties of the seawater and brine, accounting for salinity and temperature.

The following assumptions were used in the model:

- Steady state
- Thermal losses and vapor leaks to the environment are negligible
- The vapor formed in the effects contains no salt
- The demister has negligible effect on pressure drop
- The brine, feed, and distillate are in the saturated liquid phase in each effect

The MED subsystem has been validated with two models that were developed by El-Sayed [100] and Mistry et. al. [85] as shown in Figure 57. By varying the number of effects, the performance ratio of the MED subsystem, defined in Eq. 70 as the mass ratio of water produced to motive steam (Eq. 71) was compared for the three models.

$$PR = \frac{\dot{M}_D}{\dot{M}_s} \tag{70}$$

$$\dot{M}_s = [\dot{M}_f * c_{p_f} * (T_1 - T_f) + \dot{m}_1 * \lambda_1]/\lambda_s \tag{71}$$

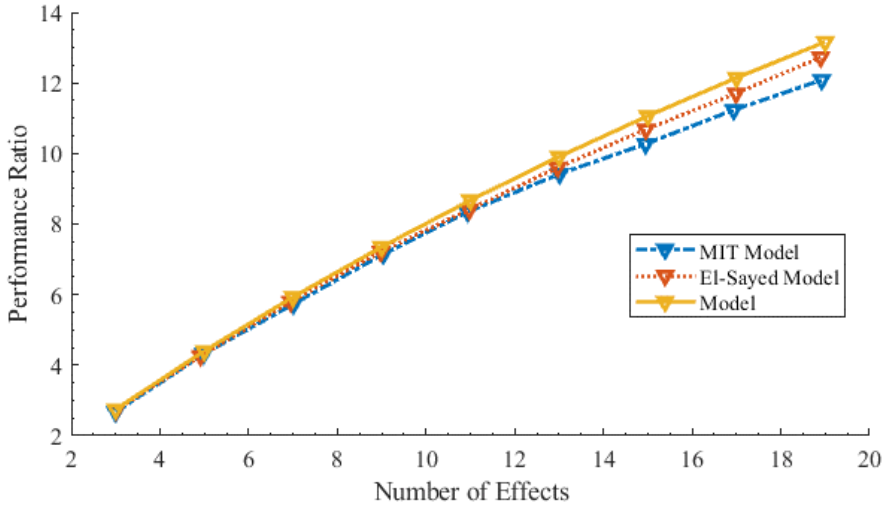

Figure 57 Validation of MED subsystem with El-Sayed [104] and Mistry et al., [85] model.

6.7 Performance Parameters

The specific thermal energy consumption and cost of water produced were considered in order to evaluate the performance of the three different MED configurations when the number of effects is increased from 4 to 16 for the conditions shown in the preliminary tables. These two parameters are the best indicators for which configuration is more useful to utilize the solar produced fresh water.

6.7.1 Specific Thermal Energy Consumption

Specific thermal energy is the heat delivered by the solar system in kWh over the total volumetric production of fresh water per hour (Eq. 72). The heat input for the three configurations is defined in equations 64, 66 and 69.

$$W_{spc_{th}} = \frac{\dot{Q}_{in}}{V_h} \tag{72}$$

6.7.2 Cost of Water Production

The cost of water production for each configuration is based on the capital cost of components in the configuration.

The cost of solar collector is calculated based on the solar collector area. For parabolic trough collector, Palenzuela et al. estimated the cost of solar collector as 150 $/m^2 [28]. Kouta et al. calculated the cost of solar tower as 330 $/m^2 [69]. For evacuated tube collectors, Mario et al. [101] estimated the cost of ETC as 680 $/collector, for a 3m^2 collector. In this analysis, ETC was considered at this cost (Eq. 73).

$$C_{solar} = 226.67 * A_{solar} \quad (73)$$

The cost of heat exchanger and condenser is calculated by Eq. 74 based on the area and the log mean temperature difference (LMTD), defined in Equations 75 and 76, respectively. The coefficient of heat removal was set to 1000 W/m^2/K [66].

$$C_{HXB/cond} = 150 * A_{HXB/cond}^{0.8} \quad (74)$$

$$A_{HXB/cond} = \frac{\dot{Q}}{U*LMTD} \quad (75)$$

$$LMTD = \frac{(T_{h,i}-T_{c,o})-(T_{h,o}-T_{c,i})}{\ln(\frac{T_{h,i}-T_{c,o}}{T_{h,o}-T_{c,i}})} \quad (76)$$

The costs of the turbine (Eq. 77) and the pump (Eq. 78) are calculated based on the net power [66]. Selection of the supercritical expander is considered one of the key factors. Quoilin et al. optimized the selection of a radial turbine over screw and scroll expanders for the power range of 100-1000 kW[102].

$$C_{turbine} = 4750 * \dot{W}_t^{0.75} \quad (77)$$

$$C_{pump} = 3500 * \dot{W}_p^{0.47} \quad (78)$$

The capital cost of the supercritical-ORC is defined as the sum of the costs of its components as shown in Eq.79.

$$C_{SORC} = C_{HXB} + C_{pump} + C_{turbine} + C_{cond} \quad (79)$$

The capital cost of the feed preheater (Eq. 80) in the MED subsystem is estimated based on the heat transfer area. The area is calculated in Eq. 81 and heat coefficient is defined as Eq. 82[38,100].

$$C_{FH} = 1000 * (12.86 + {A_{fh}}^{0.8}) \quad (80)$$

$$A_{fh} = \sum_{1}^{n-1} \frac{\dot{M}_{f} * c_{p_f} * (T_{fn} - T_{fn-1})}{U_{fh} * LMTD} \quad (81)$$

$$U_{fh} = 1.6175 + 0.1537 * 10^{-3} * T_i - 0.1825 * {T_i}^2 - 80.26 * 10^{-6} * {T_i}^3 \quad (82)$$

The capital cost of the effects in the MED subsystem is calculated in Eq. 83 and is based on the heat input in each effect and the difference of the temperature and the pressure drop in each effect. The heat input in each effect is defined in Eq. 84. The pressure drop in the shell side is set at 0.045 kPa, and the pressure drop in tube side is set at 0.205 kPa [38,100].

$$C_{Effects} = 430 * 0.582 \left(\frac{\dot{Q}_e}{\Delta T_e * dPt^{0.01} * dPs^{0.1}}\right) \quad (83)$$

$$\dot{Q}_e = \dot{M}_s * \lambda_s + \sum_{1}^{n-1} \dot{m}_\iota * \lambda_i \quad (84)$$

The capital cost of MED subsystem is the sum of the capital cost of the effects and feed preheaters (Eq. 85). That cost has been estimated by IDA Desalination Yearbook as \$1230/(m^3/day) based on the data base [15,28].

$$C_{MED} = C_{Effects} + C_{FH} \quad (85)$$

The ejector cost is represented in Eq. 86 and the cost of MVC is shown in Eq. 87 [11,18]. The pressure of the motive steam, entrained vapor pressure, mass flow rate of the motive steam, and the efficiency of MVC are listed in Table 23 and Table 24.

$$C_{Ejector} = 1500 * 0.45 * \dot{M}_s * \left(\frac{T_n}{P_n}\right)^{0.05} * \left(\frac{P_m}{1000}\right)^{-0.75} \quad (86)$$

$$C_{MVC} = 7364 * \dot{M}_s * \left(\frac{P_s}{P_n}\right)^{1} * \left(\frac{\eta_{MVC}}{1-\eta_{MVC}}\right)^{0.7} \quad (87)$$

The amortization factor, which is defined in Eq. 88, is based on the data listed in Table 25 and represents how much of the total capital cost of the system will be paid per year based on the interest rate and the life time of the plant.

$$Amortization\ Factor = AF = \frac{i_{rate}*(1+i_{rate})^{LTP}}{(1+i_{rate})^{LTP}-1} \quad (88)$$

The operation and maintenance cost for the solar subsystem is calculated based on Eq.89. It is estimated by South Africa CSP to account 10-11 % of the initial cost[103].

$$Solar_{O\&M} = 0.15 * C_{solar} \quad (89)$$

The unit product cost in \$/m^3 for each configuration is given in Eqs. 90-92.

$$TWP_{solar-MED} = AF * (\frac{C_{solar}+C_{MED}+C_{HXB}+Solar_{O\&M}}{8760*\Lambda*V_h}) \quad (90)$$

$$TWP_{solar-MED-TVC} = AF * (\frac{C_{solar}+C_{MED}+C_{HXB}+C_{Ejector}+Solar_{O\&M}}{8760*\Lambda*V_h}) \quad (91)$$

$$TWP_{solar-SORC-MVC-MED} = AF * (\frac{C_{solar}+C_{MED}+C_{SORC}+C_{MVC}+Solar_{O\&M}}{8760*\Lambda*V_h}) \quad (92)$$

Table 25 Cost data inputs.

Parameter	Value
Amortization Factor, 1/y	
Interest rate, i_{rate}, %	8.3
Annual Availability, Λ,	0.3
Life Time Plant, LTP, years	25
Hourly Water Production, V_h, m^3/h	108

6.8 Parameters of Analysis

Increasing the number of effects in the MED subsystem from 4 – 16 effects has been investigated. The other variables are held constant as shown in Table 26.

Table 26 Preliminary design parameter of the proposed system.

Parameter	Value
Temperature of HTF existing HXB entering solar field, T_{in_col}, °C	110
Temperature of the motive steam entering 1st effect in MED subsystem, T_s, °C	60
Intake feed salinity, X_F, ppm	42,000
High Pressure of supercritical ORC subsystem, P_3, MPa	5.7

6.9 Results and Discussion

The three different configurations of MED were analyzed for the performance parameters explained above holding the parameters listed in Table 21 to Table 24 as constant and changing the number of effects from 4 to 16.

The specific thermal energy consumption for solar-MED, solar-MED-TVC and solar-SORC-MVC-MED is decreased by almost 70% when the number of effects is increased from 4 to 16 (Figure 58). This decrease is a result of decreasing the amount of vapor produced in the first effect when the number of effects is increased. This leads to a decrease in the mass flow rate of the motive steam entering the first effect.

The solar-MED-TVC and solar-SORC-MVC-MED have a clear advantage over the simple solar-MED configuration regarding energy consumption. The solar-MED configuration consumed about double the power of the other configurations. The specific thermal energy consumption of solar-SORC-MVC-MED configuration is lower than the solar-MED-TVC by almost 15%, which is a clear advantage to utilize waste heat or geothermal or solar driven supercritical-ORC or work from an existing power plant compressing the vapor instead of vaporizing the motive steam as shown in Figure 58.

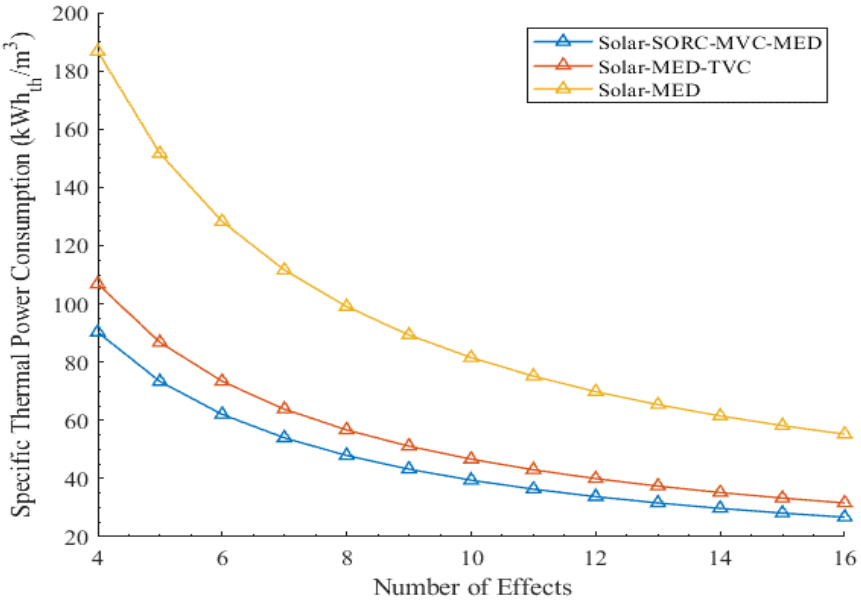

Figure 58 Specific thermal energy consumption vs. number of effects in MED subsystem.

The size of the solar field has a major impact on the cost of the different MED configurations. When the number of effects is increased, resulting in reduced heat input, the solar field decreases as shown in Figure 59.

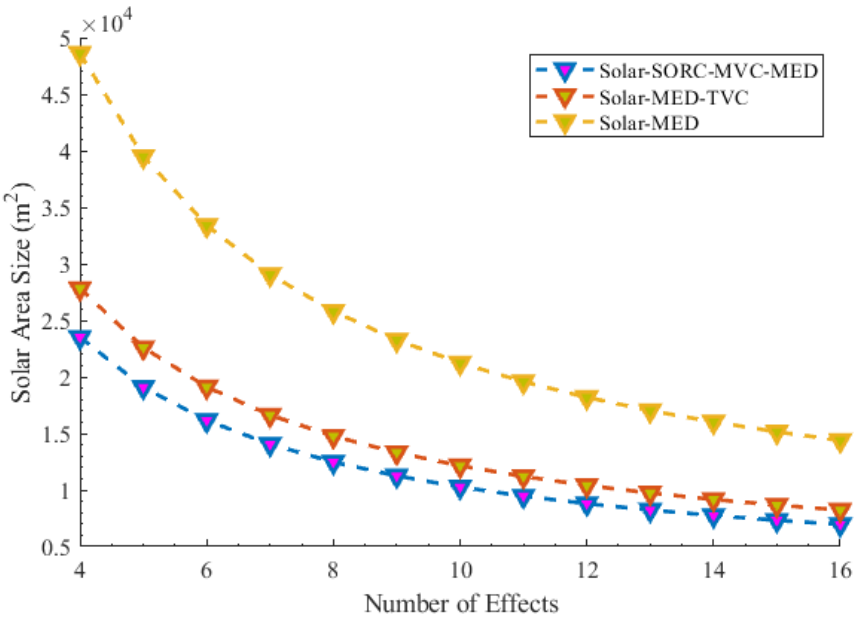

Figure 59 Solar collector area vs. number of effects in MED subsystem.

The cost to produce 1 m^3 for each configuration is defined in Eqs. 88-90 and shown in Figure 60. The trend of reduction in the cost as the number of effects increase is obvious. This decrease in cost results mainly from reducing the size of solar field shown in Figure 59. The cost of unit product for solar-MED configuration decreases from about \$3.4/m^3 to \$2.1/m^3 when the number of effects is increased from 4 to 16. For solar-MED-TVC and solar-SORC-MVC-MED configurations, the cost is dropped from about \$2.25/m^3 to \$1.8/m^3 when the number of effects is increased from 4 to 16.

The decrease of the cost for solar-MED configuration is clear due to the reduced solar field size which has the major impact, however, the reduction in the unit cost for solar-MED-TVC and solar-SORC-MVC-MED is not that clear. As the number of effects is increased from 4 to 6, the cost is dropped by about 6% with slight advantage for solar-MED-SORC-MVC-MED over solar-MED-TVC. After that, the cost remains around \$2 /m^3 as the number of effects is increased from 6 to 13. After that, the cost for both configurations is dropped by almost 12% as the effects increase to 16 with a slight advantage for solar-MED-TVC as shown in Figure 60.

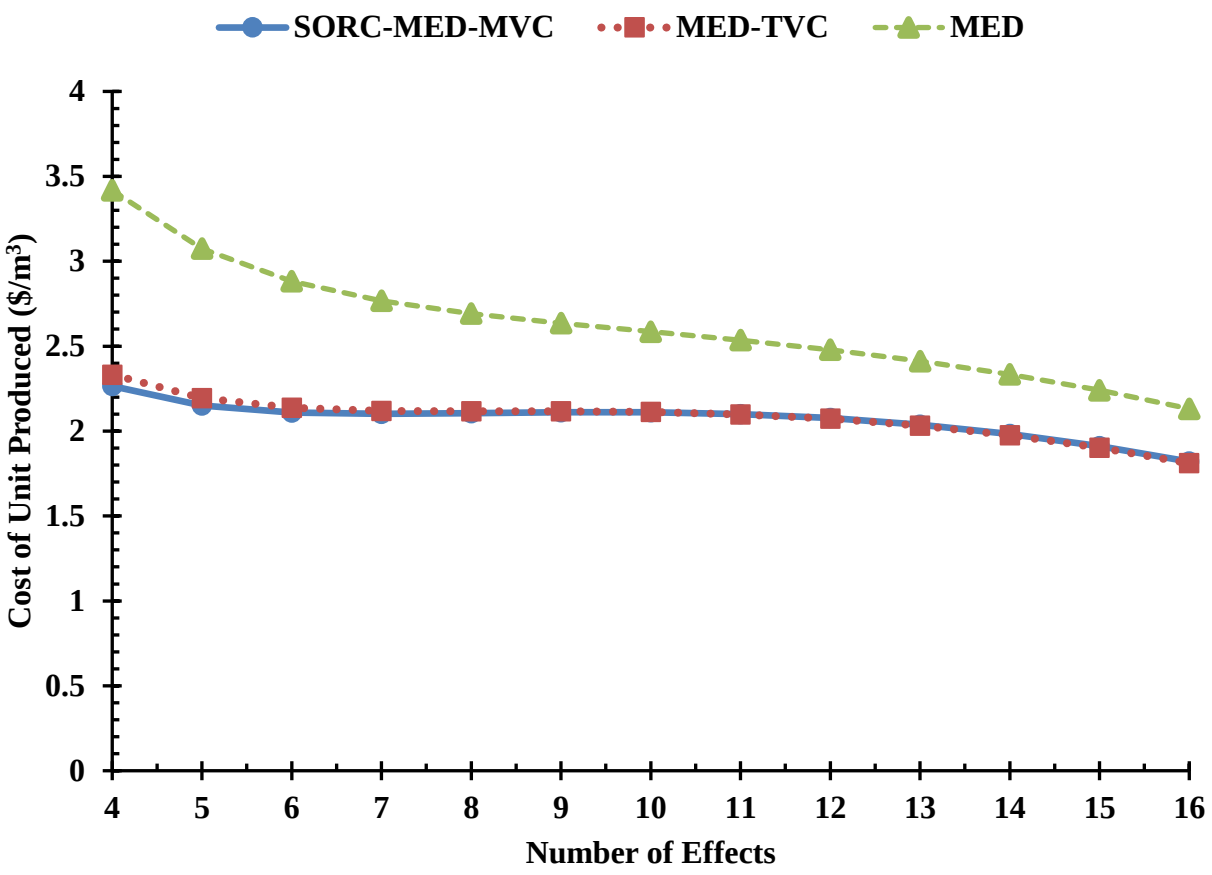

Figure 60 Cost of water production for three different configuration variations as number of effects.

For the solar-MED configuration, the cost break-down is shown in Figure 61 and is broken down into each subsystem for when the number of effects is increased from 4 to 16. Although the impact of the HXB subsystem is very small, the cost drops by almost 60% due to the decreased area of the HXB defined in Eq. 16. After the 7th effect, the cost of MED subsystem increases by almost 60% due to the increase of the specific area of MED subsystem as the difference of the temperature across the effects decreases (Eq. 83). However, the decrease in the cost of the solar field is less than the increase in the cost of the MED subsystem as the number of effects increases, reducing the total cost of the system.

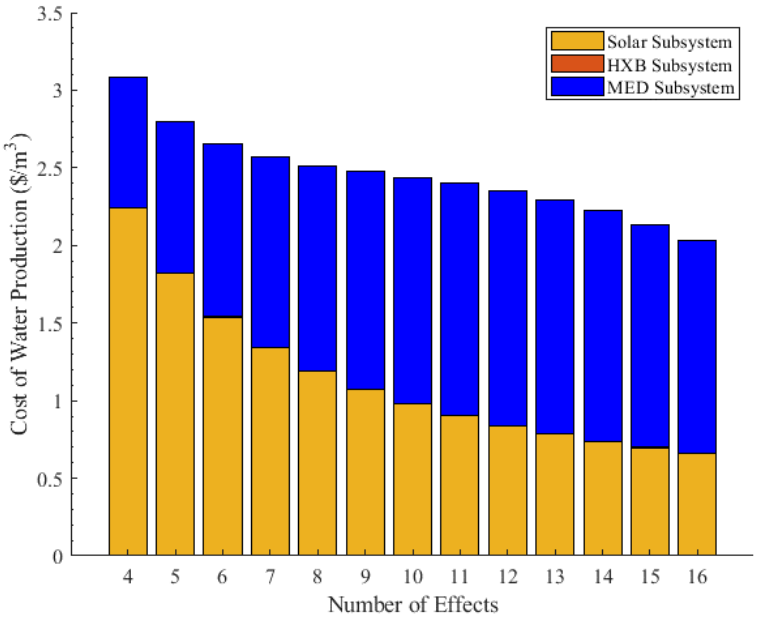

Figure 61 Cost breakdowns of solar-MED configuration showed the contribution of each subsystem as the number of effects increased.

For the solar-MED-TVC configuration, the cost breakdowns of the unit produced are shown in Figure 62 based on each component. While the costs of the ejector subsystem and HXB have a small impact, as the number of effects increased from 4 to 16, the cost of both components reduced by almost 65% due to the area of the HXB and the reduced mass flow rate of the motive steam for ejector as illustrated in Eq. 84. After the 5^{th} effect, the increasing cost of the MED subsystem keeps the total cost from going down even though the cost of solar subsystem is decreased. After the 12^{th} effect, the cost of MED subsystem is decreased due to the reduced heat input delivered to the effects (Eq. 85) and the small size of the down condenser in comparison with the solar-MED system.

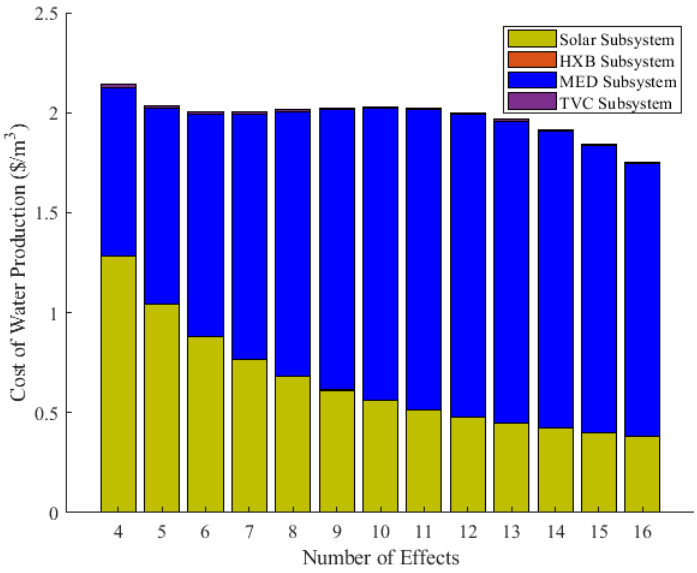

Figure 62 Cost breakdowns of solar-MED-TVC configuration showed the contribution of each subsystem as the number of effects increased.

For the solar-SORC-MVC-MED configuration, the cost of each subsystem is shown in Figure 63. The cost of the MVC subsystem drops by almost 75% due to the decreasing mass flow rate from the last effects as the number of effects is increased from 4 to 16 effects. However, it has little impact on the total cost of the system. While the cost of supercritical ORC subsystem is decreased as the number of effects is increased, the cost of MED subsystem is increased accounting for the majority of the cost for systems with more than 5 effects.

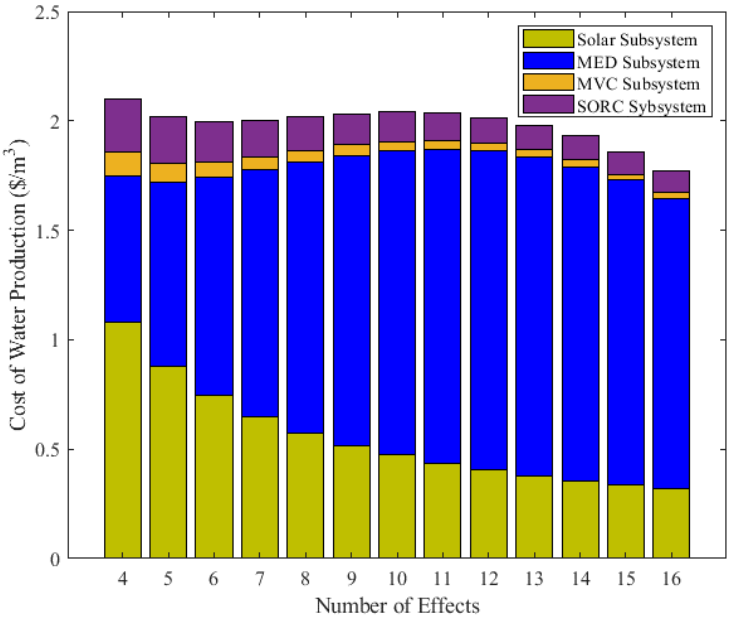

Figure 63 Cost breakdowns of solar-SORC-MVC-MED configuration showed the contribution of each subsystem as the number of effects increased.

6.10 Conclusion

In this chapter, three different configurations of MED plants powered by low temperature solar heat, where the motive steam is heated fully in solar-MED configuration or partially in solar-MED-TVC configuration or compressed through MVC coupled with supercritical-ORC in solar-SORC-MVC-MED configuration, have been analyzed. The solar-SORC-MVC-MED has a clear advantage in the specific thermal energy consumption and the size of the solar field over other configurations and a slight advantage on the cost of production over the solar-MED-TVC.

The impact of increasing the number of effects on the three configurations has been presented. The specific thermal energy consumption for each configuration decreases as the number of effects is increased. At 14 effects, solar-MED configuration consumed about 60 kWh_{th}/m^3, where the solar-MED-TVC configuration consumed about 35 kWh_{th}/m^3 and solar-SORC-MVC-MED configuration consumed about 29 kWh_{th}/m^3.

The cost of water production for the solar-MED configuration reduced from $3/m^3$ at 4 effects to almost $2/m^3$ at 16 effects. The solar-MED configuration is more sensitive to the cost of the solar field. On the other hand, the solar-MED-TVC and solar-SORC-MVC-MED systems are more sensitive to the cost of the MED subsystem. The cost of unit water production for both configurations is varied from $2/m^3$ at 4 effects to $1.75/m^3$ at 16 effects. The cost breakdowns for each configuration based on the cost of their components has been presented.

CHAPTER 7: CONCLUSIONS, RECOMMENDATIONS AND FUTURE WORK

The process of desalination is an energy intensive process which typically comes from fossil fuels, with high carbon emissions. It was estimated by Kalogirou et al. that the production of 1,000 m^3 daily requires about 10,000 tons of oil per year [104,105]. Therefore, using renewable energy in desalination instead of fossil fuels is considered one of the valuable solutions to the demand for water and a clean environment. An innovative thermal desalination system was proposed and analyzed. This proposed system is a co-generation plant that can produce power and desalination from a low-grade heat source with a supercritical-ORC and a MED-MVC thermal desalination system. The impact of the number of effects, motive steam temperature, salinity of the feed for the MED subsystem, temperature difference of the HTF for the solar subsystem, and pressure of the working fluid for the ORC subsystem were the major parameters that have been investigated. Performance ratio, specific energy consumption and cost of unit produced were analyzed for the proposed solar-supercritical ORC-LT-MED-MVC system while changing other parameters. The best performance was found for a system of 14 effects where the system efficiency was about 16% with a performance ratio of MED greater than 9 and a specific energy consumption of 3.9 kWh/m^3. A detailed exergy analysis of the innovative proposed system was conducted. The exergy efficiency of the proposed system is found to be 3% at 14 effects. The major exergy destruction was in the solar subsystem. The optimum pressure was found to be 5.7 MPa, which is in supercritical region. Increasing the temperature of the motive steam (T_s) decreases the exergy efficiency of MED subsystem while increasing the salinity of the feed entering the first effect increases it. Three different configurations of MED plants powered solar heat have been analyzed.

The solar-SORC-MVC-MED has a clear advantage in the specific thermal energy consumption and the size of the solar field over other configurations and a slight advantage on the cost of production over the solar-MED-TVC. At 14 effects, solar-MED configuration consumed about 60 kWh_{th}/m^3, where the solar-MED-TVC configuration consumed about 35 kWh_{th}/m^3 and solar-SORC-MVC-MED configuration consumed about 29 kWh_{th}/m^3. The cost of water production for the solar-MED configuration reduced from $\$3/m^3$ at 4 effects to almost $\$2/m^3$ at 16 effects. The solar-MED configuration is more sensitive to the cost of the solar field. On the other hand, the solar-MED-TVC and solar-SORC-MVC-MED systems are more sensitive to the cost of the MED subsystem. The cost of unit water production for both configurations is varied from $\$2/m^3$ at 4 effects to $\$1.75/m^3$ at 16 effects. The cost breakdowns for each configuration based on the cost of their components has been presented.

In future work, more organic working fluids could be investigated for higher temperature heat sources for supercritical-ORC. Criteria for a selection working fluid and power scheme could be proposed to drive a thermal desalination. Coupling the proposed system to be the bottom cycle of sCO_2 Brayton cycle might have a potential to supply water and power for communities in arid regions. Applying low thermal energy storage to store the waste sensible heat from rejected brine in artificial bonds to preheat the feed incoming to MED subsystem could increase the efficiency of ORC subsystem and minimize the thermal pollution of the desalination plants that affect marine life.

REFERENCES

[1] UN World Water Assessment Programme, 2014, *The United Nations World Water Development Report 2014: Water and Energy*.

[2] Hoekstra, A. Y., and Mekonnen, M. M., 2012, "The Water Footprint of Humanity.," Proc. Natl. Acad. Sci. U. S. A., **109**(9), pp. 3232–7.

[3] UN World Water Assessment Programme (WWAP), 2015, *The United Nations World Water Development Report 2015: Water for a Sustainable World*.

[4] Energy international Administration (EIA), 2017, *International Energy Outlook Executive Summary*.

[5] The 2030 Water Resources Group, 2009, *Charting Our Water Future - Economic Frameworks to Inform Decision-Making*.

[6] Sadoff, C. W. C. W., Hall, J. W., Grey, D., Aerts, J. C. J. H., Ait-Kadi, M., Brown, C., Cox, A., Dadson, S., Garrick, D., Kelman, J., McCornick, P., Ringler, C., Rosegrant, M., Whittington, D., Wiberg, D., Rosegrant, M., Whittington, D., and Wilberg, D., 2015, *Securing Water, Sustaining Growth: Report of the GWP/OECD Task Force on Water Security and Sustainable Growth*.

[7] Association, I. D., 2014, "Desalination by the Numbers | IDA," Int. Desalin. Assoc., **101**, pp. 2015–2018.

[8] Global Water Intelligence (GWI/IDA DesalData), 2012, "Market Profile and Desalination Markets" [Online]. Available: http://www.desaldata.com/. [Accessed: 16-Oct-2018].

[9] Wogan, D., Pradhan, S., and Albardi, S., 2017, "GCC Energy System Overview - 2017," GCC Energy Syst. Overv., pp. 2017–2021.

[10] Kuroda, O., Takahashi, S., Kubota, S., Kikuchi, K., Eguchi, Y., Ikenaga, Y., Sohma, N., Nishinoiri, K., Wakamatsu, S., Itoh, S., Wakamatsu, K., Itoh, S., Kubota, S., Kikuchi, K., Eguchi, Y., Ikenaga, Y., Sohma, N., and Nishinoiri, K., 1987, "An Electrodialysis Sea Water Desalination System Powered by Photovoltaic Cells," Desalination, (C).

[11] Darwish, M. A., and Al-Najem, N. M., 1987, "Energy Consumptions and Costs of Different Desalting Systems," Desalination, **64**, pp. 83–96.

[12] Sommariva, C., Hogg, H., and Callister, K., 2003, *DESALINATION Cost Reduction and Design Lifetime Increase in Thermal Desalination Plants: Thermodynamic and Corrosion Resistance Combined Analysis for Heat Exchange Tubes Material Selection*.

[13] Borsani, R., and Rebagliati, S., "Fundamentals and Costing of MSF Desalination Plants and Comparison with Other Technologies."

[14] Reddy, K. V., and Ghaffour, N., 2007, "Overview of the Cost of Desalinated Water and Costing Methodologies," Desalination, **205**(1–3), pp. 340–353.

[15] International Desalination Association, 2013, *IDA Desalination Yearbook 2012-2013, for Global Water Intelligence*.

[16] Al-Karaghouli, A., and Kazmerski, L. L., 2013, "Energy Consumption and Water Production Cost of Conventional and Renewable-Energy-Powered Desalination Processes," Renew. Sustain. Energy Rev., **24**, pp. 343–356.

[17] Karagiannis, I. C., and Soldatos, P. G., 2008, "Water Desalination Cost Literature: Review and Assessment," Desalination, **223**(1–3), pp. 448–456.

[18] Ghaffour, N., Missimer, T. M., and Amy, G. L., 2013, "Technical Review and Evaluation of the Economics of Water Desalination: Current and Future Challenges for Better Water Supply Sustainability," Desalination, **309**, pp. 197–207.

[19] Papapetrou, M., Wieghaus, M., and Biercamp, C., 2010, "Roadmap for the Development of Desalination Powered by Renewable Energy," ProDes Proj., p. 79.

[20] Isaka, M., 2012, *Water Desalination Using Renewable Energy*.

[21] European Union, 2008, *ADIRA Handbook, A Guide to Desalination System Concepts*.

[22] Delyannis, E.-E., 1987, "Status of Solar Assisted Desalination: A Review," Desalination, **67**, pp. 3–19.

[23] Delyannis, E., 2003, "Historic Background of Desalination and Renewable Energies," Sol. Energy, **75**(5), pp. 357–366.

[24] Li, C., Goswami, Y., and Stefanakos, E., 2013, "Solar Assisted Sea Water Desalination: A Review," Renew. Sustain. Energy Rev., **19**, pp. 136–163.

[25] Sharon, H., and Reddy, K. S., 2015, "A Review of Solar Energy Driven Desalination Technologies," Renew. Sustain. Energy Rev., **41**, pp. 1080–1118.

[26] Hetal, K.T., Upadhyay, D.B., Rana, A. H., 2014, "Seawater Desalination Processes," IJESRT, **3**, pp. 638–646.

[27] Qiblawey, H. M., and Banat, F., 2008, "Solar Thermal Desalination Technologies," Desalination, **220**(1–3), pp. 633–644.

[28] Palenzuela, P., Alarcón-Padilla, D. C., Zaragoza, G., and Blanco, J., 2015, "Comparison between CSP+MED and CSP+RO in Mediterranean Area and MENA Region: Techno-Economic Analysis," *Energy Procedia*, Elsevier, pp. 1938–1947.

[29] Palenzuela, P., Alarcón-Padilla, D.-C., and Zaragoza, G., "Large-Scale Solar Desalination by Combination with CSP: Techno-Economic Analysis of Different Options for the Mediterranean Sea and the Arabian Gulf," Desalination, (0).

[30] H.M.H. Al-Sheikh, 1997, "Appendix 8: Country Case Study – Water Policy Reform in Saudi Arabia," *Proceedings of the Second Expert Consultation on National Water Policy Reform in the Near East*.

[31] Ishimatsu, T., Doufene, A., Alawad, A., and de Weck, O., 2017, "Desalination Network Model Driven Decision Support System: A Case Study of Saudi Arabia," Desalination, **423**, pp. 65–78.

[32] *Meeting the GCC's Water Needs in an Environmentally Sustainable Way Energy Efficient Desalination*.

[33] Al Hashemi, R., Zarreen, S., Al Raisi, A., Al Marzooqi, F. . A., and Hasan, S. . W., 2014, "A Review of Desalination Trends in the Gulf Cooperation Council Countries," Int. Interdiscip. J. Sci. Res., **1**(2), pp. 72–96.

[34] ECRA, 2016, *Activities Report of Electricity & Co-Generation Regulatory Authority*.

[35] World Bank, T., *Renewable Energy Desalination An Emerging Solution to Close the Water Gap in the Middle East and North Africa*.

[36] Bourcier, W. L., Wolery, T. J., Wolfe, T., Haussmann, C., Buscheck, T. A., and Aines, R. D., 2011, "A Preliminary Cost and Engineering Estimate for Desalinating Produced Formation Water Associated with Carbon Dioxide Capture and Storage," Int. J. Greenh. Gas Control, **5**(5), pp. 1319–1328.

[37] Al-Karaghouli, A., and Kazmerski, L., 2012, "Economic and Technical Analysis of a Reverse-Osmosis Water Desalination Plant Using DEEP-3.2 Software," Environ. Sci. Eng., **A. 1.**

[38] Jamil, M. A., and Zubair, S. M., 2017, "Design and Analysis of a Forward Feed Multi-Effect Mechanical Vapor Compression Desalination System: An Exergo-Economic Approach," Energy, **140**, pp. 1107–1120.

[39] El-Dessouky, H. T., Ettouney, H. M., and Al-Juwayhel, F., 2000, "Multiple Effect Evaporation—Vapour Compression Desalination Processes," Chem. Eng. Res. Des., **78**(4), pp. 662–676.

[40] Aybar, H. S., 2002, "Analysis of a Mechanical Vapor Compression Desalination System," Desalination, **142**(2), pp. 181–186.

[41] Helal, A. M., and Al-Malek, S. A., 2006, "Design of a Solar-Assisted Mechanical Vapor Compression (MVC) Desalination Unit for Remote Areas in the UAE," Desalination, **197**(1–3), pp. 273–300.

[42] Nafey, A. S., Fath, H. E. S., and Mabrouk, A. A., 2008, "Thermoeconomic Design of a Multi-Effect Evaporation Mechanical Vapor Compression (MEE-MVC) Desalination Process," Desalination, **230**(1–3), pp. 1–15.

[43] Sharaf, M. A. A., Nafey, A. S. S., and García-Rodríguez, L., 2011, "Exergy and Thermo-Economic Analyses of a Combined Solar Organic Cycle with Multi Effect Distillation (MED) Desalination Process," Desalination, **272**(1–3), pp. 135–147.

[44] He, W. F. F., Zhu, W. P. P., Xia, J. R. R., and Han, D., 2018, "A Mechanical Vapor Compression Desalination System Coupled with a Transcritical Carbon Dioxide Rankine Cycle," Desalination, **425**, pp. 1–11.

[45] Mabrouk, A. N., and Fath, H. E. S., 2015, "Technoeconomic Study of a Novel Integrated Thermal MSF-MED Desalination Technology," Desalination, **371**, pp. 115–125.

[46] Shahzad, M. W., Ng, K. C., Thu, K., and Chun, W. G., 2014, "Multi Effect Desalination and Adsorption Desalination (MEDAD): A Hybrid Desalination Method," Appl. Therm. Eng., **72**(2), pp. 289–297.

[47] Darwish, M. A. A., and El-Dessouky, H., 1996, "The Heat Recovery Thermal Vapour-Compression Desalting System: A Comparison with Other Thermal Desalination Processes," Appl. Therm. Eng., **16**(6), pp. 523–537.

[48] García-Rodríguez, L., and Gómez-Camacho, C., 1999, "Thermoeconomic Analysis of a Solar Parabolic Trough Collector Distillation Plant," Desalination, **122**(2–3), pp. 215–224.

[49] García-Rodríguez, L., Palmero-Marrero, A. I., and Gómez-Camacho, C., 1999, "Application of Direct Steam Generation into a Solar Parabolic Trough Collector to Multieffect Distillation," Desalination, **125**(1–3), pp. 139–145.

[50] Thomas, A., 1996, "Solar Steam Generating Systems Using Parabolic Trough Concentrators," Energy Convers. Manag., **37**(2), pp. 215–245.

[51] Ranjan, K. R., and Kaushik, S. C., 2014, "Thermodynamic and Economic Feasibility of Solar Ponds for Various Thermal Applications: A Comprehensive Review," Renew. Sustain. Energy Rev., **32**, pp. 123–139.

[52] Lu, H., Walton, J. C., and Swift, A. H. P., 2001, "Desalination Coupled with Salinity-Gradient Solar Ponds," Desalination, **136**(1–3), pp. 13–23.

[53] Al Hawaj, O., and Darwish, M. A., 1994, "A Solar Pond Assisted Multi-Effect Desalting System," Desalination, **99**(1), pp. 119–135.

[54] Tsilingiris, P. T., 1995, “The Analysis and Performance of Large-Scale Stand-Alone Solar Desalination Plants,” Desalination, **103**(3), pp. 249–255.

[55] Caruso, G., Naviglio, A., Principi, P., and Ruffini, E., 2001, “High-Energy Efficiency Desalination Project Using a Full Titanium Desalination Unit and a Solar Pond as the Heat Supply,” Desalination, **136**(1–3), pp. 199–212.

[56] J.P. Gerofi, 1983, “The Sydney University Solar Desalination Pilot Plant Design,” Desalination, **45**(1–3), pp. 375–382.

[57] Al-Hallaj, S., Parekh, S., Farid, M. M., and Selman, J. R., 2006, “Solar Desalination with Humidification–dehumidification Cycle: Review of Economics,” Desalination, **195**(1–3), pp. 169–186.

[58] El-Nashar, A. M., and Samad, M., 1998, “The Solar Desalination Plant in Abu Dhabi: 13 Years of Performance and Operation History,” Renew. Energy, **14**(1–4), pp. 263–274.

[59] García-Rodríguez, L., and Gómez-Camacho, C., 1999, “Thermo-Economic Analysis of a Solar Multi-Effect Distillation Plant Installed at the Plataforma Solar de Almeria (Spain),” Desalination, **122**(2–3), pp. 205–214.

[60] García-Rodríguez, L., Palmero-Marrero, A. I., and Gómez-Camacho, C., 2001, “Thermoeconomic Optimization of the SOL-14 Plant (Plataforma Solar de Almería, Spain),” Desalination, **136**(1–3), pp. 219–223.

[61] Milow, B., and Zarza, E., 1997, “Advanced MED Solar Desalination Plants. Configurations, Costs, Future — Seven Years of Experience at the Plataforma Solar de Almeria (Spain),” Desalination, **108**(1–3), pp. 51–58.

[62] Kalogirou, S., 1997, “Survey of Solar Desalination Systems and System Selection,” Energy, **22**(1), pp. 69–81.

[63] García-Rodríguez, L., and Gómez-Camacho, C., 1999, “Preliminary Design and Cost Analysis of a Solar Distillation System,” Desalination, **126**(1–3), pp. 109–114.

[64] Amer, A. O. B., 2009, “Development and Optimization of ME-TVC Desalination System,” Desalination, **249**(3), pp. 1315–1331.

[65] Alarcón-Padilla, D. C., and García-Rodríguez, L., 2007, “Application of Absorption Heat Pumps to Multi-Effect Distillation: A Case Study of Solar Desalination,” Desalination, **212**(1–3), pp. 294–302.

[66] Sharaf, M. A., Nafey, A. S., and García-Rodríguez, L., 2011, “Thermo-Economic Analysis of Solar Thermal Power Cycles Assisted MED-VC (Multi Effect Distillation-Vapor Compression) Desalination Processes,” Energy, **36**(5), pp. 2753–2764.

[67] Lokiec, F., and Ophir Presenter, A., *The Mechanical Vapor Compression: 38 Years of Experience*.

[68] Patricia Palenzuela, Guillermo Zaragoza*, Diego C. Alarcón-Padilla, Elena Guillén, Mercedes Ibarra, J. B., Palenzuela, P., Zaragoza, G., Alarc??n-Padilla, D. C., Guill??n, E., Ibarra, M., Blanco, J. J., Alarcón-Padilla, D. C., Guillén, E., Ibarra, M., and Blanco, J. J., 2011, "Assessment of Different Configurations for Combined Parabolic-Trough (PT) Solar Power and Desalination Plants in Arid Regions," Energy, **36**(8), pp. 4950–4958.

[69] Kouta, A., Al-Sulaiman, F., Atif, M., and Marshad, S. Bin, 2016, "Entropy, Exergy, and Cost Analyses of Solar Driven Cogeneration Systems Using Supercritical CO2Brayton Cycles and MEE-TVC Desalination System," Energy Convers. Manag., **115**, pp. 253–264.

[70] Li, C., Kosmadakis, G., Manolakos, D., Stefanakos, E., Papadakis, G., and Goswami, D. Y., 2013, "Performance Investigation of Concentrating Solar Collectors Coupled with a Transcritical Organic Rankine Cycle for Power and Seawater Desalination Co-Generation," Desalination, **318**, pp. 107–117.

[71] Li, C., Goswami, D. Y., Shapiro, A., Stefanakos, E. K., and Demirkaya, G., 2012, "A New Combined Power and Desalination System Driven by Low Grade Heat for Concentrated Brine," Energy, **46**(1), pp. 582–595.

[72] Delgado-Torres, A. M., and García-Rodríguez, L., 2007, "Preliminary Assessment of Solar Organic Rankine Cycles for Driving a Desalination System," Desalination, **216**(1–3), pp. 252–275.

[73] Delgado-Torres, A. M., and García-Rodríguez, L., 2010, "Preliminary Design of Seawater and Brackish Water Reverse Osmosis Desalination Systems Driven by Low-Temperature Solar Organic Rankine Cycles (ORC)," Energy Convers. Manag., **51**(12), pp. 2913–2920.

[74] Nafey, A. S. S., and Sharaf, M. A. A., 2010, "Combined Solar Organic Rankine Cycle with Reverse Osmosis Desalination Process: Energy, Exergy, and Cost Evaluations," Renew. Energy, **35**(11), pp. 2571–2580.

[75] Peñate, B., and García-Rodríguez, L., 2012, "Seawater Reverse Osmosis Desalination Driven by a Solar Organic Rankine Cycle: Design and Technology Assessment for Medium Capacity Range," Desalination, **284**, pp. 86–91.

[76] Li, C., Besarati, S., Goswami, Y., Stefanakos, E., and Chen, H., 2013, "Reverse Osmosis Desalination Driven by Low Temperature Supercritical Organic Rankine Cycle," Appl. Energy, **102**, pp. 1071–1080.

[77] Al-Shammiri, M., and Safar, M., 1999, "Multi-Effect Distillation Plants: State of the Art," *Desalination*, pp. 45–59.

[78] Marcovecchioa, M., Aguirrea, P., Scennaa, N., and Mussatia, S., 2010, *Global Optimal Design of Mechanical Vapor Compression (MVC) Desalination Process*, Elsevier B.V.

[79] Belessiotis, V., Kalogirou, S., Delyannis, E., Belessiotis, V., Kalogirou, S., and Delyannis, E., 2016, "Chapter Six – Indirect Solar Desalination (MSF, MED, MVC, TVC)," Therm. Sol. Desalin., pp. 283–326.

[80] Bahar, R., Hawlader, M. N. A., and Woei, L. S., 2004, "Performance Evaluation of a Mechanical Vapor Compression Desalination System," Desalination, **166**, pp. 123–127.

[81] ECOTHERM, 2011, *Product Specifications and Design Guide Evacuated Tube Collectors*.

[82] GmbH, T. C., 2015, *Ready-to-Use Heat Transfer Fluid for Solar Thermal Systems with High Thermal Loads*.

[83] Hung, T. C., Shai, T. Y., and Wang, S. K., 1997, "A Review of Organic Rankine Cycles (ORCs) for the Recovery of Low-Grade Waste Heat," Energy, **22**(7), pp. 661–667.

[84] El-Dessouky, H., Alatiqi, I., Bingulac, S., and Ettouney, H., 1998, "Steady-State Analysis of the Multiple Effect Evaporation Desalination Process," Chem. Eng. Technol., **21**(5), pp. 437–451.

[85] Mistry, K. H., Antar, M. A., and Lienhard V, J. H., 2013, "An Improved Model for Multiple Effect Distillation," Desalin. Water Treat., **51**(4–6), pp. 807–821.

[86] E. W. Lemmon and I.H. Bell and M. L. Huber and M. O. McLinden, 2018, "NIST Standard Reference Database 23: Reference Fluid Thermodynamic and Transport Properties-REFPROP, Version 10.0, National Institute of Standards and Technology."

[87] Sharqawy, M. H., Lienhard V, J. H., and Zubair, S. M., 2011, "Erratum to Thermophysical Properties of Seawater: A Review of Existing Correlations and Data," Desalin. Water Treat., **29**(1–3), pp. 355–355.

[88] Nayar, K. G., Sharqawy, M. H., Banchik, L. D., and Lienhard, J. H., 2016, "Thermophysical Properties of Seawater: A Review and New Correlations That Include Pressure Dependence," Desalination, **390**, pp. 1–24.

[89] Le, V. L., Feidt, M., Kheiri, A., and Pelloux-Prayer, S., 2014, "Performance Optimization of Low-Temperature Power Generation by Supercritical ORCs (Organic Rankine Cycles) Using Low GWP (Global Warming Potential) Working Fluids," Energy, **67**, pp. 513–526.

[90] Fernández-Izquierdo, P., García-Rodríguez, L., Alarcón-Padilla, D. C., Palenzuela, P., and Martín-Mateos, I., 2012, "Experimental Analysis of a Multi-Effect Distillation Unit Operated out of Nominal Conditions," Desalination, **284**, pp. 233–237.

[91] Petela, R., 2010, *Engineering Thermodynamics of Thermal Radiation for Solar Power Utilization*, McGraw Hill.

[92] Petela, R., 1964, "Exergy of Heat Radiation," J. Heat Transfer, **86**(2), p. 187.

[93] Ranjan, K. R., and Kaushik, S. C., 2013, "Energy, Exergy and Thermo-Economic Analysis of Solar Distillation Systems: A Review," Renew. Sustain. Energy Rev., **27**, pp. 709–723.

[94] Goswami, D. Y., 2015, *Principles of Solar Engineering, Third Edition*, Taylor & Francis.

[95] García-Rodríguez, L., and Gómez-Camacho, C., 2001, "Exergy Analysis of the SOL-14 Plant (Plataforma Solar de Almeria, Spain)," Desalination, **137**(1–3), pp. 251–258.

[96] Al-Hallaj, S., Parekh, S., Farid, M. M., and Selman, J. R., 2006, "Solar Desalination with Humidification-Dehumidification Cycle: Review of Economics," Desalination, **195**(1–3), pp. 169–186.

[97] Chaouachi, B., 2011, "Solar Desalination," *Desalination: Trends & Technologies*, J. KUCERA, ed., JOHN WILEY, pp. 217–236.

[98] Al-Juwayhel, F., El-Dessouky, H., and Ettouney, H., 1997, "Analysis of Single-Effect Evaporator Desalination Systems Combined with Vapor Compression Heat Pumps," Desalination, **114**(3), pp. 253–275.

[99] Almatrafi, E., Moloney, F., Goswami, D. Y., and Goswami, Y., 2017, "Multi Effects Desalination-Mechanical Vapor Compression Powered By Low Temperature Supercritical Organic Rankine Cycle," *Proceedings of the IMECE2017*, ASME, Tampa, FL, p. V006T08A020.

[100] El-Sayed, Y. M., 2001, "Designing Desalination Systems for Higher Productivity," Desalination, **134**(1–3), pp. 129–158.

[101] Nájera-Trejo, M., Martin-Domínguez, I. R., and Escobedo-Bretado, J. A., 2016, "Economic Feasibility of Flat Plate vs Evacuated Tube Solar Collectors in a Combisystem," *Energy Procedia*, pp. 477–485.

[102] Quoilin, S., Broek, M. Van Den, Declaye, S., Dewallef, P., and Lemort, V., 2013, "Techno-Economic Survey of Organic Rankine Cycle (ORC) Systems," Renew. Sustain. Energy Rev., **22**, pp. 168–186.

[103] Renewable Energy Agency, I., 2012, *RENEWABLE ENERGY TECHNOLOGIES: COST ANALYSIS SERIES Concentrating Solar Power Volume 1: Power Sector Issue 2/5 Acknowledgement*.

[104] Compain, P., 2012, "Solar Energy for Water Desalination," *Procedia Engineering*, Elsevier, pp. 220–227.

[105] Kalogirou, S. A., 2005, "Seawater Desalination Using Renewable Energy Sources," Prog. Energy Combust. Sci., **31**(3), pp. 242–281.

APPENDICES

Appendix A. List of Symbols

- Nomenclature

a	heat transmission coefficient (W/m^2.K)
A	area (m^2)
avg	average
B	brine mass flow (kg/s)
BPE	boiling point elevation
c_p	Specific heat (kJ/kg-K)
DSG	direct steam generated
ETC	evacuated tube collector
FPC	flat plate collector
G	solar insolation (kW/m^2)
h	enthalpy (kJ/kg)
$\dot{M}$	mass flow (kg/s)
w	molar fraction
N	number of collectors
PR	performance ratio
s	entropy, kJ/kg-K
$SORC$	supercritical organic Rankine cycle
sA	specific heat transfer area (m^2-s/kg)
SP	solar pond
ST	solar tower
T	temperature (K)
U	heat transfer coefficient (kW/K.m^2)
$\dot{Q}$	heat rate (kW)
$\dot{W}$	power (kW)
X	Salinity of the feed (ppm)

- Greek Letters

ε	effectiveness
η	efficiency
λ	latent heat (kJ/kg)
Ψ	exergy factor
ψ	exergy flow, kJ/kg

- Subscripts

1,.. n-1	number of effect
a	ambient
atm	atmospheric
br	brine
col	collector
cw	intake seawater
d	total distillated water
e	effect
f	feed
fh	feed heater
fl	flash
fs	saturated liquid from the first effect
h	hour
HTF	heat transfer fluid
HXB	heat exchanger boiler
MED	multi effects desalination
MVC	mechanical vapor compressor
mix	mixture
n	last effect
o	dead state
op	optical efficiency
ORC	organic Rankine cycle
p	pump
ph	physical
s	steam
sat	saturation
spc	specific energy consumption
t	turbine
v	vapor
vn	saturated vapor from the last effect
vs	superheated vapor
WF	working fluid
W	water

Appendix B. Copyright Permissions

This is a copyright permission given by American Society of Mechanical Engineering (ASME) for using materials in chapter 3 &4.

From: Eydhah Almatrafi [mailto:almatrafi@mail.usf.edu]
Sent: Thursday, November 1, 2018 12:43 PM
To: permissions@asme.org
Subject: Copyright Permission for Phd Dissertation

[Quoted text hidden]

Eydhah Almatrafi <almatrafi@mail.usf.edu> Mon, Nov 5, 2018 at 6:30 PM
To: DarchiB@asme.org

Thank you

The name of the university is " University of South Florida"

Best,

Eyd
[Quoted text hidden]

Beth Darchi <DarchiB@asme.org> Thu, Nov 8, 2018 at 11:34 AM
To: Eydhah Almatrafi <almatrafi@mail.usf.edu>

Dear Mr. Almatrafi,
It is our pleasure to grant you permission to use **all or any part of** the following ASME papers:

- Performance Analysis of Solar Thermal Powered Supercritical Organic Rankine Cycle Assisted Low-Temperature Multi Effect Desalination Coupled With Mechanical Vapor Compression," by Eydhah Almatrafi; Francesca Moloney; D. Y. Goswami, Paper No. POWER2018-7307

- Multi Effects Desalination-Mechanical Vapor Compression Powered by Low Temperature Supercritical Organic Rankine Cycle, by Eydhah Almatrafi, Francesca Moloney and D. Y. Goswami, Paper No. IMECE2017-72230

cited in your letter for inclusion in a Phd Dissertation to be published by the University of South Florida.

Permission is granted for the specific use as stated herein and does not permit further use of the materials without proper authorization. Proper attribution must be made to the author(s) of the materials. **Please note:** if any or all of the figures and/or Tables are of another source, permission should be granted from that outside source or include the reference of the original source. ASME does not grant permission for outside source material that may be referenced in the ASME works.

As is customary, we request that you ensure full acknowledgment of this material, the author(s), source and ASME as original publisher. Acknowledgment must be retained on all pages where figure is printed and distributed.

Many thanks for your interest in ASME publications.

Sincerely,

Beth Darchi
Publishing Administrator
ASME
2 Park Avenue
New York, NY 10016-5990
Tel 1.212.591.7700

This is a copyright permission given by ECOS 2018 for using materials in chapter 5.

USF

Eydhah Almatrafi <almatrafi@mail.usf.edu>

Copyright Permission for Phd Dissertation

2 messages

Eydhah Almatrafi <almatrafi@mail.usf.edu> Thu, Nov 1, 2018 at 12:48 PM
To: ECOS 2018 Organization <ecos2018@dps.uminho.pt>

Dear

I am requesting a copyright permission use paper that I submitted to the ECOS2018 conference to use it in my thesis.

Almatrafi, E., Moloney, F., and Goswami, D. Y., 2018, Exergy Analysis of Solar Powered Supercritical Organic Rankine Cycle Assisted Multi-Effect Desalination Coupled with Mechanical Vapor Compressor. ECOS2018. Paper presented at 31st International Conference on Efficiency, Cost, Optimization, Simulation, and Environmental Impact of Energy Systems Conference, Guimarães, Portugal

Best wishes

Eyd

ECOS 2018 Organization <ecos2018@dps.uminho.pt> Thu, Nov 8, 2018 at 5:50 AM
To: Eydhah Almatrafi <almatrafi@mail.usf.edu>

Dear author,

You can use the following citation:

Almatrafi, E., Moloney, F., and Goswami, D. Y., (2018). Exergy Analysis of Solar Powered Supercritical Organic Rankine Cycle Assisted Multi-Effect Desalination Coupled with Mechanical Vapor Compressor. In U. do M. D. de E. Mecânica (Ed.), *Proceedings of ECOS 2018 - The 31st International Conference on Efficiency, Cost, Optimization, Simulation and Environmental Impact of Energy Systems* (pp. 1–12). Guimarães. ISBN: 978-972-99596-4-6

kind regards,

ECOS 2018

De: Eydhah Almatrafi [almatrafi@mail.usf.edu]
Enviado: 1 de Novembro de 2018 16:48
Para: ECOS 2018 Organization
Assunto: Copyright Permission for Phd Dissertation

[Quoted text hidden]

This is a copyright permission given by Michael Papapetrou for using Fig.6 in chapter 1.

USF

Eydhah Almatrafi <almatrafi@mail.usf.edu>

Copyright Permission for Phd Dissertation

Michael Papapetrou <michael.papapetrou@wip-munich.de> Fri, Nov 2, 2018 at 9:30 AM
To: Eydhah Almatrafi <almatrafi@mail.usf.edu>

Dear Eyd

You are welcome to use it as long as you reference the source:

Michael Papapetrou, Marcel Wieghaus, Charlotte Biercamp (2010), "Roadmap for the development of desalination powered by renewable energy", ISBN 978-3-8396-0147-1, by FRAUNHOFER VERLAG, 2010

Best regards

Michael

Michael Papapetrou

Senior Project Manager

WIP Renewable Energies

Sylvensteinstr. 2

81369 Munich, Germany

Phone: +49 89 720 12 712

michael.papapetrou@wip-munich.de

www.wip-munich.de

From: Eydhah Almatrafi <almatrafi@mail.usf.edu>
Sent: 01 November 2018 17:14

ABOUT THE AUTHOR

Eydhah Almatrafi is a faculty member of the college of engineering at the King Abdul-Aziz University (KAU) in Saudi Arabia. He studied physics -as an under graduate- initially at King Fahad University of Petroleum and Minerals (KFUMP) and completed his B.Sc., in mechanical engineering. When he received a PhD scholarship, he joined the Mechanical Department of University of South Florida (USF) and clean energy research center (CERC) under guidance of Dr. Yogi Goswami. His Ph.D. research is focused on solar desalination, specifically, the analysis of thermal desalination assisted by vapor compression. The ultimate goal of his research is reducing the specific energy consumption and the cost of solar thermal desalination. During his doctoral program, he served as a reviewer for journal such as: Desalination, Water Treatment, and Energy Conversion journals and conference such as: ASME power, IMECE and ECOS conferences. He was selected to participate in academic leadership program that designed by Ministry of Education (MOE) to prepare leaders for Saudi Universities. He represented Saudi Arabia in Global Solar Initiative program that designed by University of Tokyo and MISK in Japan in 2018.